POR Calabria 2014-2020 Fesr-Fse il futuro è un lavoro quotidiano

UNIONE EUROPEA FONDI STRUTTURALI E DI INVESTIMENTO EUROPEI

REPUBBLICA ITALIANA

REGIONE CALABRIA

UNIVERSITÀ DELLA CALABRIA

UNIVERSITA' DELLA CALABRIA

Dipartimento di Farmacia e Scienze della Salute e della Nutrizione

Dottorato di Ricerca in

Medicina Traslazionale

Ciclo

XXXIV

New strategies in the design of functional and bioinspired materials for therapeutic applications

Settore Scientifico Disciplinare CHIM/09

Coordinatore: Ch.mo Prof. Sebastiano Andò

Firma oscurata in base alle linee guida del Garante della privacy

Supervisore: Ch.ma Prof.ssa Roberta Cassano

Firma oscurata in base alle linee guida del Garante della privacy

Ch.ma Prof.ssa Francesca Iemma

Firma oscurata in base alle linee guida del Garante della privacy

Ch.mo Prof. Francesco Stellacci

Firma oscurata in base alle linee guida del Garante della privacy

Dottoranda: Dott.ssa Camilla Servidio

Firma oscurata in base alle linee guida del Garante della privacy

Sapere aude!
—Orazio (Epistole I, 2)

Alla mia famiglia.

TABLE OF CONTENTS

PREFACE

The works presented in this thesis are the results of the research activity performed during my three-year doctoral studies. The PhD project was mainly focused on the design of innovative materials for biomedical applications, including drug delivery and discovery. To this end, particular attention has been addressed to bioderived and bioinspired approaches to develop multifunctional smart materials able to successfully and adequately interact with biological systems, exploiting their natural or acquired functionalities. Nature has always offered bioactive complex structures that represents a source of inspiration in material science. Translating these principles in the design of engineered systems constitutes a new and promising paradigm with a potential huge impact in the pharmaceutical field.

The present thesis is divided in two different sections. In **section I** are reported the results of the projects carried out at the Laboratory of Pharmaceutical Technology of the University of Calabria (Italy) during the first-second year of my doctoral studies. In particular, they have regarded the design of functional drug delivery systems and the evaluation of their potentiality for skin delivery and cancer therapy. After a brief introduction on the new technologies developed in the last years for this purpose, the performed research works are presented in two different chapters. **Chapter I** investigates the use of hyaluronic acid-based hydrogels as delivery systems for chemotherapeutic drugs in targeted cancer therapy. This chapter begins with the analysis of the current state of the art on the newly emerged strategies for the design of hyaluronic acid-based hydrogels, with a particular focus on their use in drug delivery for cancer therapy. This is followed by the experimental part in which is reported the preparation and the characterization of a hyaluronic acid- and folic acid- based hydrogel for the delivery of cisplatin and the evaluation of its antineoplastic effect in human ovarian cancer cells. On the other hand, in **chapter II** are presented novel topical formulations developed for the dermal delivery of cyclosporine A in psoriasis treatment. In particular, given their lipophilicity and occlusive properties, solid lipid nanoparticles based on bioactive molecules are proposed as drug carriers and incorporated in different topical vehicles

including functional agents such as hyaluronic acid, obtaining gels with different degree of lipophilicity. Their potential application in psoriasis treatment is evaluated by considering the encapsulation efficiency, release profiles, *in vitro* skin permeation, and anti-inflammatory effects.

Section II is focused on the design of novel broad-spectrum virucidal antivirals. Herein are reported the results of the research project carried out at the Laboratory of Supramolecular Nanomaterials and Interfaces of the École polytechnique fédérale de Lausanne (Switzerland) during the second-third year of my doctoral studies. This section begins with the background that motivated this work, investigating the role of heparan sulfate in viral infection. In particular, the most medically relevant heparan sulfate dependent viruses are discussed, describing the current pharmacological treatments and highlighting the recent advances made in the development of glycomimetic agents. This is followed by a brief introduction on the novel concept proposing heparan sulfate mimicking gold nanoparticles as promising tools in antiviral therapy. The performed research work is then presented; its aim is to unravel the mechanism of action of this system, investigating the structure-activity relationships and identifying the key parameters required for a virucidal effect. In particular, the effect of the hydrophobicity and flexibility of the ligands, and the type and size of the core is explored.

SECTION I

Innovative functional drug delivery systems

1. Introduction

Pharmacologically active agents are fundamental tools in medicine for the treatment and the management of diseases. The global pharmaceutical market went through a significative growth over the past years, and it is expected to reach 1.6 trillion dollars by 2025[1]. Therapeutics are not intrinsically effective, and their efficacy strongly depends on their biopharmaceutical properties and route of administration. In fact, poor aqueous solubility, poor bioavailability, inactivation (i.e. enzymatic or pH-driven), lack of selectivity, non-specific toxicity and unfavorable pharmacokinetic properties are common elements that can limit the clinical use and efficacy of drugs[2]. To overcome these limitations, three main strategies have been adopted: drug modifications (i.e. chemical structural modifications and functionalization with targeting ligands), microenvironment alterations (i.e. use of solubility enhancers that act by modifying the physiological pH) and drug delivery systems[3].

The use of drug delivery systems has brought considerable benefits to the clinical development of therapeutics, converting them in effective and successful pharmacological treatments. They are formulations or devices used to introduce and transport drugs in the body to obtain a safe, effective and controlled therapeutic effect[4]. Their main aim is to improve the physicochemical properties, the biodistribution and the pharmacokinetic profile of the free drug. Most importantly, these systems can serve as drug reservoir, allowing controlled and regulated drug release rates[5]. This feature results to be useful not only for optimizing the pharmacokinetic parameters, in particular the half-life and the peak plasma concentration, but also for improving patient compliance by reducing the dosing frequency.

Drug delivery systems range from macro- to micro- to nano-scale platforms including hydrogels, microparticles and nanoparticles[6]. At present, several controlled release medications have reached the market. The first one was Spansule® (Dexedrine), approved in 1952 by the Food and Drug Administration (FDA), that started the first-generation of drug delivery systems. Into this category fall Procardia XL®, an osmotic

controlled delivery system (nifedipine), Scop®, the first transdermal patch (scopolamine) *etc*[7-8].

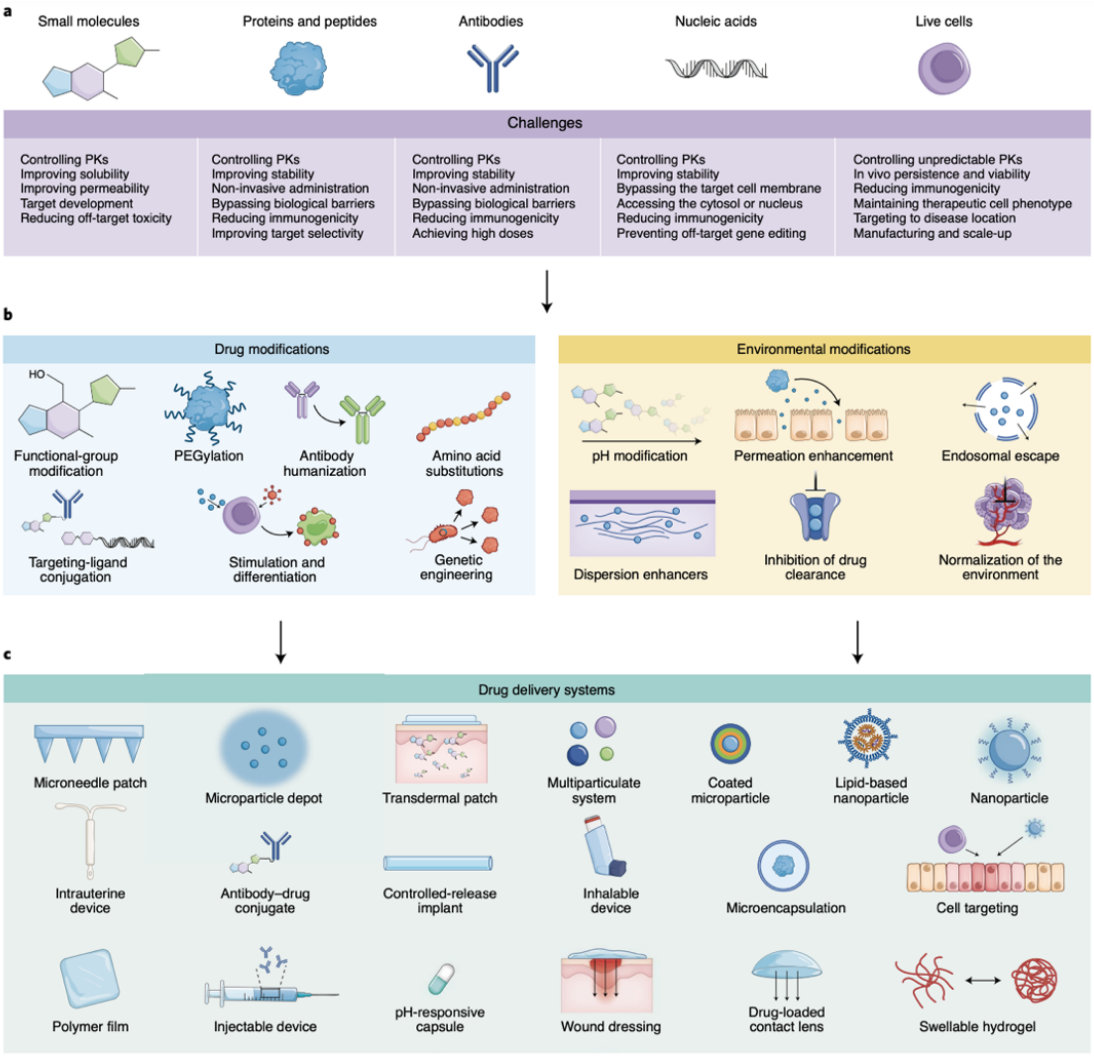

Figure 1. Schematic representation of the delivery limitations of the main classes of therapeutics (a), potential strategies to address these drawbacks (b) with a particular focus on drug delivery systems (c)[3]. Adapted with permission from Springer Nature.

In last decades, the advent of nanotechnologies has led to the start of the second generation of drug delivery systems. This latter comprises a wide group of materials such as lipid nanoparticles, polymeric nanoparticles, inorganic nanoparticles, nanogels, micelles, dendrimers, liposomes *etc*[9-10]. These systems have been mainly investigated to deliver hydrophobic drugs and/or to achieve targeted release *via* surface modifications and/or size-dependent mechanisms. Doxil®, a pegylated liposomal doxorubicin, was the first nanodrug approved (1995), and, currently, nanoparticle-based formulations are

licensed principally for cancer therapy (Abraxane, DaunoXome, Markibo) and vaccines (Comirnaty)[11-13].

Recent advances made in materials chemistry further allowed to develop new strategies, such as stimuli-responsive delivery, to optimize site-specific and controlled release. These "smart" materials are able to release drugs in response to endogenous triggers, including variation of pH, enzymes or redox state, and external triggers, such as temperature, light, magnetic field *etc*.[14]. Stimuli-responsive materials have been mostly explored for targeted cancer therapy and oral delivery of drugs[15-17]. Interesting and promising results emerged from preclinical studies; however, more *in vivo* data are required to confirm their potentiality as delivery platforms[15].

Drug delivery systems have found applications in numerous therapeutic areas, including infectious, cardiovascular, respiratory, oncological and gastrointestinal diseases. Given the topics of the experimental works that will be presented in the following chapters, we will focus on two applications: skin delivery and cancer therapy.

2. Drug delivery systems for cancer therapy

Cancer includes a large group of complex diseases characterized by uncontrolled cell growth. It is the leading cause of death globally, with approximately 10 million deaths in 2020 according to WHO[18]. In the last years, the mortality rate showed a decreasing trend thanks to the advances made in both diagnosis and treatment; however, it still remains high[19]. Conventional treatments include chemotherapy, radiotherapy, and surgery, usually in combination. Surgical resection remains the main option in case of circumscribed mass. On the other hand, chemotherapy is usually adopted as adjuvant treatment, before and/or after surgery, or in case of metastatic tumors. Chemotherapeutic drugs are cytotoxic agents that act by inducing DNA damage. However, these therapeutics are not selective and consequently act also on non-cancerous cells, causing toxicity to the patient. Moreover, the lack of selectivity leads to a low accumulation of the drug in tumor tissues, and, therefore, high dosages are required to have a significative therapeutic effect[20]. Lastly, chemotherapeutic drugs can induce multidrug resistance, which represents one of the major problems in cancer treatment[21].

In the light of these considerations, the use of drug delivery systems could bring several benefits to cancer therapy including site-specific and sustained drug release, reduced toxicity, and improved pharmacokinetic parameters and therapeutic index. Moreover, loading chemotherapeutic drugs in such vehicles could be useful for addressing common solubility issues of this class of therapeutics, since they are mostly hydrophobic[22]. To this end, in the last years, the scientific community has significantly exploited the newly emerged technologies for the design of novel drug delivery systems. In particular, numerous materials including hydrogels, micelles, polymeric, inorganic, lipid and protein-based nanoparticles, self-assembled platforms *etc.* have been synthetized and evaluated as potential formulations for cancer therapy[23-24]. Notably, some of them reached the market starting from Doxil® (1995) to Vyxeos® (2018).

As can be noted, among the different technologies, nanomedicine has had a greater scientific impact. The main reason behind this choice lies in the discovery of the enhanced permeability and retention effect (EPR), firstly described 40 years ago[25]. It is a phenomenon based on peculiar anatomical and structural features of tumor blood vessels, including irregular architecture, leaky endothelium and reduced lymphatic drainage[26-27]. These unique properties were thought to lead to the preferential accumulation and retention of nanoparticles in tumor tissue. In particular, the size of nanoparticles was identified as critical parameter for their extravasation, and the cut off dimension was assumed to range from 100 to 800 nm. However, recently, this mechanism has been heavily debated and several concerns regarding its validity have been raised[28-29].

In this context, active targeting has emerged as alternative approach that could help to address some of the passive targeting limitations (**Figure 2**). This strategy is based on the interactions between the drug carrier and the tumor microenvironment. It consists in the surface functionalization of nanoparticles with active ligands that bind with high affinity to surface-receptors overexpressed on target cells, leading therefore to enhanced particles cellular-uptake. At present, numerous biological ligands including small molecules, aptamers, peptides, glycoproteins, antigens and carbohydrates have been identified and exploited to that end[30-32]. Positive results emerged from *in vitro* and *in vivo* studies, showing a greater accumulation of the drug and the carriers in cancerous cells[33]; however, clinical studies are required to confirm the potentiality of this approach.

.

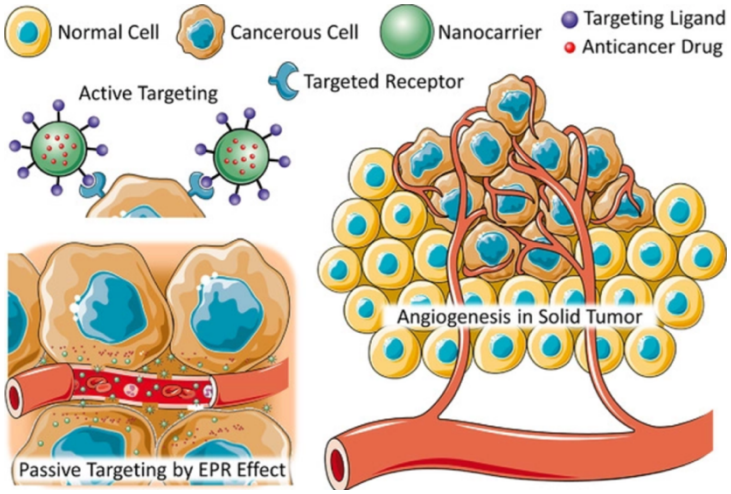

Figure 2. Schematic representation of passive and active targeting mechanisms.

In addition to the mentioned above strategies, the possibility to spatially and temporally trigger and control drug release, thanks to the development of stimuli-responsive systems, shows great potential for achieving targeted cancer therapy. It is well known that the tumor microenvironment exhibits specific changes that can be exploited as endogenous stimuli; among them we can find a lower pH, variations in the redox-state such as increased concentration of glutathione, and overexpression of enzymes such as hyaluronidase and matrix metalloproteinases[34-36]. With respect to all these approaches, pH-responsive systems are the most used and investigated for cancer therapy. In this case, the use of pH responsive polymers such as polymethacrylates, poly(β-amino ester), poly(L-histidine), and the introduction of pH labile bonds, such as imines, orthoesters and acetals, are the most common design strategies[37]. Beyond these internal stimuli, external physical triggers such as light, temperature and magnetic field were also studied for this purpose, allowing drug accumulation and release in the target site[38]. Currently, all these strategies are exploited together in order to achieve effective and selective multifunctional systems that could represent a new hope for cancer treatment.

3. Dermal drug delivery systems

In the last years, skin delivery has attracted notable interest for systemic (transdermal) and local (topical) drug administration.

In fact, this route exhibits several advantages compared to the conventional ones:

- Avoidance of first passage effect and eventual gastric inactivation;
- Sustained and prolonged drug release and reduced dosing frequency;
- Non-invasiveness and consequent enhanced patient compliance;
- Reduction of systemic side effects;
- Access to the target site in case of dermatological conditions such as psoriasis, eczema, dermatitis *etc.*

However, efficient topical drug adsorption is challenging to achieve, since the skin constitutes a considerable barrier[39-40]. As our largest organ, its main function is to protect the body from external agents such as bacteria, viruses, allergens, UV-irradations *etc.* In fact, it shows a complex multilayer structural organization; in particular, three main layers have been identified: epidermis, dermis and hypodermis. The stratum corneum is the outermost and less permeable part of epidermis, mainly responsible of these barrier properties. It is formed by dead corneocytes distributed in lipid matrix, assuming a peculiar architecture known as “brick and mortar”[41]. Given this particular composition, drug permeation mostly occurs *via* passive diffusion. In detail, three main permeation pathways have been discovered: intercellular through the lipid layer, transcellular through the epidermis corneocytes and, lastly, appendageal through sebaceous glands and hair follicles (**Figure 3**)[42]. Therefore, in addition to specific skin properties such as hydration and integrity, the physicochemical features of the drugs strongly influence the efficiency of their topical adsorption; an ideal drug should have a molecular weight < 500 Da and a logP (partition coefficient) value from 1 to 3[43].

In the light of these considerations, a notable attention has been addressed to the identification of new approaches to optimize drug permeation and penetration through the skin. In this context, we can distinguish two different methods: active and passive[44]. The first one is based on exogenous driving forces and includes electroporation, iontophoresis, microneedles, and ultrasounds. Interestingly, several iontophoretic systems reached the market, and among them we can find LidoSite®, approved for lidocaine local delivery in 2004[45]. On the other hand, the passive methods are mainly based on the use of pro-drugs or permeation enhancers. These latter are chemical agents able to temporarily alter the structure of the stratum corneum, increasing, therefore, its permeability. At present, numerous compounds such as fatty acids,

alcohols, surfactants, terpenes, cyclodextrins, phospholipids *etc.* were found to exert this effect[46].

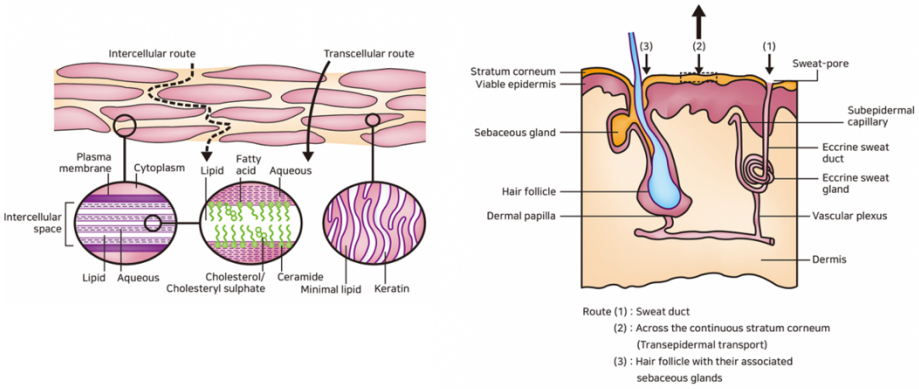

Figure 3. Schematic representation of skin structure and composition with a particular focus on the permeation pathways.

With the advent of nanotechnologies, the use of nanocarriers as topical delivery systems has emerged as attractive and promising approach for the treatment of skin disorders. In particular, among the different types, lipid-based nanoparticles, including liposomes and solid lipid nanoparticles, were mostly investigated for this purpose due to their lipophilicity[47-48]. In fact, beyond the enhanced stability, encapsulating drugs in such carriers was shown to increase their topical adsorption compared to traditional formulations[49]. In addition to the two conventional reported mechanisms (i.e. intercellular and transappendageal), it was assumed that lipid particles may also act as permeation enhancers fluidizing the lipids of the stratum corneum. These permeation mechanisms were found to be influenced by several features of the carrier including size, charge and shape[50]. For example, particles >600 nm were reported to mainly accumulate in the stratum corneum, whereas a cut-off dimension of 70 nm was observed for the dermal layer[51]. At present, beyond cosmetics, Estrasorb® is the only example of nanoparticle-based topical formulation that reached the market. However, given the promising preclinical results of these delivery systems, it is likely that they will find a place into clinical practice.

References

1. IQVIA website. Available online:https://www.iqvia.com/insights/the-iqvia-institute/reports/global-medicine-spending-and-usage-trends-outlook-to-2025
2. Allen, T. M., & Cullis, P. R. (2004). Drug delivery systems: entering the mainstream. *Science*, *303*(5665), 1818-1822.
3. Vargason, A. M., Anselmo, A. C., & Mitragotri, S. (2021). The evolution of commercial drug delivery technologies. *Nature Biomedical Engineering*, 1-17.
4. Li, C., Wang, J., Wang, Y., Gao, H., Wei, G., Huang, Y., ... & Jin, Y. (2019). Recent progress in drug delivery. *Acta pharmaceutica sinica B*, *9*(6), 1145-1162.
5. Adepu, S., & Ramakrishna, S. (2021). Controlled Drug Delivery Systems: Current Status and Future Directions. *Molecules*, *26*(19), 5905.
6. Hoffman, A. S. (2008). The origins and evolution of “controlled” drug delivery systems. *Journal of controlled release*, *132*(3), 153-163.
7. Park, K. (2014). Controlled drug delivery systems: past forward and future back. *Journal of Controlled Release*, *190*, 3-8.
8. Zhong, H., Chan, G., Hu, Y., Hu, H., & Ouyang, D. (2018). A comprehensive map of FDA-approved pharmaceutical products. *Pharmaceutics*, *10*(4), 26
9. Couvreur, P. (2013). Nanoparticles in drug delivery: past, present and future. *Advanced drug delivery reviews*, *65*(1), 21-23.
10. Mirza, A. Z., & Siddiqui, F. A. (2014). Nanomedicine and drug delivery: a mini review. *International Nano Letters*, *4*(1), 94.
11. Tran, S., DeGiovanni, P. J., Piel, B., & Rai, P. (2017). Cancer nanomedicine: a review of recent success in drug delivery. *Clinical and translational medicine*, *6*(1), 1-21.
12. Shi, J., Kantoff, P. W., Wooster, R., & Farokhzad, O. C. (2017). Cancer nanomedicine: progress, challenges and opportunities. *Nature reviews cancer*, *17*(1), 20-37.
13. Kisby, T., Yilmazer, A., & Kostarelos, K. (2021). Reasons for success and lessons learnt from nanoscale vaccines against COVID-19. *Nature Nanotechnology*, *16*(8), 843-850.
14. Raza, A., Rasheed, T., Nabeel, F., Hayat, U., Bilal, M., & Iqbal, H. (2019). Endogenous and exogenous stimuli-responsive drug delivery systems for programmed site-specific release. *Molecules*, *24*(6), 1117.

15. Mura, S., Nicolas, J., & Couvreur, P. (2013). Stimuli-responsive nanocarriers for drug delivery. *Nature materials*, *12*(11), 991-1003.
16. Rahim, M. A., Jan, N., Khan, S., Shah, H., Madni, A., Khan, A., ... & Thu, H. E. (2021). Recent Advancements in Stimuli Responsive Drug Delivery Platforms for Active and Passive Cancer Targeting. *Cancers*, *13*(4), 670.
17. Qiao, Y., Wan, J., Zhou, L., Ma, W., Yang, Y., Luo, W., ... & Wang, H. (2019). Stimuli-responsive nanotherapeutics for precision drug delivery and cancer therapy. *Wiley Interdisciplinary Reviews: Nanomedicine and Nanobiotechnology*, *11*(1), e1527.
18. WHO website. Available online: https://www.who.int/news-room/fact-sheets/detail/cancer
19. Hashim, D., Boffetta, P., La Vecchia, C., Rota, M., Bertuccio, P., Malvezzi, M., & Negri, E. (2016). The global decrease in cancer mortality: trends and disparities. *Annals of Oncology*, *27*(5), 926-933.
20. Nurgali, K., Jagoe, R. T., & Abalo, R. (2018). Adverse effects of cancer chemotherapy: Anything new to improve tolerance and reduce sequelae?. *Frontiers in pharmacology*, *9*, 245.
21. Bukowski, K., Kciuk, M., & Kontek, R. (2020). Mechanisms of multidrug resistance in cancer chemotherapy. *International journal of molecular sciences*, *21*(9), 3233.
22. Sun, T., Zhang, Y. S., Pang, B., Hyun, D. C., Yang, M., & Xia, Y. (2014). Engineered nanoparticles for drug delivery in cancer therapy. *Angewandte Chemie International Edition*, *53*(46), 12320-12364.
23. Senapati, S., Mahanta, A. K., Kumar, S., & Maiti, P. (2018). Controlled drug delivery vehicles for cancer treatment and their performance. *Signal transduction and targeted therapy*, *3*(1), 1-19.
24. Liu, G., Yang, L., Chen, G., Xu, F., Yang, F., Yu, H., ... & Li, B. (2021). A Review on Drug Delivery System for Tumor Therapy. *Frontiers in Pharmacology*, *12*.
25. Matsumura, Y., & Maeda, H. (1986). A new concept for macromolecular therapeutics in cancer chemotherapy: mechanism of tumoritropic accumulation of proteins and the antitumor agent smancs. *Cancer research*, *46*(12 Part 1), 6387-6392.
26. Fang, J., Nakamura, H., & Maeda, H. (2011). The EPR effect: unique features of tumor blood vessels for drug delivery, factors involved, and limitations and augmentation of the effect. *Advanced drug delivery reviews*, *63*(3), 136-151.

27. Islam, R., Maeda, H., & Fang, J. (2021). Factors affecting the dynamics and heterogeneity of the EPR effect: pathophysiological and pathoanatomic features, drug formulations and physicochemical factors. *Expert Opinion on Drug Delivery*, 1-14.
28. Bjornmalm, M., Thurecht, K. J., Michael, M., Scott, A. M., & Caruso, F. (2017). Bridging bio–nano science and cancer nanomedicine. *ACS nano*, *11*(10), 9594-9613.
29. Nakamura, Y., Mochida, A., Choyke, P. L., & Kobayashi, H. (2016). Nanodrug delivery: is the enhanced permeability and retention effect sufficient for curing cancer?. *Bioconjugate chemistry*, *27*(10), 2225-2238.
30. Basile, L., Pignatello, R., & Passirani, C. (2012). Active targeting strategies for anticancer drug nanocarriers. *Current drug delivery*, *9*(3), 255-268.
31. Bazak, R., Houri, M., El Achy, S., Kamel, S., & Refaat, T. (2015). Cancer active targeting by nanoparticles: a comprehensive review of literature. *Journal of cancer research and clinical oncology*, *141*(5), 769-784.
32. Kue, C. S., Kamkaew, A., Burgess, K., Kiew, L. V., Chung, L. Y., & Lee, H. B. (2016). Small molecules for active targeting in cancer. *Medicinal research reviews*, *36*(3), 494-575.
33. Yoo, J., Park, C., Yi, G., Lee, D., & Koo, H. (2019). Active targeting strategies using biological ligands for nanoparticle drug delivery systems. *Cancers*, *11*(5), 640.
34. Mi, P. (2020). Stimuli-responsive nanocarriers for drug delivery, tumor imaging, therapy and theranostics. *Theranostics*, *10*(10), 4557.
35. Jhaveri, A., Deshpande, P., & Torchilin, V. (2014). Stimuli-sensitive nanopreparations for combination cancer therapy. *Journal of controlled release*, *190*, 352-370
36. Wells, C. M., Harris, M., Choi, L., Murali, V. P., Guerra, F. D., & Jennings, J. A. (2019). Stimuli-responsive drug release from smart polymers. *Journal of functional biomaterials*, *10*(3), 34.
37. Thomas, R. G., Surendran, S. P., & Jeong, Y. Y. (2020). Tumor Microenvironment-Stimuli Responsive Nanoparticles for Anticancer Therapy. *Frontiers in Molecular Biosciences*, *7*, 414.
38. Rahim, M. A., Jan, N., Khan, S., Shah, H., Madni, A., Khan, A., ... & Thu, H. E. (2021). Recent Advancements in Stimuli Responsive Drug Delivery Platforms for Active and Passive Cancer Targeting. *Cancers*, *13*(4), 670.

39. Brown, M. B., Martin, G. P., Jones, S. A., & Akomeah, F. K. (2006). Dermal and transdermal drug delivery systems: current and future prospects. *Drug delivery*, *13*(3), 175-187.
40. Gorzelanny, C., Mess, C., Schneider, S. W., Huck, V., & Brandner, J. M. (2020). Skin barriers in dermal drug delivery: which barriers have to be overcome and how can we measure them?. *Pharmaceutics*, *12*(7), 684.
41. Menon, G. K., Cleary, G. W., & Lane, M. E. (2012). The structure and function of the stratum corneum. *International journal of pharmaceutics*, *435*(1), 3-9.
42. Iqbal, B., Ali, J., & Baboota, S. (2018). Recent advances and development in epidermal and dermal drug deposition enhancement technology. *International journal of dermatology*, *57*(6), 646-660.
43. Naik, A., Kalia, Y. N., & Guy, R. H. (2000). Transdermal drug delivery: overcoming the skin's barrier function. *Pharmaceutical science & technology today*, *3*(9), 318-326.
44. Brown, M. B., Martin, G. P., Jones, S. A., & Akomeah, F. K. (2006). Dermal and transdermal drug delivery systems: current and future prospects. *Drug delivery*, *13*(3), 175-187.
45. Alkilani, A. Z., McCrudden, M. T., & Donnelly, R. F. (2015). Transdermal drug delivery: innovative pharmaceutical developments based on disruption of the barrier properties of the stratum corneum. *Pharmaceutics*, *7*(4), 438-470.
46. Marwah, H., Garg, T., Goyal, A. K., & Rath, G. (2016). Permeation enhancer strategies in transdermal drug delivery. *Drug delivery*, *23*(2), 564-578.
47. Schäfer-Korting, M., Mehnert, W., & Korting, H. C. (2007). Lipid nanoparticles for improved topical application of drugs for skin diseases. *Advanced drug delivery reviews*, *59*(6), 427-443.
48. Puglia, C., & Bonina, F. (2012). Lipid nanoparticles as novel delivery systems for cosmetics and dermal pharmaceuticals. *Expert Opinion on Drug Delivery*, *9*(4), 429-441.
49. Yu, Y. Q., Yang, X., Wu, X. F., & Fan, Y. B. (2021). Enhancing Permeation of Drug Molecules Across the Skin via Delivery in Nanocarriers: Novel Strategies for Effective Transdermal Applications. *Frontiers in Bioengineering and Biotechnology*, *9*, 200.
50. Hua, S. (2015). Lipid-based nano-delivery systems for skin delivery of drugs and bioactives. *Frontiers in pharmacology*, *6*, 219.

51. Verma, D. D., Verma, S., Blume, G., & Fahr, A. (2003). Liposomes increase skin penetration of entrapped and non-entrapped hydrophilic substances into human skin: a skin penetration and confocal laser scanning microscopy study. *European Journal of Pharmaceutics and Biopharmaceutics*, *55*(3), 271-277.

CHAPTER I. INTRODUCTORY PART: "Strategies for hyaluronic acid-based hydrogels design for biomedical applications"*

1. Introduction

Hydrogels are three dimensional hydrated systems formed by crosslinked polymers with high affinity for water and biological fluids, capable of absorbing from ten up to thousands of times of their dry weight in water[1]. In the last decades, given their unique properties such as biocompatibility, biodegradability and flexibility, they have been widely investigated for biomedical applications including cell therapy, tissue engineering, drug delivery and diagnostic[2]. For example, hydrogels made of pectin or carboxymethylcellulose and propylene glycol are used as wound dressings, keratin or polyvinyl alcohol-based hydrogels as scaffolds for cell growth *etc.*[3-6]. Among them we can find DEXTENZA®, a polyethylene glycol based hydrogel recently approved by FDA as ophthalmic insert[7].

Hyaluronic acid (HA) represents one of the most used biopolymers in the design of hydrogels for biomedical applications due to its biocompatibility, native biofunctionality, biodegradability, non-immunogenicity and versatility. Structurally, HA is a natural linear polysaccharide that consists of alternating units of D-glucuronic acid and N- acetyl-D-glucosamine, connected by β-1,3- and β-1,4-glycosidic bonds. It is the main component of the extracellular matrix, and its biosynthesis, mainly mediated by the hyaluronic acid synthase, occurs at the plasma membrane[8-9]. Around 30% of the HA present in the body is rapidly degraded by the hyaluronidases and oxidative species, while the remaining 70% is catabolized by the liver and the endothelial cells of lymphatic vessels, exhibiting tissue half-lives going from minutes to weeks in the bloodstream and cartilage, respectively[10]. Upon physiological conditions, it exists as a polyanion associated with extracellular cations (Na^+, Ca^{2+}, Mg^{2+}, K^+), known as hyaluronan[11].

***Published on Pharmaceutics, 2019 Aug 12;11(8):407. doi: 10.3390/pharmaceutics11080407.**

HA exerts important physiological functions in the human body. In the extracellular matrix of most tissues, it contributes to maintain their mechanical integrity, homeostasis, viscoelasticity and lubrication[12]. Interestingly, it was also found to mediate several signaling pathways such as cell adhesion, migration, proliferation and differentiation, *via* its binding to the cellular receptors CD44 and RHAMM[13].

For these reasons, in recent years, hydrogels built from HA have been widely developed and investigated for biomedical applications. Nowadays several HA-based hydrogels are already used in medicine as dermal fillers, viscosupplements and wound dressings, and their market is continuously increasing worldwide.

2. Physical and chemical hydrogels

Hydrogels can be classified into "physical" or "chemical" gels, on the basis of the nature of the binding occurring between their macromolecular chains. Hydrogels are called "reversible" or "physical" if they are based on weak physical interactions such as H-bonds, Van der Waals, hydrophobic or electrostatic interactions and molecular entanglements[14]. They can be synthesized by warming or cooling polymers solution, mixing solutions of polyanions and polycations *etc.*[1]. Physical hydrogels often appear not homogenous, instable and reversible; in fact, they are not able to maintain their structural integrity and can be dissolved easily by changing environmental factors such as temperature, pH *etc.* On the other hand, hydrogels are called "permanent" or "chemical" if their polymeric chains are connected by covalent bonds[15]. For this reason, these materials, after swelling, retain their structural integrity; however, degradation can occur if particular bonds, sensitive to chemical or enzymatic hydrolysis, are present in the structure. In this case, the crosslinking of polymers with radiations, chemical crosslinkers, polyfunctional compounds and free radical-generating agents are the most common employed design strategies[1].

Although HA, due to its conformation and molecular weight, can form molecular networks in solution, it is not able to form physical gels alone. For this reason, chemical modifications, covalent crosslinking or gelling agents are needed in order to obtain hydrogels. Luckily, HA turns out to be a suitable polymer for chemical modifications thanks to its structure; in particular, to this end, three functional groups were mainly exploited: the carboxylic group, the hydroxyl group and the amino group (after deacetylation)[16]. This section reviews the different modified HA macromers and the main

strategies adopted for the design and preparation of physical and chemical HA-based hydrogels.

2.1 Chemical hydrogels

Chemical crosslinking represents a viable strategy to obtain hydrogels with excellent mechanical and thermal stability. In this context, the most adopted preparation methods are condensation reactions, enzymatic or disulfide crosslinking, polymerization *etc.* However, unfortunately, this approach can show some limitations such as the use of metal catalysts and/or photoinitiators, low reaction yields *etc.*[17]. For these reasons, in the last years, click chemistry has emerged as attractive and promising strategy due to its high specificity and yield, bioorthogonality and mild reaction conditions[18]. Interestingly, HA can also be directly crosslinked by divinyl sulfone, glutaraldehyde, carbodiimide, bisepoxide *etc.*[19-22]; however, this latter cannot be considered a suitable approach since it requires harsh reaction conditions, toxic by-products can be formed, and the crosslinking agents used are mostly cytotoxic.

2.1.1 Diels Alder reaction (click chemistry)

In recent years, a particular interest has been addressed to the Diels-Alder reaction between furan and maleimide moieties for hydrogels design, due to its selectivity, efficiency and thermoreversibility[23]. In this regard, Fisher *et al.* recently developed a HA-based hydrogel with tunable properties to use as platform to investigate breast cancer cells invasion. With the aim of mimicking the extracellular matrix, the gel was obtained *via* a Diels Alder click reaction between furan modified HA and bismaleimide functional peptides[24]. A similar approach was reported by Yu *et al*. that designed a 3D patterned system to use for cell culture. In this work, Diels Alder click chemistry between furyl-modified HA and bismaleimide PEG was exploited in order to get a hydrogel with a peculiar structure thanks to which it can further go through thiol-ene reactions, allowing its spatiotemporal patterning[25].

2.1.2 Azide-alkyn Huisgen cycloaddition (click chemistry)

Huisgen reaction is a cycloaddition between an azide and an alkyne to produce triazoles; it requires the presence of a catalyst (Cu^{+}) as reported by Rostovtsev *et al.*[26]. In the last years, it has become one of the most used strategies for hydrogels preparation thanks to its high yield, efficiency, excellent bioorthogonality, fast reaction rate *etc.*[27-28]. For example, Manzi *et a*l. adopted this method to obtain nanohydrogels by using HA derivatives and riboflavin[29]. Despite the various advantages offered by this reaction, the use of copper as a catalyst can be problematic since it is a cytotoxic element. However, recently, it has been reported that cyclooctyne functionalized molecules are able to react rapidly with azide without the presence of copper[30]. This alternative reaction, called strain-promoted azide-alkyne cycloaddition, is currently more used for hydrogels design since it shows "biocompatibility" as well as the previously reported advantages. Following this approach, Fu *et al.* fabricated an injectable HA-PEG based hydrogel[31]. In particular, cyclooctyne modified HA was synthesized by reacting HA with 2-(aminoethoxy)cyclooctyne (**Figure 1**); subsequently, it was reacted with azide functionalized PEG in order to obtain the hydrogel. Interestingly, this latter showed fast gelation time, excellent mechanical properties and high stability.

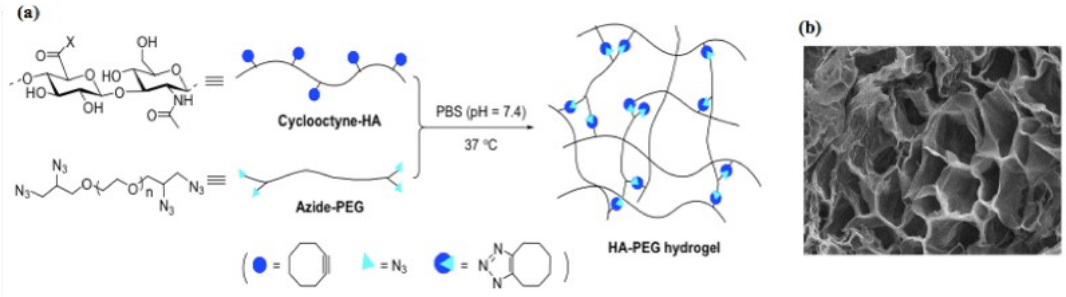

Figure 1. Preparation of the HA-PEG hydrogel (a), SEM image of the hydrogel (b) 31. Reproduced with permission from Elsevier, 2017.

2.1.3 Thiol-ene photocoupling (click chemistry)

The thiol-ene reaction consists in the radical addition (induced by light) of thiols to alkenes; it has a high yield, efficiency, specificity and fast reaction rate[32]. This method is particularly attractive for hydrogels preparation because it is solvent free and allows their spatiotemporal control; for this reason, it is mostly investigated for tissue engineering, cell culture matrices and drug delivery systems[33-34]. Different vinyl groups are employed for thiol-ene click chemistry like norbornene, vinyl sulfone, maleimide *etc*. Among them,

the thiol-norbornene reaction is characterized by greater specificity[36-35]. For example, Gramlich *et al.* employed this method for the synthesis of a photopatterned HA-based hydrogel by reacting norbornene modified HA (NorHA) with dithiothreitol (**Figure 2**)[37]. Hydrogels with an elastic modulus ranging from 1kPa to 70kPa were obtained by varying the quantity of crosslinker. Furthermore, they reported that a secondary thiol-norbornene reaction could be performed by reducing the initial amount of crosslinker. In this context we can also find the thiol-Michael addition which, however, is characterized by lower orthogonality. In this regard, Khetan *et al.* designed and prepared a 3D hydrogel *via* a two-step crosslinking process: firstly *via* a thiol-Michael addition between methacrylate-maleimide functionalized HA and the thiol groups of the peptides and, subsequently, *via* methacrylates photopolymerization[38].

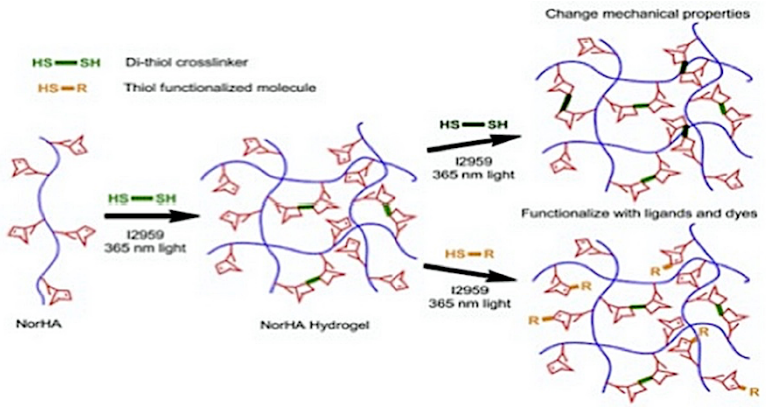

Figure 2. Schematic representation of the synthesis of the hydrogel *via* thiol-norbornene reaction[37]. Reproduced with permission from Elsevier.

2.1.4 Aldehyde-hydrazide coupling (click chemistry)

The aldehyde-hydrazide reaction has currently attracted interest in hydrogels design due to its high efficiency, cytocompatibility, simplicity, reversibility and mild reaction conditions[39-41]. In particular, hydrazone crosslinked hydrogels have been widely investigated for tissue engineering. In this regard, Chen *et al*. recently developed an injectable HA-pectin based hydrogel by reacting HA adipic dihydrazide with biofunctionalized pectin-dialdehyde and investigated its potential use as scaffold for cartilage tissue engineering (**Figure 3**)[42]. Interestingly, the resulting hydrogel exhibited a fast gelation rate, good mechanical properties, biocompatibility and cytocompatibility that make it a suitable candidate for tissue regeneration. To further improve the structural integrity of hydrazone crosslinked hydrogels, Wang *et al.* recently reported the design

and the preparation of an elastin-like protein/HA based hydrogel by combining two different crosslinking mechanisms (covalent and thermal)[43]. Firstly, the hydrogel was obtained *via* aldehyde-hydrazide coupling between hydrazine modified elastin-like protein and aldehyde modified HA; the use of a thermoresponsive protein allowed a secondary thermal crosslinking, improving its structural integrity and stability. The resulting hydrogel showed shear-thinning and self-healing properties, easy injectability and protection of cells from the mechanical stress of injection.

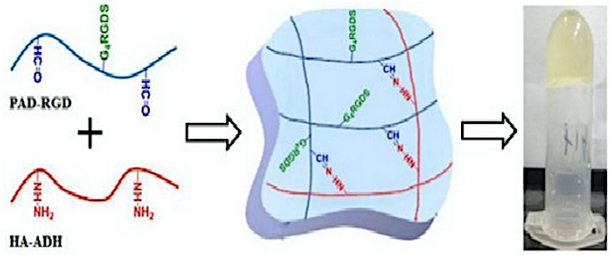

Figure 3. Schematic representation of the synthesis of the hydrogel *via* Aldehyde-hydrazide coupling[47]. Adapted with permission from Elsevier, 2017

2.1.5 Enzymatic crosslinking

Enzymatic crosslinking constitutes an interesting approach for HA based hydrogels preparation, since it is characterized by mild reaction conditions, fast gelation rate and allows to obtain hydrogels with excellent mechanical properties[44-45]. Among different enzymes, horseradish peroxidase (HRP) results to be one of the most employed; it is usually used in combination with hydrogen peroxide, and the reaction can be summarized as follows: $2Ph + H_2O_2 \rightarrow 2Ph\cdot + H_2O$ [46]. In literature are reported various tyramine modified HA-based hydrogels, obtained *via* an enzymatic crosslinking process that occurs through the oxidation of tyramine residues with the consequent formation of di-tyramine bonds[47]. In this regard, Xu *et al.* designed and fabricated HA-tyramine hydrogels by crosslinking the tyramine moieties of modified HA in the presence of HRP and H_2O_2[48]. By varying the amounts of the two enzymes, hydrogels with different mechanical strength were obtained and investigated as scaffolds for stem cells culture. Interestingly, it was observed that the hydrogel with an elastic modulus of 350 Pa supported the proliferation of stem cells. A similar approach was reported by Raia *et al.* that enzymatically crosslinked tyramine functionalized HA and silk fibroin in order to increase the mechanical strength and the stability of tyramine-HA based hydrogels[49]. By

changing the concentration of the polymers, systems with tunable properties were obtained, resulting in versatile platforms.

2.1.6 Crosslinking by radical polymerization

Hydrogels can be obtained *via* radical polymerization of monomers in the presence of crosslinking agents and an initiator, such as a redox pair or a photoinitiator[50]. Methacrylates represent the most common groups used for HA-based hydrogels preparation. They can be introduced to HA by reacting it with glycidyl methacrylate or methacrylic anhydride[51-52]. An advantage of methacrylated HA based hydrogels is that it is possible to tune their properties by varying the concentration and the molecular weight of the functional monomer, the degree of substitution *etc.*[53]. In this regard, Tavsanli *et al.* developed silk/HA based hydrogels and investigated their mechanical properties[54]. The hydrogels were prepared by reacting methacrylated HA and silk fibroin in aqueous solution in the presence of N,N,N',N'-tetramethylethylenediamine, ammonium persulfate and N, N-dimetylacrylamide, which has the function of connecting methacrylated HA macromers *via* their vinyl groups. Interestingly, the resulting hydrogels showed biocompatibility, excellent mechanical properties and stability thanks to the presence of silk fibroin, since its β-sheet domains act as physical crosslinks.

2.1.7 Crosslinking by condensation reactions

Condensation reactions are often applied for hydrogels synthesis. Considering the chemical structure of HA, among the different condensation reactions, esterification results to be one of the most commonly employed for this purpose. In this regard, Larrañeta *et al.* recently developed an attractive eco-friendly strategy for the synthesis of HA-based hydrogels[55]. In particular, Gantrex S97 was used as crosslinking agent, and the hydrogels were prepared *via* esterification between the hydroxyl groups of HA and the carboxylic groups of Gantrex S97 (**Figure 4**); interestingly, the reaction was performed in solid phase inside a microwave and, thus, this process can be considered advantageous because it does not need organic solvents or toxic substances. Furthermore, the release profile and the antimicrobial properties were investigated. Notably, the resulting hydrogel showed a sustained release and excellent anti-infective properties resulting in a promising candidate for the design of drug delivery systems and wound dressings.

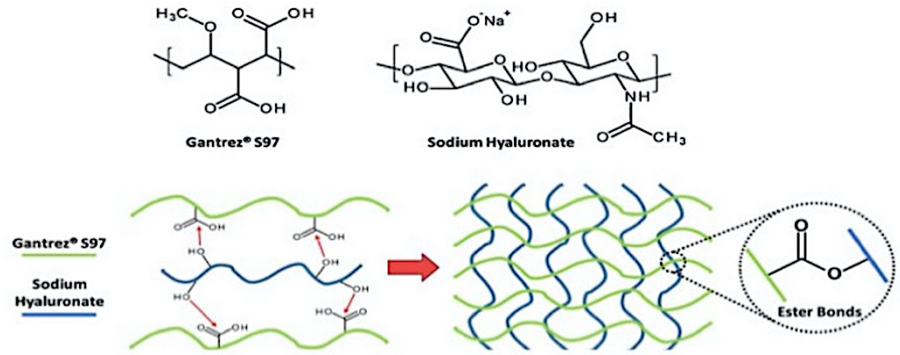

Figure 4. Schematic crosslinking mechanism between sodium hyaluronate and Gantrez®S97[55]. Reproduced with permission from Elsevier, 2018.

2.2 Physical hydrogels

In the last years, noncovalent bonds and supramolecular interactions have been widely exploited for hydrogels design thanks to their peculiar features. First of all, since these interactions are reversible, the non-covalent assembly allows to obtain hydrogels with tunable properties and responsivity to various cues like light, pH, temperature *etc.* [56-57]. In contrast to covalent crosslinking, physical crosslinking leads to the formation of less mechanically and chemically stable hydrogels. However, this aspect can be considered an advantageous feature since it can be exploited to achieve shear-thinning and self-healing properties[17].

In this context, inclusion complexation represents one of the most used strategies for the preparation of physical gels. It is based on the supramolecular interactions and the structural complementarity between two molecules called “host” and “guest”[58]. Cyclodextrins are one of the mostly employed hosts; structurally they are formed by hydrophobic cavities with a high affinity for hydrophobic guests. Several guest molecules employed in pair with cyclodextrins have been reported in literature, and among these the most representative is adamantane. In this regard, Rodell *et al.* designed a self-assembling HA hydrogel by using adamantane functionalized HA and β-cyclodextrin functionalized HA[59]. Hydrogel formation occurred rapidly by mixing the two compounds in aqueous solution. Its physical properties were investigated and were shown to be dependent on the crosslinking density and to be influenced by several factors including host and guest concentrations, molar ratio *etc.* The obtained hydrogel displayed shear-thinning properties resulting in a promising injectable system. Another investigated pair for inclusion complexation broadly reported in literature is represented by α or β-

cyclodextrin and azobenzene. In detail, trans-azobenzene has a high binding affinity for α or β-cyclodextrin, while cis-azobenzene has a low binding affinity for them. On this subject, Rosales *et al.* recently reported the preparation of a supramolecular HA hydrogel by using HA functionalized with β-cyclodextrin and azobenzene[60]. It was shown that it was possible to modulate the properties of the hydrogel with light; in fact, upon irradiation (λ=365 nm), isomerization of azobenzene occurs, changing the binding affinity between host/guest molecules and, consequently, the network connectivity and the elastic modulus. Furthermore, the release profiles were investigated, highlighting the possibility to tune drug release with light exposure. A similar approach was reported by Rowland *et al.* that adopted cucurbit[8]uril and cysteine-phenylalanine as host/guest pair[61].

Another interesting noncovalent approach is represented by the functionalization of HA with hydrophobic molecules in order to render it amphiphilic and consequently determine the macromers self-assembly in nanogels. In this regard, Montanari *et al.* prepared HA based hydrogels *via* the self-assembly of macromers in water after the functionalization of HA with cholesterol[62].

Moreover, the use of gelling agents in combination with HA can be considered a valid strategy for physical hydrogels design. For example, Jung *et al.* recently reported the preparation of a thermosensitive hydrogel based on HA and Pluronic F-127[63]. This latter is a tryblock copolymer able to form rapidly thermoresponsive hydrogels, which however are instable in physiological conditions due to their low mechanical strength. To overcome this problem, in this study, HA was mixed with Pluronic F-127 in water in order to obtain a hydrogel with improved structural integrity and stability ascribable to the hydrophobic interactions occurring between the acetyl groups of HA and the methyl groups of Pluronic. Interestingly, the resulting hydrogel not only showed an increased mechanical strength but also a sustained drug release, reducing the typical burst release observed in Pluronic F-127 based hydrogels.

3. HA based hydrogels for biomedical applications

Currently, HA based hydrogels are widely investigated for biomedical purposes like drug delivery, tissue engineering, regenerative medicine thanks to their biocompatibility, biodegradability, non–immunogenicity, responsivity to various cues and tunable properties[64-66]. This section reviews the main biomedical applications of HA based

hydrogels reported in literature in the last few years, focusing in particular on drug delivery for cancer therapy.

3.1 Drug delivery

HA based hydrogels are particularly interesting for drug delivery since, in addition to above cited features, allow to have a controlled and targeted drug release in response to different triggers, that turns out to be attractive when aiming for targeted therapy[68-69].

3.1.1 Stimuli-responsive hydrogels

Various smart hydrogels responsive to different environmental factors such as pH, temperature, light and biochemical molecules have been developed and investigated as drug delivery systems. With regard to stimuli-responsive platforms, physical crosslinking is preferred since supramolecular interactions are reversible and consequently results easier to tune their properties. In this context, Highley *et al.* recently proposed an interesting strategy for the design of a near infrared light (NIR)/temperature responsive system[69]; in detail, it was prepared in a microfluidic mixing device by combining gold nanorods with a HA supramolecular hydrogel previously obtained *via* the inclusion complexation of β-cyclodextrin and adamantane. The presence of nanorods caused heating in response to NIR irradiation, leading consequently to the breakage of the supramolecular interactions and of the networks. The release capability of the resulting platform in response to different NIR exposures was evaluated. Interestingly, it was observed that the drug release could be modulated by varying two parameters: irradiation time and light intensity; specifically, the quantity of the molecule released from the platform increased with increasing power and irradiation time.

Inclusion complexation employing azobenzene/cyclodextrin as host/guest pair has been broadly investigated for photoresponsive hydrogels design, since these specific supramolecular host/guest interactions can be disrupted upon trans-cis photoisomerization of azobenzene induced by ultraviolet (UV) light[70]. An interesting example of a photoresponsive drug delivery platform has been described by Rosales *et al.*[60]. Herein, HA was functionalized with azobenzene and β-cyclodextrin in order to obtain self-assembled hydrogels. These latter showed reversible changes in crosslink density, and consequently, in mesh size, upon UV exposures. These changes were

exploited to modulate the drug release and, therefore, *in vitro* release studies under UV irradiation were performed. In particular, a fluorescently labeled protein was loaded as model drug and it was noted that upon irradiation the hydrogel released a double amount of protein compared to the non-irradiated one.

Even if physical crosslinking is preferred for smart hydrogels preparation, also the chemical approach has been recently investigated. In this regard, Kwon *et al.* reported the preparation of pH-sensitive hydrogels based on hydroxyethyl cellulose and HA, and investigated their potential use as transdermal delivery systems for the treatment of skin lesions[71]. In this study, the hydrogels were synthesized *via* Michael addition between HA and hydroxyethyl cellulose by using divinyl sulfone as crosslinking agent, and their physicochemical properties were investigated. The obtained hydrogels were then loaded with isoliquiritigenin, which has antimicrobial activity, and its release efficiency was evaluated by *in vitro* measurements at different pH values. Experimental data showed that the quantity of released drug increased with increasing pH beyond 7, due to electrostatic repulsions occurring between the carboxylate groups of HA that consequently lead to an increase of mesh size.

3.1.2 HA based hydrogels for targeted cancer treatment

As already reported, HA regulates different cellular functions such as cell adhesion, differentiation, migration, proliferation *etc.*, due to its binding to specific membrane surface receptors such as CD44, LYVE-1 and RHAMM[72]. In particular, CD44 was found to be the main receptor involved in proliferation, differentiation, and migration pathways and, consequently, in tumor progression and metastasis; moreover, it is overexpressed in various types of tumors like melanoma, chondrosarcoma, breast, gastrointestinal, prostate, bladder, lung and pancreatic cancers, and different studies have reported a positive correlation between CD44 expression and poor prognosis[73]. For these reasons, HA has recently emerged as promising agent for the design of anticancer drug delivery systems for active targeting of malignant tumors[74]. Comprehensive reviews by Huang *et al.* and Choi *et al.* supply an interesting description of HA based drug delivery systems developed for targeted cancer treatment[75-76]. In the last years, several HA based hydrogels have been studied for the delivery of different antitumor drugs such as doxorubicin, paclitaxel, cisplatin, *etc.* in order to improve their efficacy and reduce their systemic side effects[77-78]; some of the most interesting and recent examples will now be presented.

Aiming at preparing a suitable drug delivery platform for the targeted release of doxorubicin, Yang *et al*. prepared various HA based nanogels *via* copolymerization of methacrylated HA with di(ethylene glycol) diacrylate[79]. Nanogels with a diameter of about 70 nm and a spherical shape were obtained and were loaded with doxorubicin by incubation method. *In vitro* studies showed a CD44-dependent cellular uptake, and, consequently, a greater internalization of these carriers in tumor cell lines that overexpress CD44 receptor (**Figure 8**).

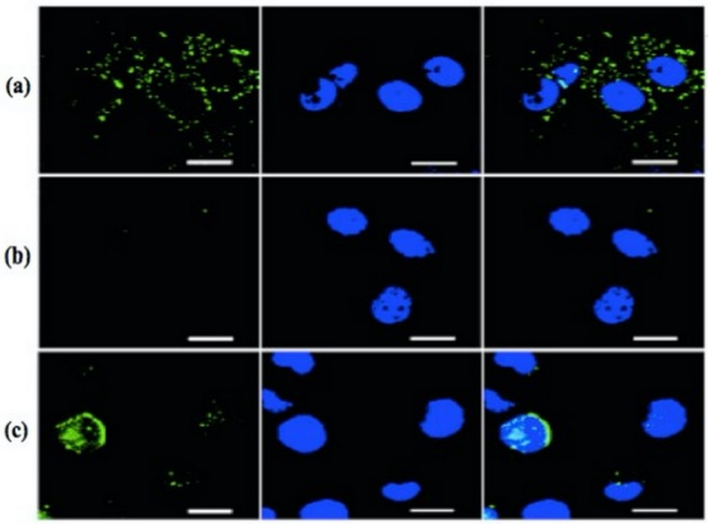

Figure 8. Confocal laser scanning microscopy of (a) A549, (b) NIHT3T and (c) H22 cells incubated with FITC-labeled HA nanogels[79]. Reproduced with permission from Elsevier, 2015.

Furthermore, the nanogels showed higher accumulation in the tumor site and a superior antineoplastic effect compared to the free doxorubicin, resulting in a promising drug delivery system for cancer therapy. A noteworthy further example of doxorubicin delivery system has been reported by Jhan *et al.*[80]. In this study, injectable thermosensitive hydrogels based on Pluronic F-127 and HA-doxorubicin nanocomplexes were prepared *via* physical mixing and their physiochemical properties were investigated. Doxorubicin release profile was studied *in vitro*, while nanogels antitumor activity both *in vivo* and *in vitro*. Experimental data showed a pH sensitive and sustained release of doxorubicin with a faster release rate at tumoral pH. Moreover, they exhibited excellent cytotoxic activity against tumor cell lines that overexpress CD44 receptor and high affinity to lymphonodes, resulting in promising injectable formulations for the treatment of local and metastatic tumors. Furthermore, in this context, an efficient approach for metastatic

breast cancer treatment has been recently described by Chen *et al*.[81]. In particular, the authors prepared epidermal growth factor receptor (EGFR) and CD44 dual targeted HA nanogels by combining inverse nanoprecipitation and tetrazole-alkene photocoupling. Nanogels with a diameter of about 160 nm and a spherical shape were obtained and evaluated for the treatment of metastatic breast cancer. *In vitro* studies showed an excellent internalization of nanogels in 4T1 breast cancer cell line that overexpresses both EGFR and CD44. Furthermore, *in vivo* studies in metastatic 4T1-luc breast tumor bearing mice displayed that the nanogels enhanced the therapeutic efficacy of saporin, showing an excellent inhibition of tumor growth and lung metastasis.

Currently, intraperitoneal (IP) chemotherapy is emerging as an efficient strategy for the treatment of solid tumors present in the peritoneal cavity[82]. However, to this end, an ideal delivery system should have the following requirements: biocompatibility, biodegradability, non-immunogenicity and controlled and sustained drug release profiles. Since HA hydrogels exhibit these features, currently, they are also studied for this purpose. In this regard, Cho *et al*. recently reported the design of *in situ* crosslinkable HA based gels and evaluated their potential use as IP carriers of platinum for the treatment of ovarian cancer[83]. Firstly, they prepared platinum loaded nanoparticles that were subsequently incorporated in HA based hydrogels obtained *via* aldehyde-hydrazide coupling. These platforms showed sustained platinum release, good anti-tumor activity and a long permanence in the peritoneal cavity resulting attractive for IP chemotherapy of ovarian cancer.

Unfortunately, one of the most frequent problem that can occur when hydrogels are used as drug delivery systems is the burst release[84]; with the attempt to overcome this limitation, Zhang *et al.* proposed an innovative strategy for HA based hydrogels design[85]. In this regard, they prepared multilayer hydrogel capsules based on chitosan, HA and doxorubicin *via* ionotropic crosslinking. Notably, the release studies showed a pH-sensitive, controlled release of doxorubicin with a significant reduction of the burst release due to their peculiar structure; in fact, the multilayer architecture reduced the drug concentration gradient between the capsules external layer and the surrounding environment, limiting the release of doxorubicin adsorbed on the surface.

References

1. Hoffman, A. S. (2012). Hydrogels for biomedical applications. *Advanced drug delivery reviews*, *64*, 18-23.
2. Seliktar, D. (2012). Designing cell-compatible hydrogels for biomedical applications. *Science*, *336*(6085), 1124-1128.
3. ConvaTec website. Available online: https://www.convatec.it/
4. Covidien website. Available online: https://www.medtronic.com/
5. Blanchard CR, Timmons SF, Smith RA. US Patent 6,379,690 B2; 2002.
6. Kumar A. US Patent 2013/0236971 A1; 2013
7. Ocular Therepeutix website. Available online: https://www.ocutx.com/products/dextenza/
8. Fraser, J. R. E., Laurent, T. C., & Laurent, U. B. G. (1997). Hyaluronan: its nature, distribution, functions and turnover. *Journal of internal medicine*, *242*(1), 27-33.
9. Prehm, P. (1984). Hyaluronate is synthesized at plasma membranes. *Biochemical Journal*, *220*(2), 597-600.
10. Fallacara, A., Baldini, E., Manfredini, S., & Vertuani, S. (2018). Hyaluronic acid in the third millennium. *Polymers*, *10*(7), 701.
11. Laurent, T. C., & Fraser, J. R. E. (1992). Hyaluronan 1. *The FASEB journal*, *6*(7), 2397-2404.
12. Dicker, K. T., Gurski, L. A., Pradhan-Bhatt, S., Witt, R. L., Farach-Carson, M. C., & Jia, X. (2014). Hyaluronan: a simple polysaccharide with diverse biological functions. *Acta biomaterialia*, *10*(4), 1558-1570.
13. Toole, B. P. (2004). Hyaluronan: from extracellular glue to pericellular cue. *Nature Reviews Cancer*, *4*(7), 528-539.
14. Ahmed, E. M. (2015). Hydrogel: Preparation, characterization, and applications: A review. *Journal of advanced research*, *6*(2), 105-121.
15. Caló, E., & Khutoryanskiy, V. V. (2015). Biomedical applications of hydrogels: A review of patents and commercial products. *European Polymer Journal*, *65*, 252-267.
16. Schanté, C. E., Zuber, G., Herlin, C., & Vandamme, T. F. (2011). Chemical modifications of hyaluronic acid for the synthesis of derivatives for a broad range of biomedical applications. *Carbohydrate polymers*, *85*(3), 469-489.
17. Appel, E. A., del Barrio, J., Loh, X. J., & Scherman, O. A. (2012). Supramolecular polymeric hydrogels. *Chemical Society Reviews*, *41*(18), 6195-6214.

18. Jiang, Y., Chen, J., Deng, C., Suuronen, E. J., & Zhong, Z. (2014). Click hydrogels, microgels and nanogels: Emerging platforms for drug delivery and tissue engineering. *Biomaterials*, *35*(18), 4969-4985
19. Ibrahim, S., Kang, Q. K., & Ramamurthi, A. (2010). The impact of hyaluronic acid oligomer content on physical, mechanical, and biologic properties of divinyl sulfone-crosslinked hyaluronic acid hydrogels. *Journal of Biomedical Materials Research Part A*, *94*(2), 355-370
20. Crescenzi, V., Francescangeli, A., & Taglienti, A. (2002). New gelatin-based hydrogels via enzymatic networking. *Biomacromolecules*, *3*(6), 1384-1391.
21. Kuo, J. W., Swann, D. A., & Prestwich, G. D. (1991). Chemical modification of hyaluronic acid by carbodiimides. *Bioconjugate chemistry*, *2*(4), 232-241.
22. Segura, T., Anderson, B. C., Chung, P. H., Webber, R. E., Shull, K. R., & Shea, L. D. (2005). Crosslinked hyaluronic acid hydrogels: a strategy to functionalize and pattern. *Biomaterials*, *26*(4), 359-371.
23. Gandini, A. (2013). The furan/maleimide Diels–Alder reaction: A versatile click–unclick tool in macromolecular synthesis. *Progress in Polymer Science*, *38*(1), 1-29.
24. Fisher, S. A., Anandakumaran, P. N., Owen, S. C., & Shoichet, M. S. (2015). Tuning the microenvironment: click-crosslinked hyaluronic acid-based hydrogels provide a platform for studying breast cancer cell invasion. *Advanced Functional Materials*, *25*(46), 7163-7172.
25. Yu, F., Cao, X., Li, Y., & Chen, X. (2015). Diels–Alder click-based hydrogels for direct spatiotemporal postpatterning via photoclick chemistry. *ACS Macro Letters*, *4*(3), 289-292.
26. Rostovtsev, V. V., Green, L. G., Fokin, V. V., & Sharpless, K. B. (2002). A stepwise huisgen cycloaddition process: copper (I)-catalyzed regioselective "ligation" of azides and terminal alkynes. *Angewandte Chemie*, *114*(14), 2708-2711.
27. Pahimanolis, N., Sorvari, A., Luong, N. D., & Seppälä, J. (2014). Thermoresponsive xylan hydrogels via copper-catalyzed azide-alkyne cycloaddition. *Carbohydrate polymers*, *102*, 637-644.
28. Gong, T., Adzima, B. J., Baker, N. H., & Bowman, C. N. (2013). Photopolymerization reactions using the photoinitiated copper (I)-catalyzed azide-alkyne cycloaddition (CuAAC) reaction. *Advanced Materials*, *25*(14), 2024-2028.
29. Manzi, G., Zoratto, N., Matano, S., Sabia, R., Villani, C., Coviello, T., ... & Di Meo, C. (2017). "Click" hyaluronan based nanohydrogels as multifunctionalizable carriers for hydrophobic drugs. *Carbohydrate polymers*, *174*, 706-715.

30. Laughlin, S. T., Baskin, J. M., Amacher, S. L., & Bertozzi, C. R. (2008). In vivo imaging of membrane-associated glycans in developing zebrafish. *Science*, *320*(5876), 664-667.
31. Fu, S., Dong, H., Deng, X., Zhuo, R., & Zhong, Z. (2017). Injectable hyaluronic acid/poly (ethylene glycol) hydrogels crosslinked via strain-promoted azide-alkyne cycloaddition click reaction. *Carbohydrate polymers*, *169*, 332-340.
32. Hoyle, C. E., Lee, T. Y., & Roper, T. (2004). Thiol–enes: Chemistry of the past with promise for the future. *Journal of Polymer Science Part A: Polymer Chemistry*, *42*(21), 5301-5338.
33. Sawicki, L. A., & Kloxin, A. M. (2014). Design of thiol–ene photoclick hydrogels using facile techniques for cell culture applications. *Biomaterials science*, *2*(11), 1612-1626.
34. Yang, C., Mariner, P. D., Nahreini, J. N., & Anseth, K. S. (2012). Cell-mediated delivery of glucocorticoids from thiol-ene hydrogels. *Journal of controlled release*, *162*(3), 612-618.
35. Fairbanks, B. D., Schwartz, M. P., Halevi, A. E., Nuttelman, C. R., Bowman, C. N., & Anseth, K. S. (2009). A versatile synthetic extracellular matrix mimic via thiol-norbornene photopolymerization. *Advanced materials*, *21*(48), 5005-5010.
36. Lutolf, M. P., & Hubbell, J. A. (2005). Synthetic biomaterials as instructive extracellular microenvironments for morphogenesis in tissue engineering. *Nature biotechnology*, *23*(1), 47-55.
37. Gramlich, W. M., Kim, I. L., & Burdick, J. A. (2013). Synthesis and orthogonal photopatterning of hyaluronic acid hydrogels with thiol-norbornene chemistry. *Biomaterials*, *34*(38), 9803-9811.
38. Khetan, S., Guvendiren, M., Legant, W. R., Cohen, D. M., Chen, C. S., & Burdick, J. A. (2013). Degradation-mediated cellular traction directs stem cell fate in covalently crosslinked three-dimensional hydrogels. *Nature materials*, *12*(5), 458-465.
39. Yan, S., Wang, T., Feng, L., Zhu, J., Zhang, K., Chen, X., ... & Yin, J. (2014). Injectable in situ self-cross-linking hydrogels based on poly (L-glutamic acid) and alginate for cartilage tissue engineering. *Biomacromolecules*, *15*(12), 4495-4508.
40. Tian, W. M., Zhang, C. L., Hou, S. P., Yu, X., Cui, F. Z., Xu, Q. Y., ... & Li, H. D. (2005). Hyaluronic acid hydrogel as Nogo-66 receptor antibody delivery system for the repairing of injured rat brain: in vitro. *Journal of Controlled Release*, *102*(1), 13-22.

41. Ito, T., Fraser, I. P., Yeo, Y., Highley, C. B., Bellas, E., & Kohane, D. S. (2007). Anti-inflammatory function of an in situ cross-linkable conjugate hydrogel of hyaluronic acid and dexamethasone. *Biomaterials*, *28*(10), 1778-1786.
42. Chen, F., Ni, Y., Liu, B., Zhou, T., Yu, C., Su, Y., ... & Zhou, Y. (2017). Self-crosslinking and injectable hyaluronic acid/RGD-functionalized pectin hydrogel for cartilage tissue engineering. *Carbohydrate polymers*, *166*, 31-44.
43. Wang, H., Zhu, D., Paul, A., Cai, L., Enejder, A., Yang, F., & Heilshorn, S. C. (2017). Covalently adaptable elastin-like protein–hyaluronic acid (ELP–HA) hybrid hydrogels with secondary thermoresponsive crosslinking for injectable stem cell delivery. *Advanced functional materials*, *27*(28), 1605609.
44. Kurisawa, M., Lee, F., Wang, L. S., & Chung, J. E. (2010). Injectable enzymatically crosslinked hydrogel system with independent tuning of mechanical strength and gelation rate for drug delivery and tissue engineering. *Journal of Materials Chemistry*, *20*(26), 5371-5375.
45. Tran, N. Q., Joung, Y. K., Lih, E., Park, K. M., & Park, K. D. (2010). Supramolecular hydrogels exhibiting fast in situ gel forming and adjustable degradation properties. *Biomacromolecules*, *11*(3), 617-625
46. Roberts, J.J.; Naudiyal, P.; Lim, K.S.; Poole-Warren, L.A.; Martens, P.J. A comparative study of enzyme initiators for crosslinking phenol-functionalized hydrogels for cell encapsulation. *Biomaterials research* **2016**
47. Rizzuto, F., & Spikes, J. D. (1977). The eosin-sensitized photooxidation of substituted phenylalanines and tyrosines. *Photochemistry and photobiology*, *25*(5), 465-476.
48. Xu, K., Narayanan, K., Lee, F., Bae, K. H., Gao, S., & Kurisawa, M. (2015). Enzyme-mediated hyaluronic acid–tyramine hydrogels for the propagation of human embryonic stem cells in 3D. *Acta biomaterialia*, *24*, 159-171.
49. Raia, N. R. , Partlow, B. P., McGill, M., Kimmerling, E. P., Ghezzi, C. E., & Kaplan, D. L. (2017). Enzymatically crosslinked silk-hyaluronic acid hydrogels. *Biomaterials*, *131*, 58-67.
50. Hennink, W. E., & van Nostrum, C. F. (2012). Novel crosslinking methods to design hydrogels. *Advanced drug delivery reviews*, *64*, 223-236.
51. Ibrahim, S., Kothapalli, C. R., Kang, Q. K., & Ramamurthi, A. (2011). Characterization of glycidyl methacrylate–Crosslinked hyaluronan hydrogel scaffolds incorporating elastogenic hyaluronan oligomers. *Acta biomaterialia*, *7*(2), 653-665.

52. Poldervaart, M. T., Goversen, B., De Ruijter, M., Abbadessa, A., Melchels, F. P., Öner, F. C., ... & Alblas, J. (2017). 3D bioprinting of methacrylated hyaluronic acid (MeHA) hydrogel with intrinsic osteogenicity. *PloS one*, *12*(6), e0177628.
53. Burdick, J. A., Chung, C., Jia, X., Randolph, M. A., & Langer, R. (2005). Controlled degradation and mechanical behavior of photopolymerized hyaluronic acid networks. *Biomacromolecules*, *6*(1), 386-391.
54. Tavsanli, B., & Okay, O. (2019). Mechanically robust and stretchable silk/hyaluronic acid hydrogels. *Carbohydrate polymers*, *208*, 413-420.
55. Larrañeta, E., Henry, M., Irwin, N. J., Trotter, J., Perminova, A. A., & Donnelly, R. F. (2018). Synthesis and characterization of hyaluronic acid hydrogels crosslinked using a solvent-free process for potential biomedical applications. *Carbohydrate polymers*, *181*, 1194-1205.
56. Zheng, Z., Hu, J., Wang, H., Huang, J., Yu, Y., Zhang, Q., & Cheng, Y. (2017). Dynamic softening or stiffening a supramolecular hydrogel by ultraviolet or near-infrared light. *ACS applied materials & interfaces*, *9*(29), 24511-24517.
57. Rombouts, W. H., De Kort, D. W., Pham, T. T., van Mierlo, C. P., Werten, M. W., de Wolf, F. A., & van der Gucht, J. (2015). Reversible temperature-switching of hydrogel stiffness of coassembled, silk-collagen-like hydrogels. *Biomacromolecules*, *16*(8), 2506-2513.
58. Chen, G., & Jiang, M. (2011). Cyclodextrin-based inclusion complexation bridging supramolecular chemistry and macromolecular self-assembly. *Chemical Society Reviews*, *40*(5), 2254-2266.
59. Rodell, C. B., Kaminski, A. L., & Burdick, J. A. (2013). Rational design of network properties in guest–host assembled and shear-thinning hyaluronic acid hydrogels. *Biomacromolecules*, *14*(11), 4125-4134.
60. Rosales, A. M., Rodell, C. B., Chen, M. H., Morrow, M. G., Anseth, K. S., & Burdick, J. A. (2018). Reversible control of network properties in azobenzene-containing hyaluronic acid-based hydrogels. *Bioconjugate chemistry*, *29*(4), 905-913.
61. Rowland, M. J., Atgie, M., Hoogland, D., & Scherman, O. A. (2015). Preparation and supramolecular recognition of multivalent peptide–polysaccharide conjugates by cucurbit [8] uril in hydrogel formation. *Biomacromolecules*, *16*(8), 2436-2443.
62. Montanari, E., D'arrigo, G., Di Meo, C., Virga, A., Coviello, T., Passariello, C., & Matricardi, P. (2014). Chasing bacteria within the cells using levofloxacin-loaded hyaluronic acid nanohydrogels. *European Journal of Pharmaceutics and Biopharmaceutics*, *87*(3), 518-523.

63. Jung, Y. S., Park, W., Park, H., Lee, D. K., & Na, K. (2017). Thermo-sensitive injectable hydrogel based on the physical mixing of hyaluronic acid and Pluronic F-127 for sustained NSAID delivery. *Carbohydrate polymers*, *156*, 403-408.
64. Huang, G., & Huang, H. (2018). Application of hyaluronic acid as carriers in drug delivery. *Drug delivery*, *25*(1), 766-772.
65. Hemshekhar, M., Thushara, R. M., Chandranayaka, S., Sherman, L. S., Kemparaju, K., & Girish, K. S. (2016). Emerging roles of hyaluronic acid bioscaffolds in tissue engineering and regenerative medicine. *International Journal of Biological Macromolecules*, *86*, 917-928
66. Liu, Z., Tang, M., Zhao, J., Chai, R., & Kang, J. (2018). Looking into the future: toward advanced 3D biomaterials for stem-Cell-based regenerative medicine. *Advanced Materials*, *30*(17), 1705388.
67. Dosio, F., Arpicco, S., Stella, B., & Fattal, E. (2016). Hyaluronic acid for anticancer drug and nucleic acid delivery. *Advanced drug delivery reviews*, *97*, 204-236.
68. Li, J., & Mooney, D. J. (2016). Designing hydrogels for controlled drug delivery. *Nature Reviews Materials*, *1*(12), 1-17.
69. Highley, C. B., Kim, M., Lee, D., & Burdick, J. A. (2016). Near-infrared light triggered release of molecules from supramolecular hydrogel-nanorod composites. *Nanomedicine*, *11*(12), 1579-1590.
70. Yamaguchi, H., Kobayashi, Y., Kobayashi, R., Takashima, Y., Hashidzume, A., & Harada, A. (2012). Photoswitchable gel assembly based on molecular recognition. *Nature communications*, *3*(1), 1-5.
71. Kwon, S. S., Kong, B. J., & Park, S. N. (2015). Physicochemical properties of pH-sensitive hydrogels based on hydroxyethyl cellulose–hyaluronic acid and for applications as transdermal delivery systems for skin lesions. *European journal of pharmaceutics and biopharmaceutics*, *92*, 146-154.
72. Mattheolabakis, G., Milane, L., Singh, A., & Amiji, M. M. (2015). Hyaluronic acid targeting of CD44 for cancer therapy: from receptor biology to nanomedicine. *Journal of drug targeting*, *23*(7-8), 605-618.
73. Chen, C., Zhao, S., Karnad, A., & Freeman, J. W. (2018). The biology and role of CD44 in cancer progression: therapeutic implications. *Journal of hematology & oncology*, *11*(1), 1-23.
74. Rao, N. V., Yoon, H. Y., Han, H. S., Ko, H., Son, S., Lee, M., ... & Park, J. H. (2016). Recent developments in hyaluronic acid-based nanomedicine for targeted cancer treatment. *Expert opinion on drug delivery*, *13*(2), 239-252.

75. Choi, K. Y., Han, H. S., Lee, E. S., Shin, J. M., Almquist, B. D., Lee, D. S., & Park, J. H. (2019). Hyaluronic acid–based activatable nanomaterials for stimuli-responsive imaging and therapeutics: beyond CD44-mediated drug delivery. *Advanced Materials*, *31*(34), 1803549.
76. Huang, G., & Huang, H. (2018). Hyaluronic acid-based biopharmaceutical delivery and tumor-targeted drug delivery system. *Journal of Controlled Release*, *278*, 122-126
77. Fu, C., Li, H., Li, N., Miao, X., Xie, M., Du, W., & Zhang, L. M. (2015). Conjugating an anticancer drug onto thiolated hyaluronic acid by acid liable hydrazone linkage for its gelation and dual stimuli-response release. *Carbohydrate polymers*, *128*, 163-170.
78. Bajaj, G., Kim, M. R., Mohammed, S. I., & Yeo, Y. (2012). Hyaluronic acid-based hydrogel for regional delivery of paclitaxel to intraperitoneal tumors. *Journal of Controlled Release*, *158*(3), 386-392.
79. Yang, C., Wang, X., Yao, X., Zhang, Y., Wu, W., & Jiang, X. (2015). Hyaluronic acid nanogels with enzyme-sensitive cross-linking group for drug delivery. *Journal of Controlled Release*, *205*, 206-217.
80. Jhan, H. J., Liu, J. J., Chen, Y. C., Liu, D. Z., Sheu, M. T., & Ho, H. O. (2015). Novel injectable thermosensitive hydrogels for delivering hyaluronic acid–doxorubicin nanocomplexes to locally treat tumors. *Nanomedicine*, *10*(8), 1263-1274.
81. Chen, J., He, H., Deng, C., Yin, L., & Zhong, Z. (2019). Saporin-loaded CD44 and EGFR dual-targeted nanogels for potent inhibition of metastatic breast cancer in vivo. *International journal of pharmaceutics*, *560*, 57-64.
82. Dakwar, G. R., Shariati, M., Willaert, W., Ceelen, W., De Smedt, S. C., & Remaut, K. (2017). Nanomedicine-based intraperitoneal therapy for the treatment of peritoneal carcinomatosis—Mission possible?. *Advanced drug delivery reviews*, *108*, 13-24.
83. Cho, E. J., Sun, B., Doh, K. O., Wilson, E. M., Torregrosa-Allen, S., Elzey, B. D., & Yeo, Y. (2015). Intraperitoneal delivery of platinum with in-situ crosslinkable hyaluronic acid gel for local therapy of ovarian cancer. *Biomaterials*, *37*, 312-319.
84. Qiu, Y., & Park, K. (2001). Environment-sensitive hydrogels for drug delivery. *Advanced drug delivery reviews*, *53*(3), 321-339.
85. Zhang, W., Jin, X., Li, H., Wei, C. X., & Wu, C. W. (2019). Onion-structure bionic hydrogel capsules based on chitosan for regulating doxorubicin release. *Carbohydrate polymers*, *209*, 152-

CHAPTER I. EXPERIMENTAL PART: "Characterization of a hyaluronic acid and folic acid based hydrogel for cisplatin delivery: antineoplastic effect in human ovarian cancer cells *in vitro*" *

Abstract

We successfully prepared and characterized a hyaluronic acid- and folic acid-based hydrogel for the delivery of cisplatin (GEL-CIS) with the aim to induce specific and efficient incorporation of CIS into ovarian cancer (OC) cells, improve its antineoplastic effect and avoid CIS-resistance. The slow and controlled release of the drug from the polymeric network and its swelling degree at physiologic pH suggested its suitability for CIS delivery in OC. We compared here the effects of pure CIS to that of GEL-CIS on human OC cell lines, either wild type or CIS-resistant, in basal conditions and in the presence of macrophage-derived conditioned medium, mimicking the action of tumor-associated macrophages *in vivo*. GEL-CIS inhibited OC cell growth and migration more efficiently than pure CIS and modulated the expression of proteins involved in the Epithelial Mesenchymal Transition, a process playing a key role in OC metastatic spread and resistance to CIS.

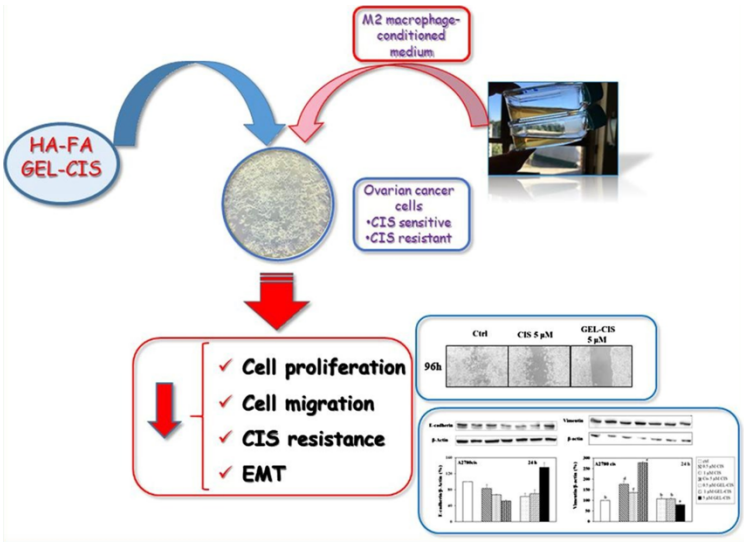

***Published on International Journal of Pharmaceutics, 2021 Sep 5; 606, 120899; doi: https://doi.org/10.1016/j.ijpharm.2021.120899**

1. Materials and methods

1.1 Chemicals

All solvents, analytical grade, were purchased from Carlo Erba Reagents (Milan, Italy): diethyl ether, acetone, methanol (MeOH), N,N-dimethylacetamide (DMAc), ethanol and hydrochloric acid (HCl) 0.1 N. Lithium chloride (LiCl), folic acid (FA), N,N′-Dicyclohexylcarbodiimide (DCC), 4-Dimethylaminopyridine (DMAP), sodium hydrogenphosphate, sodium dihydrogen phosphate, potassium dihydrogen phosphate, phenophtalein, sodium hydroxide (NaOH), methyl red and cisplatin were purchased from Sigma Aldrich (Milan, Italy). Hyaluronic acid (HA) MW 300 kDa and Poloxamer 407 were purchased from FarmaLabor.

1.2 Instruments

FT-IR spectra were measured by a Jasco 4200 IR spectrophotometer using KBr disks. The UV–vis spectra were carried out using a Jasco UV-530 spectrophotometer.

1.3 Esterification of HA with FA

The esterification was carried out according to Steglich reaction[1]. In a three necked flask equipped with a reflux condenser and dropping funnel, under stirring and maintained under N_2, 0.225 g of LiCl was dissolved in 20 ml of DMAc at 80 °C. After 30 min, the reaction mixture was cooled to 40 °C, and then HA (12 mM) was added. The system was further cooled to 25 °C and subsequently FA (37 mM), DCC (37 mM) and DMAP (0.4 mM) were added; the reaction mixture was kept under stirring for 72 h at 40 °C. The product was collected by precipitation in water and then washed with hot methanol to remove dicyclohexylurea, acetone, and, finally, diethyl ether. The resulting compound was dried under vacuum obtaining an orange solid (yield 90%). The compound was characterized by FT-IR.

1.4 Determination of the substitution degree

The substitution degree was calculated by volumetric analysis[2]. 25 mg of the sample was dissolved in an ethanolic sodium hydroxide solution and kept under stirring and reflux at

80 °C for 17 h. Then, a titration with 0.1 N HCl was performed by using phenolphtaleine and methyl red for the first and second equivalence point, respectively. The moles of HCl between the first and second equivalence points correspond to the moles of the free ester. The degree of substitution (DS) was calculated by using the following equation (1):

$$DS = \frac{MM\ HA\ unit}{(g\ sample - n\ free\ ester) - MM\ free\ ester - MM\ H2O}$$

where n free ester are the moles of the free HA-FA ester and are calculated as follows: V_2 eq- V_1 eq × [HCl]; MM HA unit is the molecular weight of the repetitive unit of HA; MM free ester is the molecular weight of the unit of the HA-FA ester; MM H_2O is the molecular weight of water.

1.5 Preparation of HA-FA based hydrogel

The HA-FA based hydrogel was prepared by dissolving 0.1 g of HA-FA ester in 5 ml of NaOH aqueous solution. Then, 3 g of Poloxamer 407 were added and physically mixed until obtaining a homogeneous gel.

1.6 Swelling studies

The affinity of hydrogels towards the aqueous environment was determined by studying their swelling degree (WR%). The sample (200 mg) was placed in glass filters (porosity G2/3), previously wetted, centrifuged (2000 rpm for 5 min) and then weighted. Subsequently, the filters were put in contact with solutions at different pH values: 1.2, 5.0, 6.2, 6.8 and 7.4 at 37 °C. At predetermined times (1 h, 3 h, 6 h, 9 h, 24 h) the excess of water was removed from the filters by percolation at atmospheric pressure. Subsequently, the filters were centrifuged (3500 rpm for 15 min) and then weighted. The weights recorded at the times indicated above were averaged and used to calculate the swelling degree by the following equation (2):

$$WR\% = \frac{(Ws - Wd)}{Wd} \cdot 100$$

where Ws and Wd are the weights of the swollen and dried sample, respectively.

1.7 Preparation of the GEL-CIS

CIS (10 mg) and HA-FA ester (100 mg) were dissolved in 5 ml of NaOH aqueous solution under stirring. Then, after complete dissolution, 3 g of Poloxamer 407 was added and physically mixed until obtaining a homogeneous gel.

1.8 *In vitro* release studies

The samples (100 mg) were placed in glass filters (porosity G2/3). Subsequently the filters were immersed in 6 ml of phosphate buffer at pH 7.4 and maintained at 37 °C in a horizontal shaking bath. The release medium of each sample was withdrawn at specific time points (1 h, 2 h, 4 h, 8 h, 24 h, 48 h, 72 h) and replaced with fresh one. The samples were analyzed through UV–Vis spectrophotometry, and drug release profiles were expressed as percentage of drug released with respect to the total loaded amount in function of time.

1.9 Cell lines and treatments

The human ovarian carcinoma (OC) cells A2780wt and A2780cis, sensitive and resistant to CIS, respectively, were kindly gifted by Dr. Anna Bagnato (IRCCS-Istituto Nazionale Tumori Regina Elena, Rome, Italy) and were maintained in RPMI 1640 culture medium containing glutamine (2 mM), penicillin (100 U/ml), streptomycin (100 µg/ml) and fetal bovine serum (10%) in humidified atmosphere at 37 °C and 5% CO2. Human THP-1 monocytic cell line was obtained by the American Type Culture Collection (ATCC, Manassas, VA, USA) and was maintained in RPMI 1640 culture medium containing glutamine (2 mM) and FBS (10%). All the cells were maintained in an exponential growth phase by seeding them at 3 × 105 cells/ml twice a week. THP-1 cells were induced to differentiate into M2 macrophages (similar to tumor associated macrophages, TAM) by exposing them to 320 nM phorbol-12-myristate acetate (PMA, Sigma-Aldrich, St. Louis, MO, USA) for 24 h, as previously indicated by Zeng *et al.*, [3]. The morphology of differentiated macrophages was observed and photographed by using an inverted microscope (Leica, Buccinasco, MI, Italia). For the experiments regarding the study of the effect of tumor microenvironment on the epithelial-mesenchymal transition (EMT) in the OC cells, the conditioned culture medium (CM) from the M2 differentiated macrophages was starved and maintained at −20 °C until its use.

1.10 Cell proliferation evaluation

For the evaluation of cell proliferation in the human OC cells treated with pure cisplatin (CIS) or with GEL-CIS, a commercial colorimetric kit was used (Cell proliferation Assay Kit, BioVision, Milpitas, CA, USA). This assay allows to reveal the incorporation of the pyrimidinic analog 5-bromo-deoxyuridine (BrdU) in the neosynthesized DNA of proliferating cells in place of thymidine. A2780wt and A2780cis cells were seeded at the concentration of 5×10^3 cells/well in a 96-well multi-well plate. After 24 h, cell culture medium was removed and replaced with fresh culture medium containing or not CIS or GEL-CIS at the concentrations of 1 and 5 μM. Pure CIS was solubilized in water containing 0.9% NaCl. Aliquots of 1 μL/mL and 5 μL/ml, taken from a 1 mM CIS stock solution, were added to the culture medium to obtain the final concentrations of 1 and 5 μM, respectively. CIS stock solution was prepared freshly for each experiment. Since in preliminary experiments we determined that CIS contained in the hydrogel was 0.132% (w/w), we dissolved 34.5 mg of GEL-CIS (corresponding to 0.455 mg of pure cisplatin) in 1 mL of culture medium, obtaining a 0.15 mM GEL-CIS stock solution. Aliquots of 6.7 μL/mL and 33.5 μL/mL taken from the stock solution were used to obtain the 1 and 5 μM final concentrations, respectively. In preliminary experiments, we exposed the cells to the empty HA-FA hydrogel (not containing CIS), in the same amounts used for the GEL-CIS to establish if the formulationl itself could affect the proliferation of OC cells. We found that the empty hydrogel did not induce significant effects on cell proliferation at the concentrations utilized (data not shown).

After 72 h incubation, BrdU solution was added in each well, and the plate was incubated at 37 °C for 4 h. Then the cell culture medium was removed and 100 μL of fixing/denaturing solution was added into each well. The plate was incubated for 30 min at room temperature and, after gently removing the fixing/denaturing solution, 100 μL of anti-BrdU antibody were added into each well. Cell culture plate was incubated for 1 h at room temperature with gentle shaking. The wells were then washed with 300 μL wash buffer and 100 μL of secondary anti-mouse HRP-linked antibody were added into the wells. After 1 h incubation, wells were washed again with 300 μL washing buffer and 100 μL of TMB solution (HRP substrate) were added into the wells. A blue color developed in the wells, proportional to the BrdU incorporation into the cells. A stop solution (2 N H2SO4, 100 μL) was then added into the wells, resulting in the development of a yellow color, and the absorbance was read with a spectrophometer set at 450 nm.

1.11 Wound healing assay *in vitro*

The migrating ability of the OC cells was analyzed by the Wound healing assay *in vitro*. To this aim disposable silicon inserts (Ibidi, Munchen, Germany) were used. The silicon inserts consist of two chambers separated by a silicon sept with a 500 μm thickness. The inserts were put into the wells of a 6-well multi-well plate and 70 μL of a cell suspension of A2780wt and A2780cis cells (at the concentration of 3×10^5 cells/mL) were seeded in each of the silicon insert chambers. Fresh culture medium (1.3 mL) was put in the well outside the silicon inserts. After 24 h, the silicon inserts were gently removed, and two monolayers of cells separated by a 500 μm free-from-cell space were obtained. Samples were photographed at the microscope (representing time 0), the cell culture medium was removed and replaced with fresh culture medium containing or not CIS and GEL-CIS at the concentrations of 1 and 5 μM. The ability of cells to migrate was evaluated at the indicated time points (24, 48, 72 and 96 h) by measuring the residual cell free area in the wells. We prolonged the observation until 96 h, since in preliminary experiments it was observed that only at this time point the wound area was almost completely filled by cells in the control conditions. Cell cultures were observed daily at the microscope and photographed. The saved images were then analyzed by a dedicated software (developed by Dr. Koumoutsakos, CSE Lab, at the ETH, Zurich, Switzerland).

1.12 Analysis of protein expression by Western blotting

A2780wt and A2780cis cells were seeded in a 100 mm Petri dish (3×10^5 cells/mL). After 24 h cell culture medium was removed and replaced by fresh culture medium containing or not CIS and GEL-CIS (1 and 5 μM). THP-1 cells (which usually grow in suspension) were seeded at the concentration of 2 × 105 cells/mL in 10 mL cell culture medium containing 320 nM PMA and, after 24 h, the CM was withdrawn and stored at −20 °C for the following treatment of A2780wt and A2780cis cells. THP-1 cells, which, following the PMA treatment, had adhered to the bottom of the culture flask and changed their morphology, were trypsinized and centrifuged at 1000 × g for 10 min to obtain the cell pellet. A2780wt and A780cis cells, treated with CIS and GEL-CIS for 24 h in basal conditions or in the presence of THP-1 CM, were trypsinized and centrifuged at 1200 rpm for 5 min to obtain the cell pellets.

Total cell lysates from THP-1, A2780wt and A2780cis cells were prepared according to Serini et al.,[4]. Briefly, the pellet obtained from 5 × 106 cells were resuspended in 100 μL

of cold lysis buffer containing 1 mM MgCl2, 350 mM NaCl, 20 mM HEPES, 0.5 mM EDTA, 0.1 mM EGTA, 1 mM Na4P2O4, 1 mM phenylmethylsulfonyl fluoride (PMSF), 1 mM aprotinin, 1.5 mM leupeptin, 20% glycerol, 1% NP-40. Samples were incubated on ice for 30 min and then centrifuged at 14000 rpm for 15 min to remove cell debris. Protein concentration in the samples was evaluated by the Biorad assay (Hercules, CA, USA).

Equal amounts of proteins for each sample (50 µg) were separated on a SDS-polyacrylamide gel and transferred on a nitrocellulose membrane. The membrane was then blocked in TBST containing 5% low fat dried milk for 1 h at room temperature and incubated at 4 °C overnight with primary antibodies against E-cadherin (clone 5F-133, Santa Cruz Biotechnology, Santa Cruz, CA, USA), vimentin (clone 5G3F10, sc-66002, Santa Cruz Biotechnology) (for A2780wt and A2780cis cells) and against CD206 (clone D-1, sc-376108, Santa Cruz Biotechnology) and CD11c (clone B-6, sc-46676, Santa Cruz Biotechnology) (for THP-1 cells). As a loading control, membranes were stripped and reincubated with antibodies against β-actin (clone AC40, sc-A-4700, Sigma-Aldrich, Milan, Italy) or against α-actinin (clone B-12, sc-166524, Santa Cruz Biotechnology). After incubation with secondary anti-mouse antibody, immunocomplexes were visualized by the Enhanced Chemiluminescence Detection system (ECL, GE Healthcare Life Sciences, Pittsburgh, PA, USA) and quantitated through densitometric analysis utilizing the UVITEC Alliance system (Cambridge, UK).

1.13 Statistical analysis

Data were analyzed by the one-way analysis of variance (ANOVA) followed by Tukey's test in Fig. 3, Fig. 5, Fig. 8, Fig. 9. Student t-test was used to evaluate the significance of data in Fig. 2 and Fig. 7. Both the tests were performed by the InStat GraphPad software (San Diego, CA, USA). P-Values ≤ 0.05 were considered statistically significant.

2. Results and discussion

2.1 Synthesis of GEL-CIS

Given their biofunctionality and biodegradability, FA and HA were chosen as starting materials to develop an effective drug delivery system for CIS targeted and sustained release [5-6]. HA is an endogenous non-sulfated glycosaminoglycan, and its receptor, the cluster of differentation-44 (CD44), is overexpressed in different malignant tumors such as gastrointestinal, pancreatic, breast, cervical and ovarian cancers[7]. To improve the selectivity of the drug delivery system, HA was conjugated with FA, a widely used ligand for this purpose, since one of its receptors, FR-α, was found to be overexpressed in different cancer cell lines, including OC[6]. With the aim to obtain a suitable functional compound, the hydroxyl groups of HA were functionalized with the carboxylic groups of FA *via* Steglich reaction by using DCC as crosslinking agent and DMAP as nucleophilic activator. Given the different hydrophilicity/hydrophobicity of the two starting materials, the reaction was performed in a binary mixture of LiCl/DMAc, in order to increase the solubilization of the reagents and, consequently, the reaction yield[8]. Furthermore, the polar aprotic nature of the solvent enhances the activity of the nucleophilic reagents.

The product formation was confirmed by FT-IR (**Figure 1**). In particular, the spectra of HA (**Figure 1a**), FA (**Figure 1b**) and that of the ester HA-FA (**Figure 1c**) were compared. The spectrum of the ester HA-FA shows a new band at 1731 cm^{-1}, corresponding to the stretching of the carbonyl group of the ester, and a sharper and broader peak at 3500 cm^{-1}, corresponding to the –OH groups of FA and HA, therefore confirming the successful derivatization.

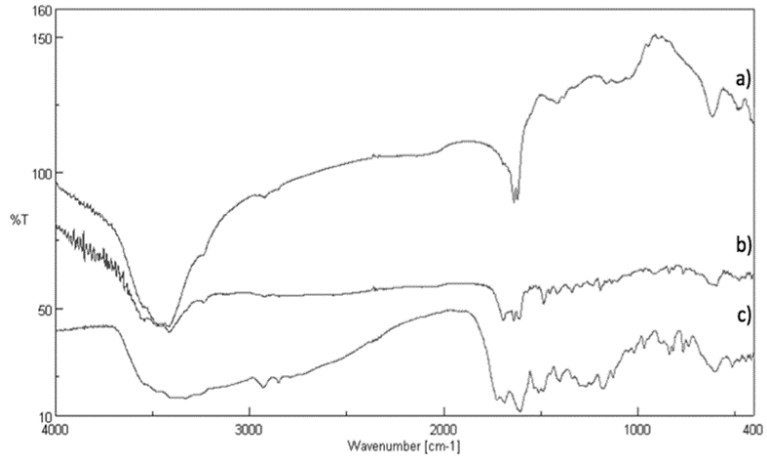

Figure 1. NMR spectra of HA(a), FA(b) and the ester HA-FA(c).

To quantify the functionalized groups of HA, a volumetric analysis was performed, and the degree of substitution was calculated. This latter indicates the average number of –OH groups functionalized *per* repetitive unit and, considering the chemical structure of HA, it should range from 0 to 4.0. The calculated substitution degree was found to be 2.3, which seems to be a satisfying result given the different chemical features of the two starting materials and the heterogeneous synthetic route adopted. On the basis of the reactivity and steric hindrance, it is possible to hypothesize that the derivatization mainly involved the –OH in position 6 and 2.

To develop a formulation for CIS sustained release, we prepared a physical thermosensitive hydrogel by using Poloxamer 407 as gelling agent[9]; in particular, it is a biocompatible non-ionic triblock copolymer showing a thermo-reversible sol-gel behavior that results a very advantageous feature for the development of self-healing and shear-thinning hydrogels as suitable systems for intraperitoneal chemotherapy[10-11]. This latter has recently emerged as promising approach for post-surgical treatment of solid tumors within the peritoneum including ovarian and gastric cancer. Moreover, advanced stage ovarian cancer is usually associated with peritoneal carcinomatosis. The major benefit of intraperitoneal chemotherapy is the possibility to achieve a direct release within the tumor tissue, maximizing the locoregional effect and reducing the systemic adsorption of the drug. However, the amphiphilic nature of Poloxamer 407 leads to the formation of hydrogels that undergo rapid degradation in the aqueous environment, determining fast release rates[12]. The use of HA in combination with Poloxamer 407 could enhance the stability and mechanical strength of the resulting hydrogel, due to the hydrophobic interactions occurring between HA and Poloxamer 407[13].

2.2 Chemical-physical characterization of GEL- CIS

In the present study, the hydrogel was prepared by physically mixing the HA-FA ester with Poloxamer 407 in aqueous solution. This approach shows several advantages such as fast gelation rate, cytocompatibility, high yield, and mild reaction conditions. Moreover, it allowed to obtain a 100% loading efficiency. To assess the stability of the hydrogel and its affinity towards the physiological environment, swelling studies were performed at different pH values (1.2, 5.0, 6.2, 6.8 and 7.4) mimicking gastric, intestinal, tumor and physiological conditions.

	α %				
pH	1h	2h	6h	9h	24h
1.2	1.4	1.4	1.4	1.4	1.4
5.0	40.7	55.8	85.5	95.0	101.6
6.2	1.4	36.6	71.9	108.5	108.5
6.8	2.7	33.7	65.9	75.8	75.8
7.4	0	17.8	31.3	31.3	37.3

Table 1. Swelling degree values (α %) in function of time. The swelling studies were carried out in duplicate, and the mean values are reported.

The obtained data (**Table 1**) show that, above strongly acidic pH (1.2) and below physiological pH (7.4), the swelling degree increased with increasing pH, reaching its maximum value at pH 6.2. This behavior may be ascribed to the electrostatic repulsions occurring between the ionized carboxylic groups of HA and FA, resulting in a less compact network. In fact, HA has a pKa ~ 3.0, while the following pKa values were reported for FA in physiological conditions: pKa_1 ~ 2.4, pKa_2 ~ 3.5 and pKa_3 ~ 5.0; this means that it results to be positively or negative charged at pH values below and above pKa_1, respectively[14-15]. In view of these observations, in acidic or slightly acidic environment, a significant and protracted erosion process is likely to occur, leading to a lower stability and complete dissolution of the delivery system within 24 h.

To assess the suitability of this delivery platform for CIS release, *in vitro* release studies were performed at different time intervals (1, 2, 4, 8, 24, 48, 72 h), at pH 7.4 and 37 °C, to mimic the physiological conditions. Drug release profile was determined by UV-Vis spectrometry and expressed as the percentage of the drug released with respect to the total loaded amount in function of time (**Figure 2**). In detail, the obtained data showed a slow and controlled release of the drug from the polymeric network. While no release was reported in the first hour, the burst release occurred in the second hour, with about 25% of drug released. A progressive reduction in the release rate was observed from the third hour onwards, with approximately 90% of the loaded drug released within 72 h. Therefore, we can consider this release profile very advantageous, as the initial burst release is useful for reaching the therapeutic window, whereas the slow and prolonged release observed in the following hours could allow to minimize the side effects of the drug ascribable to its high systemic concentration. Moreover, the almost complete release of the loaded drug within 72 h seems quite satisfactory. The absence of drug release in the first hour may be due to the lack of swelling of the system, resulting in the

entrapment of the drug in the polymeric network. Based on these findings, it is possible to hypothesize that the drug release is mainly driven by gel erosion rather than diffusion.

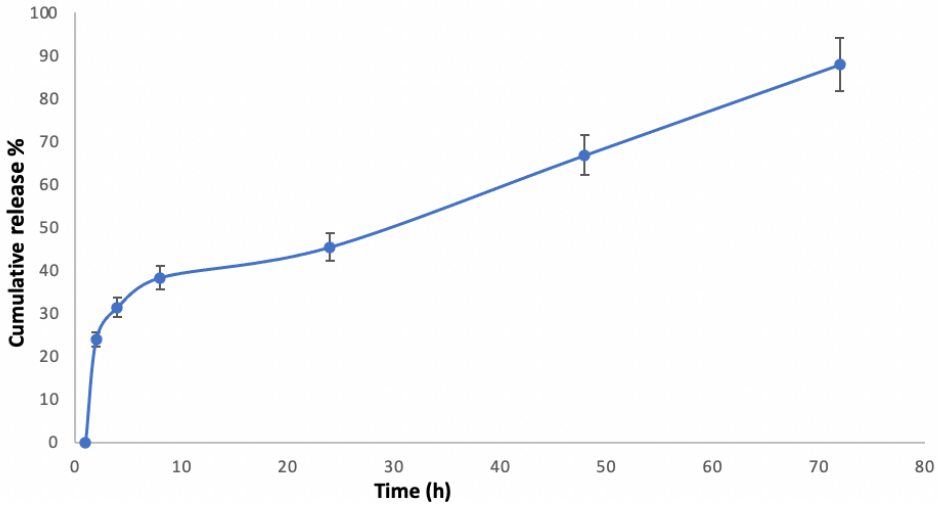

Figure 2. *In vitro* release profile of CIS at pH 7.4 and 37°C. Data are expressed as the mean of two independent experiments.

2.3 Effect of HA-FA based hydrogel containing CIS on OC cell proliferation

Having characterized the physical-chemical properties of GEL-CIS, we next investigated the effect of the hydrogel on the proliferation of the two human OC cell lines A2780wt and A2780cis, which are sensitive and resistant to CIS, respectively. **Figure 3** shows the effect on the proliferation of A2780wt and A2780cis cells following a 72 h treatment with 1 μM and 5 μM pure CIS, and with the same concentrations of CIS included in the GEL-CIS. The concentrations used were chosen since they are in the range of the concentrations administered in most of the *in vitro* studies, mirroring the actual drug level in the circulation of patients[16-17]. We evaluated cell proliferation at 72 h, since we had observed from the release measurements *in vitro* that the maximal release of CIS from GEL-CIS occurred at this time point.

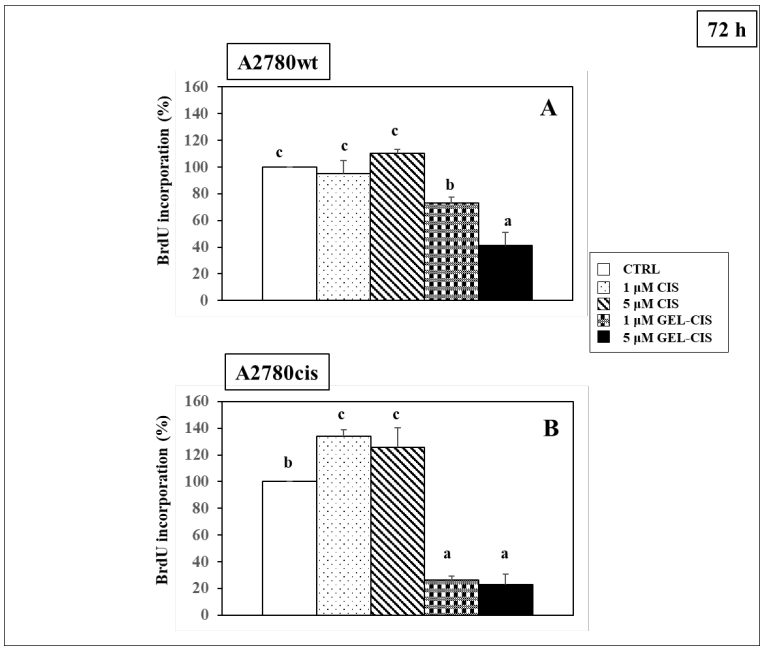

Figure 3. Effect of pure cisplatin (CIS) and of the HA-FA based hydrogel containing cisplatin (GEL-CIS) at the concentrations of 1 and 5 μM on the proliferation of A2780wt (A) and A2780cis (B) after 72 h treatment. Data are the means ± SD of three different experiments. Values with different letters (a, b, c) are significantly different ($p<0.05$, one-way ANOVA followed by Tukey's test).

We observed that 1 μM CIS did not significantly inhibit the proliferation of A2780wt cells (**Figure 3A**) after 72 h treatment, as compared to control, whereas at 5 μM it induced a small but not significant increase of cell proliferation (% increase vs control, 10%). On the other hand, when CIS was delivered as GEL-CIS, a dose-dependent inhibition of cell proliferation was observed (% inhibition vs control: 1 μM GEL-CIS, 26.7%; 5 μM GEL-CIS, 58.7%, $p<0.05$). Similarly to what observed in A2780wt cells with the highest CIS concentration (5 μM), in A2780cis cells CIS treatment increased cell proliferation as compared to control cells at both the concentrations used (33.8% and 29.5% increase vs control at 1 and 5 μM CIS, respectively). Interestingly, in A2780cis cells GEL-CIS was able to significantly reduce cell proliferation at both the concentrations used (1 μM GEL-CIS 73.6%; 5 μM GEL-CIS 77.0 %, $p<0.05$) (**Figure 3B**). The results obtained suggest that the presence of FA and HA in GEL-CIS may significantly improve the growth inhibitory efficiency of this antineoplastic agent.

In the attempt to demonstrate the possibility that a FA-based hydrogel could increase the anticancer effect of CIS in OC cells, Patra *et al.* previously developed gold decorated FA-based nanoparticles for the delivery of this drug[18]. However, they did not find any improvement in the growth inhibitory effect of CIS when they tested their CIS containing

FA-based hydrogel in the OC cell lines OV-167 and OVCAR-5, although they used concentrations of CIS (0-10 μM) comparable to those used in our experimental model. In any case, a beneficial effect was observed also in this case, since the authors found that CIS delivered through the formulation showed a lower toxicity towards normal cells (human umbilical vein endothelial cells, HUVEC and ovarian surface epithelial, OSE). On the other hand, and in agreement with our results, Li *et al.* used FA-based nanoparticles containing different chemotherapic drugs, i.e. Docetaxel and Gemcitabine (DTX/GEM), and observed that the drug growth inhibitory effects resulted amplified following their inclusion in the FA-based nanoparticles[19]. These authors demonstrated that the drugs delivered through the FA-based nanoparticles were able to induce a 3.6-fold higher tumor cell cytotoxicity than the drugs administered in their pure form. Similar results were also obtained by Mo *et al.* who synthesized FA-based nanoparticles containing carboplatin/paclitaxel and observed that the drugs delivered through the nanoparticles were significantly more efficacious in inhibiting the growth of the SKOV-3 human OC cells, either cultured *in vitro* or transplanted in nude mice, as compared to the combination of the pure drugs. In agreement to what suggested by us, these authors ascribed the higher efficacy of the hydrogel to the controlled release of the drugs occurring in conditions of physiologic pH (pH 7.4) [20].

We suggest that also HA may have contributed to the increased antineoplastic efficacy of CIS delivered by GEL-CIS, and that is in agreement with the results of plenty of works previously performed by using HA-based nanomaterials for the delivery of CIS and other chemotherapic drugs in different cancers, such as breast, stomach, lung and larynx cancer, and in melanoma[21-25]. However, very few studies have so far evaluated the efficacy of HA-based nanoformulations for CIS delivery in OC. For the formulation developed in the present study, we used HA with a molecular weight of 300 kDa. This is a crucial point, since it was recently observed that the effect elicited by HA on tumor growth is different depending on its molecular weight.

It was reported that low molecular weight HA (< 200 kDa) may induce pro-cancerogenic effects, whereas high molecular weight HA (> 200 kDa) has the capacity to control the normal tissue homeostasis and induce antitumor effects [26-27]. Correspondingly, *Cho et al.*, who used as OC animal model mice transplanted with the human OC cells SKOV-3 and injected them intraperitoneally with a CIS-containing hydrogel obtained by using 35 kDa HA, not only lacked to observe an improved anti-tumor efficacy of pure CIS but, after four weeks from the treatment, even registered a tumor mass increase[28]. The authors

hypothesized that, despite a sustained release of CIS from the nanoparticles, an efficacious endocytosis mediated by the CD44 receptor, and a good retention of the gel in the animal peritoneum, such a tumor inducing effect could be attributable to the HA-based material used for the drug delivery as well as to the growth promoting effect of HA degradation products formed lately *in vivo*[28]. Instead, the results recently obtained by Pang *et al.* are in agreement with our findings[29]. They used a different type of nanoparticles (a cross-linked hyaluronan-based hydrogel, CHAG), and demonstrated that the HA-based material administered into the pelvic cavity of nude mice was able to reduce the growth of human OC cells implanted in this cavity. Moreover, tumor cell growth inhibition was also accompanied by the inhibition of the activation of EGF signaling pathway and of metalloproteinase expression *in vitro*. Similar results were obtained earlier by the same group of authors also in gastric and hepatic cancer cells [30]. Moreover, in agreement with all these results and with our findings, Bae *et al.* found that an intraperitoneal treatment with a HA-based nanocomplex containing CIS in combination with epigallocatechin gallate, an antioxidant able to counteract the prooxidant activity of CIS, reduced the growth of OC cells transplanted intraperitoneally and decreased their intraperitoneal (i.p.) metastatic spread in a murine experimental model[31]. The therapeutic strategy of inoculating intraperitoneally HA-based hydrogels for the treatment of OC used by different authors appears to us very interesting, being HA an extremely suitable material for i.p. drug delivery due to its biocompatibility, fast rate of degradation and incorporation[28-29,31]. Furthermore, intraperitoneal chemotherapy itself represents a very promising therapeutic approach for OC following the first line surgical resection, since the most common route of OC spread is direct exfoliation of cells from the ovary into the peritoneal cavity[32]. Moreover, a drug administered intraperitoneally shows a longer half-life compared to drugs administered systemically and can reach higher concentrations in the target cancer cells [33-35]. Thus, improving the delivery and the effect of a first line chemotherapic agent such as CIS in OC may represent a winning strategy, since it is through this route that the drug may more easily target tumor cells [36-37].

2.4 Effect of GEL-CIS on OC cell invasive ability and EMT-related proteins

Since one of the reasons underlying the high mortality observed in OC patients is the high invasive ability and metastatic potential of these tumor cells, we also evaluated the effect of the HA-FA based hydrogel containing CIS on the migration of A2780wt and

A2780cis cells by using the Wound healing assay *in vitro* (**Figure 4**), which is a method widely used for studying *in vitro* the invasive and metastatic potential of cells *in vivo*.

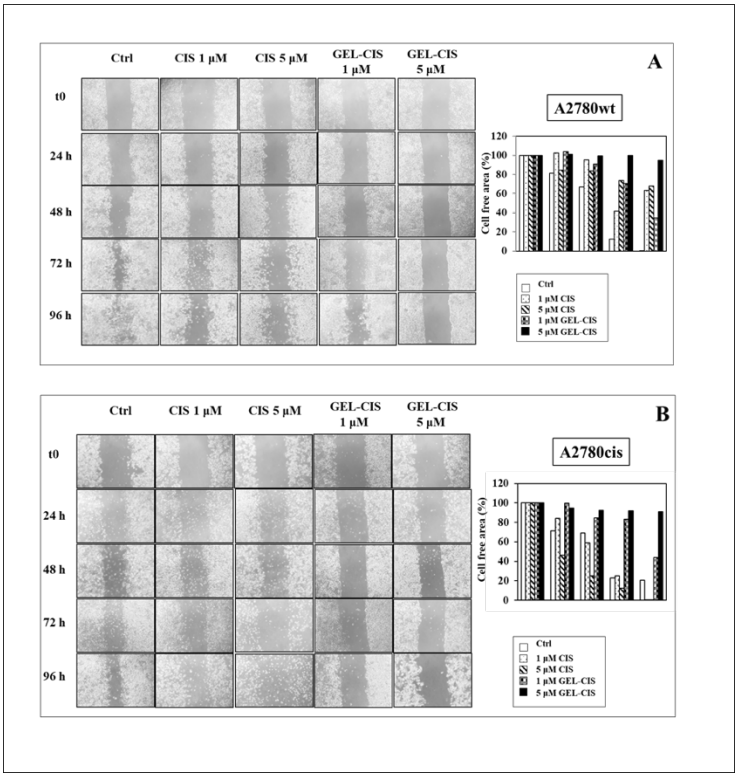

Figure 4. Effect of CIS (1 and 5 μM) and of GEL-CIS (1 and 5 μM) on the migration ability of A2780wt (A) and A2780cis (B) evaluated at the indicated time points (0-96 h) by Wound healing assay *in vitro* (for further details, see Materials and Methods section). In the Figure, representative images from two different experiments are shown. Data in the histograms represent the percent cell free area observed in the experiment shown in the Figure.

In the CIS-sensitive cells (A2780wt), we observed that pure CIS was able to inhibit cell migration at a similar extent of GEL-CIS at the same concentrations and until the 48 h of treatment, as evidenced by the larger cell free area in the CIS-treated wells as compared to control wells. At longer time-points (72-96 h), pure CIS progressively lost its inhibitory activity (5 μM CIS, about 73% and 67% of the initial cell free area at 72 h and 96 h, respectively). Instead, GEL-CIS always exhibited very high efficiency in inhibiting cancer cell migration, especially at the highest concentration (5 μM), that, after 72 h and 96 h of treatment, and therefore allowed the cell free area to still remain around 99% and 94% of the initial free area, respectively (**Figure 4A**). This suggests that the delivery of CIS

through the HA-FA based hydrogel allows a more controlled and prolonged effect of the drug.

Even more interesting results were obtained in the CIS resistant A2780cis cells, where pure CIS, already after 48 h of treatment and even at the higher concentration used (5 μM), showed a very low efficacy (about 25% of the initial cell free area). Then, after 96 h of treatment, it completely lost its ability to inhibit tumor cell migration confirming the CIS-resistant behavior of this cell line. On the contrary, GEL-CIS used at the same concentrations was able to maintain a marked inhibitory effect over the entire duration of the experiment (about 92% of the initial cell free area after 96 h of treatment) (**Figure 4B)**. This strongly suggests that the inclusion of CIS in GEL-CIS makes this drug able to overcome the resistance of these OC cells towards its therapeutic action.

On the basis of the above reported results, we hypothesized that the enhancement or even the induction of the inhibiting effect on migration elicited by CIS enclosed in GEL-CIS, as well as its ability to overcome CIS-resistance, could be related to its capacity to negatively influence the EMT process, which is involved in cancer cell invasion and metastasis, as well as in the development of CIS-resistance[38]. In fact, increasing evidence show that EMT plays a key role in the metastatic spread of OC cells, and several *in vitro* and *in vivo* studies have demonstrated that EMT is also involved in the mechanisms of OC cell drug resistance towards antineoplastic drugs, including CIS[39-42]. EMT is a process through which epithelial cells lose their apical-basal polarization and their intercellular adhesion molecules and transform themselves into spindle-shaped mesenchymal cells possessing an increased ability to invade healthy surrounding tissues and to spread metastases to distant organs and tissues[43-44]. Typically, during EMT, the expression of E-cadherin, a fundamental component of intercellular junctions, is reduced, while proteins such as vimentin, fibronectin, and neural-cadherin (N-cadherin) and different metalloproteinases result to be overexpressed [45]. Based on all these observations, we evaluated the effect of GEL-CIS on the expression of the two main proteins involved in EMT, E-cadherin and vimentin in our experimental cell model (**Figure 5**).

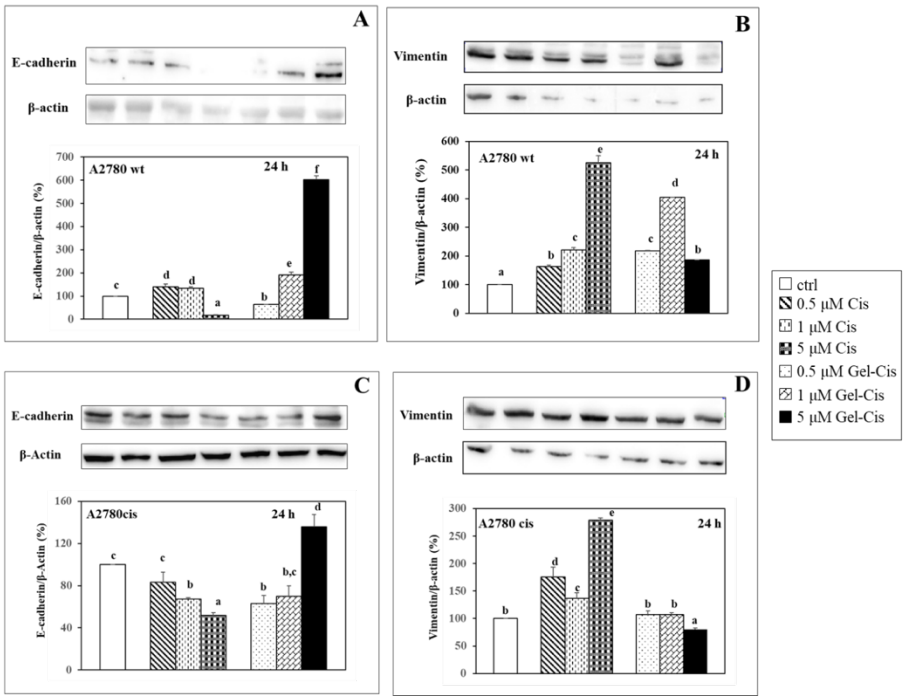

Figure 5. Effect of increasing concentrations of pure CIS and GEL-CIS (0.5-5 μM) on the expression of E-cadherin (A,C) and vimentin (B,D) in A2780wt (A,B) and A2780cis (C,D) treated for 24 h. In the Figure a representative Western Blotting experiment is shown for each protein. Data are the means ± SD of three different experiments. Values with different letters (a, b, c, d, e, f) are significantly different ($p<0.05$, one-way ANOVA followed by Tukey's test).

We preferred to evaluate the effect of the GEL-CIS on the expression of E-cadherin (a negative marker of EMT) and vimentin (a positive marker of EMT) at 24 h, when a large amount of CIS has already been released (**see Figure 2**). Moreover, it is possible that at this time-point, the molecular changes underlying the CIS-induced inhibition of invasion *in vitro*, starting at 24 h (**see Figure 4**), could have already taken place. We observed that, in A2780wt cells, pure CIS at the highest concentration used (5 μM), markedly and significantly reduced the expression of this protein (83.7% reduction vs control conditions, $p<0.05$), thus demonstrating its ability to induce EMT at this high concentration. Instead, at the lower concentrations (0.5 and 1 μM), it even induced a slight increase in E-cadherin expression. On the contrary, we observed a marked and significant increase of E-cadherin expression when CIS was given included in GEL-CIS, both at 1 and 5 μM (% increase vs control: GEL-CIS 1 μM, 90.2%, GEL-CIS 5 μM, 501.9%, $p<0.05$) (**Figure 5A),** suggesting that the inclusion of CIS in the hydrogel made it unable to induce EMT, particularly at the highest concentration. This observation is very interesting, since it was especially at 5 μM that we observed the greatest differences

between the effects of pure CIS and GEL-CIS on cell migration *in vitro* in A2780wt cells (**Figure 4**). In the same cells, we observed a significant increase of vimentin expression following the treatment with CIS at all the concentrations used (% increase vs control: 63.1%, 120.3 and 425.5%, at the concentrations 0.5, 1 and 5 μM, respectively, $p<0.05$) (**Figure 5B**). This effect further confirmed the EMT-inducing capacity of pure CIS, being vimentin a positive marker of EMT. In this case, the inclusion of CIS in the hydrogel was not able to contrast the inducing effect of CIS on vimentin expression. However, when used at the highest concentration (5 μM), its inducing effects on vimentin expression was much lower than that observed with pure CIS at the same concentration (86 % and 425 % increase vs control with 5 μM GEL-CIS and 5 μM pure CIS, respectively) (**Figure 5B**). This could be related to slow release of CIS from the hydrogel.

In A2780cis cells, CIS induces a reduction of E-cadherin expression at any concentration used (% inhibition vs control: 16.8, 23.8 and 49.4% at 0.5, 1 and 5 μM, respectively, $p<0.05$), whereas GEL-CIS was able to markedly and significantly increase E-cadherin expression only at 5 μM (35.9% increase vs control conditions, $p<0.05$) (**Figure 5C**). This finding shows that also in A2780cis it was necessary to reach this concentration for CIS and GEL-CIS to induce critically different effects. Confirming this point, we observed that the treatment of A2780cis with 5 μM GEL-CIS was able to significantly reduce the expression of vimentin (20% inhibition vs control, $p<0.05$), whereas its lower concentrations (0.5 and 1 μM) left it unaltered as compared to the control. Such effect was in stark contrast to what observed by treating the cells with pure CIS, which was found to induce a significant increase of vimentin expression at any concentration used (% increase vs control: 76, 36.9 e 178.5% at the concentrations 0.5, 1 e 5 μM, respectively, $p<0.05$) (**Figure 5D**).

Overall, these results are of interest since demonstrate that the GEL-CIS was able to significantly contrast the effects of pure CIS on the proteins involved in EMT. This is particularly interesting also in view of the findings of several *in vitro* and *in vivo* studies demonstrating that EMT is also involved in the mechanisms of drug resistance of OC cells towards antineoplastic drugs, including CIS [40-42]. Our results also confirm the recent findings by Aghamiri *et al.* who synthesized HA-based nanoparticles for the delivery of TWIST siRNA[46]. TWIST is a protein involved in EMT regulation, in tumor neoangiogenesis and in the drug resistance development [47]. These authors transplanted OC cancer cells in mice and treated them both intravenously and intraperitoneally with a combination of the TWIST siRNA containing nanoparticles and pure CIS and observed

that the combined treatment increased the antitumor efficacy of CIS and modulated the expression of several proteins involved in EMT[46].

2.5 Effect of GEL-CIS on the proliferation of OC cells in the presence of M2 macrophage CM

Even though plenty of experimental studies have demonstrated the central role played by the genetic alterations in the development and progression of OC, an increasing number of studies have recently evidenced the crucial influence exerted also by the microenvironment in the progression of this kind of tumor[48]. Among immune cells infiltrating OC tissues, tumor associated macrophages (TAM) are those present in the highest amount [49]. Plenty of evidence suggest that TAM may play different roles depending on their polarization towards a M1 phenotype reacting to the developing tumor, or a M2 phenotype which promotes tumor growth and progression. Several cytokines (i.e., IL-4, IL-10 and IL-13) and hypoxia may drive M2 polarization. In turn, M2 macrophages secrete several factors (i.e., Arginase 1, IL-10, TGF-β, VEGF, MMP9 and PGE2) able to subvert anti-tumor adaptive immunity and promote tumor development progression[50-51].

OC cells produce a variety of cytokines attracting mononuclear blood cells, which then differentiate into macrophages inside tumor tissue. Moreover, OC cells secrete high amounts of colony stimulating factor (CSF)-1, which, in turn, induces the macrophage polarization towards the M2 phenotype[52]. Previous studies demonstrated that the higher the number of M2 macrophages, the worst is the prognosis in patients with advanced OC [53]. Zhang *et al.* by performing an immunohistochemical analysis of M1 and M2 macrophages in OC tissue samples, observed that patients with higher M1/M2 ratios showed better prognosis, suggesting that TAM play an extremely important role in OC progression[54]. In addition, Zeng *et al.* demonstrated that TAM were also involved in the EMT process in OV90 and OVCA429 OC cells when co-cultured with M2 macrophages or when exposed to M2-conditioned medium[55]. In this study, the expression of E-cadherin was significantly reduced, while that of N-cadherin and vimentin was significantly increased in both the OC cell lines in the presence of M2-differentiated macrophages, suggesting that the macrophages present in the tumor microenvironment may induce EMT, thus contributing to tumor metastatic spread.

In view of such observation, in the present study we aimed to evaluate if the GEL-CIS could also be able to modulate the TAM effect on the proliferation of OC cells, as well as on the expression of the proteins involved in EMT. To obtain macrophages with M2 phenotype, similar to TAM, the human monocytic THP-1 cells were differentiated by treating them with PMA, as described in the Materials and Methods section. The differentiation of THP-1 cells into macrophages was demonstrated by both the morphological analysis of the cells (**Figure 6**) and the expression of biomarkers typical of M1 (CD11c) and M2 (CD206) macrophages (**Figure 7**).

The treatment of THP-1 cells with PMA induced changes in both growth and morphology of the cells, which normally grow in suspension like circulating monocytes, and are round-shaped. Instead, after 24 h exposure to PMA, they became completely adherent to the bottom of the culture flask (**Figure 6A**), similarly to tissue macrophages that adhere to the surrounding environment and acquired a spindle shape (**Figure 6B**).

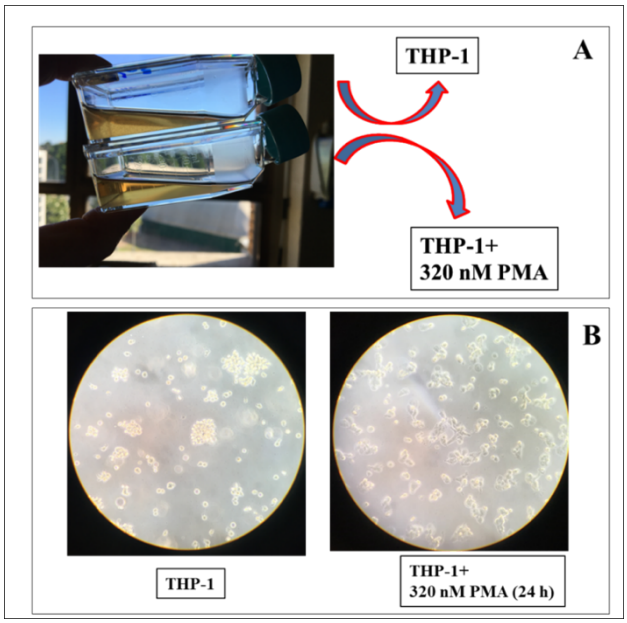

Figure 6. Morphological analysis of THP-1 monocytes in the absence and in the presence of a 24 h treatment with 320 nM PMA (A) macroscopic appearance of THP-1 in suspension before PMA treatment and completely adherent to the flask bottom following PMA treatment. (B) Microscopic appearance of THP-1 cells before and after PMA treatment.

In addition, PMA treatment was able to induce a significant increase in the expression of both the macrophage biomarkers (CD11c and CD206) (**Figure 7$_1$**), with a particularly evident effect on the expression of CD206, typical surface marker of M2 macrophages,

thus demonstrating that most of the obtained macrophages could be effectively considered M2 macrophages that represent the macrophage phenotype usually associated with the most aggressive OCs.

Next, we evaluated if the M2 macrophage conditioned medium could influence the effect of CIS on A2780wt cell proliferation finding that it was not inhibited by pure CIS (% inhibition vs control: 12.6 and 4.3% with 1 and 5 μM CIS, respectively) (**Figure 7**$_2$). This was in agreement with what observed by us in basal conditions (**Figure 3**, absence of CM).

1) **2)**

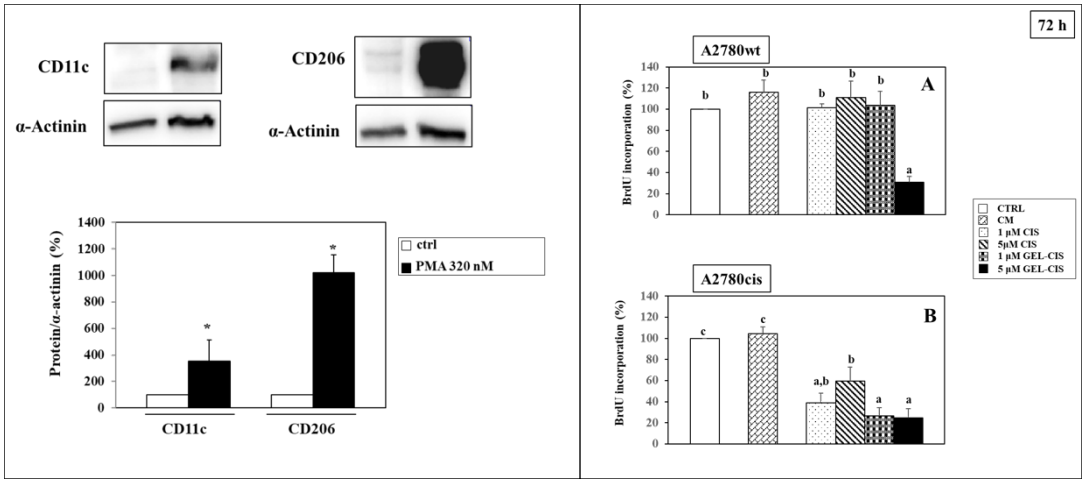

Figure 7. Expression of macrophage biomarkers CD11c and CD206 in THP-1 cells before and after 24 h treatment with 320 nM PMA. In the Figure a representative Western Blot experiment is shown. Values in the histograms are the mean ± SD of two different experiments. Values with asterisk are significantly different from the respective control $p<0.05$, Student t-test) **(1)**; Effect of 72 h treatment with pure cisplatin (CIS) and cisplatin delivered through the HA-FA-based hydrogel (GEL-CIS) on the proliferation of A2780 wt (A) and A2780 cis (B**)** cells. Cells were exposed to macrophage conditioned medium for all the duration of the experiment. The percentage of BrdU incorporation was calculated with respect to untreated control cells. Data are the means ± SD of three different experiments. Values with different letters (a, b, c) are significantly different ($p<0.05$, one-way ANOVA followed by Tukey's test) (**2**).

Instead, we observed that GEL-CIS was able to induce a substantial inhibition of A2780wt cell proliferation at the highest concentration used (5 μM: % inhibition vs control: 73.4%, $p<0.05$), even though this activity was not yet evident at 1 μM. This finding confirmed the higher efficacy of GEL-CIS as compared to pure CIS in inhibiting the growth of A2780wt cells, also in the presence of macrophage CM, a condition better

reflecting the *in vivo* tumor surrounding conditions (**Figure 7$_2$A**). Moreover, in the presence of CM, both 1 μM and 5 μM CIS exerted a marked antiproliferative effect on A2780cis cells (62.6% and 43.1% inhibition of proliferation vs control), whereas we observed that in basal conditions (absence of CM) CIS exerted even an inducing effect on proliferation (**see Figure 3B**). Interestingly, also in the presence of CM, GEL-CIS at both the concentrations tested was still able to markedly and significantly reduce the proliferation of A2780cis cells (1 and 5 μM: % inhibition vs control, 74.6 and 76.5%, $p<0.05$, respectively) (**Figure 7$_2$B**) at levels comparable to those observed in basal conditions (**see Figure 3**).

2.6 Effect of GEL-CIS on the EMT in OC cells in the presence of M2 macrophage CM

We next investigated (**Figure 8**) the effect of GEL-CIS on the expression of the proteins E-cadherin and vimentin (markers negatively and positively associated to EMT, respectively) in A2780wt and A2780cis cells following the treatment with macrophage CM, which mimics the action of TAM *in vivo*. In fact, it was reported that TAM may promote the invasive and metastatic process of OC cells through a multiplicity of mechanisms, including the induction of the EMT in cancer cells[3].

We observed (**Figure 8A**) that in A2780wt cells, the presence of macrophage CM was able to significantly reduce E-cadherin expression with respect to control conditions (21.4% inhibition in the presence of macrophage CM, $p<0.05$). This confirms the EMT inducing effect of the macrophage CM. When we combined the addition of macrophage CM to pure CIS, a further reduction of E-cadherin expression (57.6% inhibition vs control cells, $p<0.05$) was observed, confirming that the resistance to CIS induced by the drug itself may be also related to its EMT-inducing effect. However, when CIS was administered loaded in the hydrogel, the EMT-promoting activity of CIS resulted attenuated. Again, this favorable effect of GEL-CIS was observed at the maximal concentration used (5 μM). However, it is possible that prolonging the time of observation beyond the 24 h, thus allowing the complete release of the drug from the polymeric network, this effect could be observed also at lower concentrations of the enclosed drug.

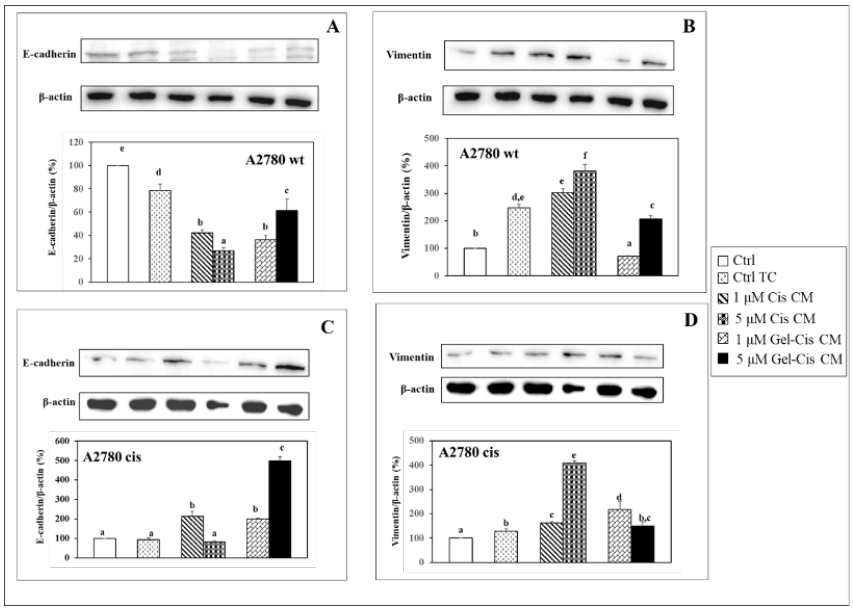

Figure 8. Effect of 24 h treatment with pure CIS and of GEL-CIS (1 and 5 μM) on the expression of E-cadherin (A,C) and vimentin (B,D) in A2780wt (A,B) and A2780cis (C,D) cells exposed to macrophage CM. In the Figure, a representative Western Blotting experiment is shown for each protein. Data are the means ± SD of three different experiments. Values with different letters (a, b, c, d, e) are significantly different, $p<0.05$, one-way ANOVA followed by Tukey's test).

On the contrary, vimentin expression (**Figure 8B**) resulted markedly increased in the presence of macrophage CM (147.1% increase vs control, $p<0.05$) and the treatment with pure CIS induced an even more evident increase in the expression of this protein (202.6 and 282.2% increase vs control, at 1 and 5 μM CIS, respectively, $p<0.05$). In this case, the incorporation of CIS in the hydrogel significantly reduced vimentin expression, as compared to pure CIS at both the concentrations used (GEL-CIS 1 μM: 29.6% reduction vs control, $p<0.05$; GEL CIS 5 μM: 45.8 % decrease vs pure CIS at the same concentration) (**Figure 8B**).

Overall, these data confirm the hypothesis that pure CIS may induce drug resistance development in OC cells through EMT induction, but also demonstrate that the GEL-CIS formulation is able to revert such tendency in A2780wt cells. In the A2780cis cells, already resistant to the drug, the exposure to macrophage CM is not able to further reduce E-cadherin expression, probably since these cells already show very low levels of this protein. We observed, however, that pure CIS at the lowest concentration tested (1 μM) was able to even increase E-cadherin levels (113% increase vs control, $p<0.05$),

whereas 5 μM CIS reverted E-cadherin levels to those observed in control conditions. This suggests that, to elicit its EMT-promoting activity, high concentrations of pure CIS are needed in the CIS-resistant cells. However, also in these cells, the incorporation of CIS in the hydrogel made it able to substantially and significantly increase E-cadherin expression at each concentration used, and in a dose-dependent manner (% increase vs control: 99.4 and 399% with 1 and 5 μM GEL-CIS, respectively, $p<0.05$) (**Figure 8C**).

In A2780cis cells, the presence of macrophage CM leads to a modest, but still significant increase of vimentin expression (28.6% increase vs control, $p<0.05$) and the concomitant presence of pure CIS was able to further increase the expression of this protein (62.8 e 307.5% increase vs control with 1 e 5 μM, respectively, $p<0.05$). CIS administered as GEL-CIS reduced the ability of pure CIS to increase the expression of vimentin, positive marker of EMT, when used at the highest concentration (5 μM GEL-CIS: 63.1% decrease vs pure CIS at the same concentration, $p<0.05$) (**Figure 8D**).

Overall, the data obtained support the hypothesis that CIS delivered through the hydrogel could significantly limit EMT and, possibly, also the development of CIS resistance in OC cells. At the best of our knowledge, this is the first study demonstrating that a HA-FA-based hydrogel containing CIS is able to modulate EMT induced by M2 macrophages in OC cells. Our finding is also supported by recent observations by Ding *et al*.,[55]. These authors, based on the evidence that iron plays a key role in the acquisition of the metastatic potential in tumor cells, and that metastatic cells are less sensitive to the anti-neoplastic effects of CIS, synthesized nanoparticles for the delivery of the iron chelator Dp44mT, and performed a combined treatment with CIS in mice bearing human breast cancer cells. They demonstrated that the nanoparticles were able to reduce the growth of breast cancer cells in mice, as well as to reduce metastasis development through an inhibition of the expression of MMP-2, VEGFα and vimentin[55].

3. Conclusions

In the present study, a hydrogel based on HA and FA loading cisplatin (GEL-CIS), was synthesized and characterized. We found that the swelling degree of GEL-CIS as well as its *in vitro* drug release rendered it suitable for the delivery of CIS to cancer cells in physiological pH conditions. The results demonstrate that GEL-CIS was able to inhibit the proliferation of the two human OC cell lines A2780wt and A2780cis (sensitive and resistant to CIS, respectively) more efficiently than pure CIS. Moreover, our data show

that GEL-CIS was able to inhibit the migration of both the OC cells almost completely in our experimental conditions. Worth noticing, the HA-FA based hydrogel was able to modulate the expression of two of the most important proteins involved in EMT, a process playing a key role not only in the metastatic potential of tumor cells, but also in the drug resistance to CIS.

Interestingly, GEL-CIS modulated the proliferation and the expression of EMT-related proteins also when OC cells were exposed to M2 macrophage CM. Such macrophages were recently recognized as essential for the production of factors influencing not only tumor cell growth, but also tumor cell invasive potential and EMT.

The results obtained here appear very promising for improving the CIS chemotherapic treatment of OC. However, further work using *in vivo* animal models of OC is needed to definitely establish the potential that the HA-FA based hydrogel containing CIS may have in improving the outcome of intraperitoneal CIS-chemotherapy of OC. It would be also necessary to define the hydrogel capacity to increase the *in vivo* the efficacy of CIS, and to reduce its systemic toxicity.

References

1. Neises, B., & Steglich, W. (1978). Simple method for the esterification of carboxylic acids. *Angewandte Chemie International Edition in English*, *17*(7), 522-524
2. Trombino, S., Cassano, R., Bloise, E., Muzzalupo, R., Leta, S., Puoci, F., & Picci, N. (2008). Design and synthesis of cellulose derivatives with antioxidant activity. *Macromolecular bioscience*, *8*(1), 86-95.
3. Zeng, X. Y., Xie, H., Yuan, J., Jiang, X. Y., Yong, J. H., Zeng, D., ... & Xiao, S. S. (2019). M2-like tumor-associated macrophages-secreted EGF promotes epithelial ovarian cancer metastasis via activating EGFR-ERK signaling and suppressing lncRNA LIMT expression. *Cancer biology & therapy*, *20*(7), 956-966.
4. Serini, S., Fasano, E., Piccioni, E., Monego, G., Cittadini, A. R., Celleno, L., ... & Calviello, G. (2012). DHA induces apoptosis and differentiation in human melanoma cells in vitro: involvement of HuR-mediated COX-2 mRNA stabilization and β-catenin nuclear translocation. *Carcinogenesis*, *33*(1), 164-173.
5. Dosio, F., Arpicco, S., Stella, B., & Fattal, E. (2016). Hyaluronic acid for anticancer drug and nucleic acid delivery. *Advanced drug delivery reviews*, *97*, 204-236
6. Zwicke, G. L., Ali Mansoori, G., & Jeffery, C. J. (2012). Utilizing the folate receptor for active targeting of cancer nanotherapeutics. *Nano reviews*, *3*(1), 18496.
7. Mattheolabakis, G., Milane, L., Singh, A., & Amiji, M. M. (2015). Hyaluronic acid targeting of CD44 for cancer therapy: from receptor biology to nanomedicine. *Journal of drug targeting*, *23*(7-8), 605-618.
8. Tosh, B., Saikia, C. N., & Dass, N. N. (2000). Homogeneous esterification of cellulose in the lithium chloride–N, N-dimethylacetamide solvent system: effect of temperature and catalyst. *Carbohydrate research*, *327*(3), 345-352.
9. Trombino, S., Servidio, C., Curcio, F., & Cassano, R. (2019). Strategies for hyaluronic acid-based hydrogel design in drug delivery. *Pharmaceutics*, *11*(8), 407.
10. Russo, E., & Villa, C. (2019). Poloxamer hydrogels for biomedical applications. *Pharmaceutics*, *11*(12), 671.
11. Guvendiren, M., Lu, H. D., & Burdick, J. A. (2012). Shear-thinning hydrogels for biomedical applications. *Soft matter*, *8*(2), 260-272.
12. Klouda, L., & Mikos, A. G. (2008). Thermoresponsive hydrogels in biomedical applications. *European journal of pharmaceutics and biopharmaceutics*, *68*(1), 34-45.

13. Jung, Y. S., Park, W., Park, H., Lee, D. K., & Na, K. (2017). Thermo-sensitive injectable hydrogel based on the physical mixing of hyaluronic acid and Pluronic F-127 for sustained NSAID delivery. *Carbohydrate polymers*, *156*, 403-408.
14. Mero, A., & Campisi, M. (2014). Hyaluronic acid bioconjugates for the delivery of bioactive molecules. *Polymers*, *6*(2), 346-369.
15. Hofsäss, M. A., de Souza, J., Silva-Barcellos, N. M., Bellavinha, K. R., Abrahamsson, B., Cristofoletti, R., ... & Dressman, J. B. (2017). Biowaiver monographs for immediate-release solid oral dosage forms: Folic acid. *Journal of pharmaceutical sciences*, *106*(12), 3421-3430.
16. Xie, F., Van Bocxlaer, J., Colin, P., Carlier, C., Van Kerschaver, O., Weerts, J., ... & Vermeulen, A. (2020). PKPD Modeling and Dosing Considerations in Advanced Ovarian Cancer Patients Treated with Cisplatin-Based Intraoperative Intraperitoneal Chemotherapy. *The AAPS Journal*, *22*(5), 1-12.
17. Perez, R. P., Chen, E., Thaddeus Beck, J., Shirai, K., Neil Hayes, D., Shen, T., ... & Chin, S. (2019). Evaluation of pharmacokinetics and safety of cetuximab with cisplatin/carboplatin in patients with advanced solid tumor: Result from phase II studies. *Pharmacology research & perspectives*, *7*(6), e00519.
18. Patra, C. R., Bhattacharya, R., & Mukherjee, P. (2010). Fabrication and functional characterization of goldnanoconjugates for potential application in ovarian cancer. *Journal of materials chemistry*, *20*(3), 547-554.
19. Li, S., Li, X., Ding, J., Han, L., & Guo, X. (2019). Anti-tumor efficacy of folate modified PLGA-based nanoparticles for the co-delivery of drugs in ovarian cancer. *Drug design, development and therapy*, *13*, 1271.
20. Mo, J., Wang, L., Huang, X., Lu, B., Zou, C., Wei, L., ... & Zhao, W. (2017). Multifunctional nanoparticles for co-delivery of paclitaxel and carboplatin against ovarian cancer by inactivating the JMJD3-HER2 axis. *Nanoscale*, *9*(35), 13142-13152.
21. Yu, T., Li, Y., Gu, X., & Li, Q. (2020). Development of a Hyaluronic Acid-Based Nanocarrier Incorporating Doxorubicin and Cisplatin as a PH-Sensitive and CD44-Targeted Anti-Breast Cancer Drug Delivery System. *Frontiers in Pharmacology*, *11*, 1370.
22. Yang, F., Li, A., Liu, H., & Zhang, H. (2018). Gastric cancer combination therapy: synthesis of a hyaluronic acid and cisplatin containing lipid prodrug coloaded with sorafenib in a nanoparticulate system to exhibit enhanced anticancer efficacy and reduced toxicity. *Drug design, development and therapy*, *12*, 3321.

23. Zhang, R., Ru, Y., Gao, Y., Li, J., & Mao, S. (2017). Layer-by-layer nanoparticles co-loading gemcitabine and platinum (IV) prodrugs for synergistic combination therapy of lung cancer. *Drug design, development and therapy*, *11*, 2631.
24. Sim, M. W., Grogan, P. T., Subramanian, C., Bradford, C. R., Carey, T. E., Forrest, M. L., ... & Cohen, M. S. (2016). Effects of peritumoral nanoconjugated cisplatin on laryngeal cancer stem cells. *The Laryngoscope*, *126*(5), E184-E190.
25. Yang, Q., Aires, D. J., Cai, S., Fraga, G. R., Zhang, D., Li, C. Z., & Forrest, M. L. (2014). In vivo efficacy of nano hyaluronan-conjugated cisplatin for treatment of murine melanoma. *Journal of drugs in dermatology: JDD*, *13*(3), 283.
26. Wolny, P. M., Banerji, S., Gounou, C., Brisson, A. R., Day, A. J., Jackson, D. G., & Richter, R. P. (2010). Analysis of CD44-hyaluronan interactions in an artificial membrane system: insights into the distinct binding properties of high and low molecular weight hyaluronan. *Journal of Biological Chemistry*, *285*(39), 30170-30180.
27. Arslan, E., Talih, T., Oz, B., Halaclar, B., Caglayan, K., & Sipahi, M. (2014). Comparison of lovastatin and hyaluronic acid/carboxymethyl cellulose on experimental created peritoneal adhesion model in rats. *International Journal of Surgery*, *12*(2), 120-124.
28. Cho, E. J., Sun, B., Doh, K. O., Wilson, E. M., Torregrosa-Allen, S., Elzey, B. D., & Yeo, Y. (2015). Intraperitoneal delivery of platinum with in-situ crosslinkable hyaluronic acid gel for local therapy of ovarian cancer. *Biomaterials*, *37*, 312-319.
29. Pang, J., Jiang, P., Wang, Y., Jiang, L., Qian, H., Tao, Y., ... & Wu, Y. (2018). Cross-linked hyaluronan gel inhibits the growth and metastasis of ovarian carcinoma. *Journal of ovarian research*, *11*(1), 1-8.
30. Lan, T., Pang, J., Wu, Y., Zhu, M., Yao, X., Wu, M., ... & Chen, Y. (2016). Cross-linked hyaluronic acid gel inhibits metastasis and growth of gastric and hepatic cancer cells: in vitro and in vivo studies. *Oncotarget*, *7*(40), 65418.
31. Bae, K. H., Tan, S., Yamashita, A., Ang, W. X., Gao, S. J., Wang, S., ... & Kurisawa, M. (2017). Hyaluronic acid-green tea catechin micellar nanocomplexes: Fail-safe cisplatin nanomedicine for the treatment of ovarian cancer without off-target toxicity. *Biomaterials*, *148*, 41-53.
32. Chandrashekhara, S. H., Triveni, G. S., & Kumar, R. (2016). Imaging of peritoneal deposits in ovarian cancer: a pictorial review. *World journal of radiology*, *8*(5), 513.
33. Chambers, S. K., Ww, H. S., Janicek, M. F., Cragun, J. M., Hatch, K. D., Cui, H., ... & Alberts, D. S. (2012). Phase I trial of intraperitoneal pemetrexed, cisplatin, and

paclitaxel in optimally debulked ovarian cancer. *Clinical cancer research*, *18*(9), 2668-2678.

34. Hasovits, C., & Clarke, S. (2012). Pharmacokinetics and pharmacodynamics of intraperitoneal cancer chemotherapeutics. *Clinical pharmacokinetics*, *51*(4), 203-224.
35. Lu, Z., Wang, J., Wientjes, M. G., & Au, J. L. (2010). Intraperitoneal therapy for peritoneal cancer. *Future oncology*, *6*(10), 1625-1641.
36. Markman, M. (2001). Intraperitoneal drug delivery of antineoplastics. *Drugs*, *61*(8), 1057-1065.
37. Nissan, A., Stojadinovic, A., Garofalo, A., Esquivel, J., & Piso, P. (2009). Evidence-based medicine in the treatment of peritoneal carcinomatosis: Past, present, and future. *Journal of surgical oncology*, *100*(4), 335-344.
38. Roche, J. (2018). The epithelial-to-mesenchymal transition in cancer.
39. Hojo, N., Huisken, A. L., Wang, H., Chirshev, E., Kim, N. S., Nguyen, S. M., ... & Unternaehrer, J. J. (2018). Snail knockdown reverses stemness and inhibits tumour growth in ovarian cancer. *Scientific reports*, *8*(1), 1-
40. Baribeau, S., Chaudhry, P., Parent, S., & Asselin, É. (2014). Resveratrol inhibits cisplatin-induced epithelial-to-mesenchymal transition in ovarian cancer cell lines. *PLoS One*, *9*(1), e86987.
41. Chowanadisai, W., Messerli, S. M., Miller, D. H., Medina, J. E., Hamilton, J. W., Messerli, M. A., & Brodsky, A. S. (2016). Cisplatin resistant spheroids model clinically relevant survival mechanisms in ovarian tumors. *PloS one*, *11*(3), e0151089.
42. Haslehurst, A. M., Koti, M., Dharsee, M., Nuin, P., Evans, K., Geraci, J., ... & Feilotter, H. (2012). EMT transcription factors snail and slug directly contribute to cisplatin resistance in ovarian cancer. *BMC cancer*, *12*(1), 1-10.
43. Kim, D. H., Xing, T., Yang, Z., Dudek, R., Lu, Q., & Chen, Y. H. (2018). Epithelial mesenchymal transition in embryonic development, tissue repair and cancer: a comprehensive overview. *Journal of clinical medicine*, *7*(1), 1.
44. Van Zijl, F., Krupitza, G., & Mikulits, W. (2011). Initial steps of metastasis: cell invasion and endothelial transmigration. *Mutation Research/Reviews in Mutation Research*, *728*(1-2), 23-34.
45. Dongre, A., & Weinberg, R. A. (2019). New insights into the mechanisms of epithelial–mesenchymal transition and implications for cancer. *Nature reviews Molecular cell biology*, *20*(2), 69-84.

46. Aghamiri, S., Mehrjardi, K. F., Shabani, S., Keshavarz-Fathi, M., Kargar, S., & Rezaei, N. (2019). Nanoparticle-siRNA: a potential strategy for ovarian cancer therapy?. *Nanomedicine*, *14*(15), 2083-2100.
47. Terauchi, M., Kajiyama, H., Yamashita, M., Kato, M., Tsukamoto, H., Umezu, T., ... & Kikkawa, F. (2007). Possible involvement of TWIST in enhanced peritoneal metastasis of epithelial ovarian carcinoma. *Clinical & experimental metastasis*, *24*(5), 329-339.
48. Ghoneum, A., Afify, H., Salih, Z., Kelly, M., & Said, N. (2018). Role of tumor microenvironment in ovarian cancer pathobiology. *Oncotarget*, *9*(32), 22832.
49. Colvin, E. K. (2014). Tumor-associated macrophages contribute to tumor progression in ovarian cancer. *Frontiers in oncology*, *4*, 137
50. Mantovani, A., Marchesi, F., Malesci, A., Laghi, L., & Allavena, P. (2017). Tumour-associated macrophages as treatment targets in oncology. *Nature reviews Clinical oncology*, *14*(7), 399-416.
51. Sica, A., Larghi, P., Mancino, A., Rubino, L., Porta, C., Totaro, M. G., ... & Mantovani, A. (2008, October). Macrophage polarization in tumour progression. In *Seminars in cancer biology* (Vol. 18, No. 5, pp. 349-355). Academic Press.
52. Kawamura, K., Komohara, Y., Takaishi, K., Katabuchi, H., & Takeya, M. (2009). Detection of M2 macrophages and colony-stimulating factor 1 expression in serous and mucinous ovarian epithelial tumors. *Pathology international*, *59*(5), 300-305.
53. Barros, M. H. M., Hauck, F., Dreyer, J. H., Kempkes, B., & Niedobitek, G. (2013). Macrophage polarisation: an immunohistochemical approach for identifying M1 and M2 macrophages. *PloS one*, *8*(11), e80908
54. Zhang, M., He, Y., Sun, X., Li, Q., Wang, W., Zhao, A., & Di, W. (2014). A high M1/M2 ratio of tumor-associated macrophages is associated with extended survival in ovarian cancer patients. *Journal of ovarian research*, *7*(1), 1-16.
55. Ding, F., Zhang, L., Chen, H., Song, H., Chen, S., & Xiao, H. (2020). Enhancing the chemotherapeutic efficacy of platinum prodrug nanoparticles and inhibiting cancer metastasis by targeting iron homeostasis. *Nanoscale horizons*, *5*(6), 999-1015.

Chapter II: "Viscosified solid lipid nanoparticles based on naringenin and linolenic acid for cyclosporine A release on the skin"*

Abstract

Psoriasis is one of the most common human skin disorders. Although its pathogenesis is complex and not completely known, the hyperactivation of the immune system seems to have a key role. In this regard, among the most effective systemic therapeutics used in psoriasis we find cyclosporine, an immunosuppressive medication. However, one of the major problems associated with its use is the occurrence of systemic side effects such as nephrotoxicity, hypertension, *etc.* The present work fits in this context, and its aim is the design of suitable platforms for cyclosporine topical release in psoriasis treatment. The main objective is to achieve local administration of cyclosporine in order to reduce its systemic absorption and, consequently, its side effects. In order to improve dermal penetration, solid lipid nanoparticles (SLNs) are used as carriers, due to their lipophilicity and occlusive properties, and naringenin and linolenic acid are chosen, due to their properties, as starting materials for SLNs design. In order to have dermatological formulations and further modulate drug release, SLNs are incorporated in several topical vehicles obtaining gels with different degree of lipophilicity. Potential applications for psoriasis treatment were evaluated by considering the encapsulation efficiency, release profiles, *in vitro* skin permeation and anti-inflammatory effects.

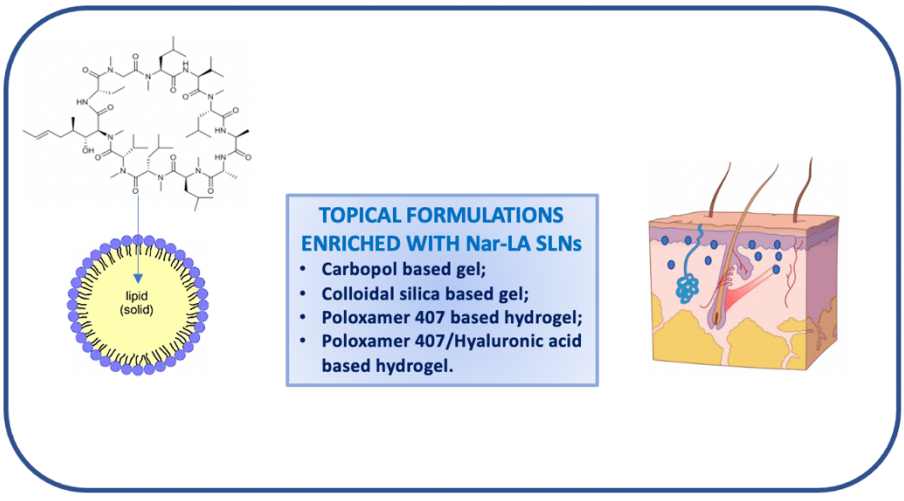

***Published on Molecules, 2020 Aug 02; 25(15), 3535; doi: https://doi.org/10.3390/molecules25153535**

1. Introduction

Psoriasis is a multifactorial chronic inflammatory skin disorder that affects approximately 2-3% of the worldwide population. It is characterized by the hyperproliferation and atypical differentiation of keratinocytes resulting in itchy, erythematous and squamous plaques[1-2]. Psoriasis can present clinical features with a different degree of severity ranging from mild/moderate to severe manifestations with a large portion of cutaneous surface affected, negatively impacting the quality of life of the patient[3]. Moreover, it is associated with rheumatological, metabolic and cardiovascular comorbidities[4].

The etiology of psoriasis is multifactorial and is considered to have an important genetic component. Regarding its pathogenesis, is not completely elucidated but the hyperactivation of the immune system seems to have a key role. In particular, several cell types are involved such as lymphocytes T, dendritic cells and macrophages that infiltrate in dermis and epidermis and secrete proinflammatory mediators that stimulate, in their turn, the hyperproliferation of keratinocytes [5-6].

Current treatments include corticosteroids, keratolytics, phototherapy, calcineurin inhibitors, biologics targeting proinflammatory mediators and vitamin D analogues[7]. One of the most effective drugs approved for psoriasis treatment is oral cyclosporine A, an immunosuppressive medication. Its mechanism of action is attributable to the inhibition of calcineurin that consequently leads to the inactivation of T cells and the downregulation of the expression of proinflammatory mediators, particularly IL-2 and IL-4[8].

Although its proven efficacy, one of the major problems associated with cyclosporine is that its long-term use can cause systemic adverse effects like hypertension, nephrotoxicity, hyperlipidaemia *etc*[9]. Therefore, cyclosporine topical administration would be advantageous. However, several attempts to achieve local administration of cyclosporine, by using numerous topical vehicles, have been made and failed[10-13]. This can be attributed to its unfavorable physicochemical properties for dermal penetration such as high molecular weight, low hydrophilicity and rigid structure[14-16].

In this regard, solid lipid nanoparticles (SLNs) have been widely investigated as potential topical delivery systems. In fact, their lipophilicity promotes topical drug penetration without damaging the skin [17-19]. Moreover, SLNs show several advantages compared to other types of nanoparticles (i.e. polymeric and inorganic) such as biocompatibility, biodegradability, high loading efficiency and easy scalability[20].

The aim of this work is the design of suitable platforms for cyclosporine topical release in psoriasis treatment. The main objective is to achieve site specific release of cyclosporine in order to reduce its systemic absorption and, consequently, its side effects. In order to improve dermal penetration, SLNs have been used as carriers and naringenin and linolenic acid were chosen due to their properties as starting materials for SLNs design.

Naringenin is a natural flavonoid exerting broad biological effects such as antioxidant, antibacterial, anti-inflammatory and cardioprotective activities[21]. Interestingly, *in vitro* naringenin inhibited T-cells proliferation and reduced the levels of proinflammatory mediators such as TNF-alpha and IL-6 [22-23]. Linolenic acid is a polyunsaturated fatty acid belonging to omega-3 family. It shows potent anti-inflammatory activity attributable to the inhibition of TNF-alpha, inducible nitric oxide synthase and cyclooxygenase-2[24]. Moreover, clinical studies reported that intravenous infusions of omega-3 fatty acids, in combination with oral supplementation, determined a reduction of psoriasis skin lesions[25]. For these reasons, in addition to the pharmacological activity of cyclosporine, the use of naringenin and linolenic acid could be useful in reducing the inflammatory state that intervenes in the pathogenesis of psoriasis.

In order to have dermatological formulations and further modulate drug release, SLNs have been incorporated in several topical vehicles such as Poloxamer 407, Carbopol and colloidal silica. Potential applications for psoriasis treatment were evaluated by considering the encapsulation efficiency, release profiles, *in vitro* skin permeation and anti-inflammatory effects.

2. Materials and Method

2.1 Chemicals

All solvents, analytical grade, were purchased from Carlo Erba Reagents (Milan,Italy): diethyl ether, dichloromethane (DCM), ethanol, methanol, acetone, dimethylformamide (DMF), 1-butanol, trichloroacetic acid (TCA), acetonitrile and n-hexane. Naringenin, linolenic acid, N,N-diisopropylethylamine (DIPEA), sodium sulfate, N, N-dicyclohexylcarbodiimide (DCC), sodium hydroxide, sodium taucholorate, polyoxyethylene sorbitan monolaurate (Tween 20), tert-butyl alcohol(TBA), butylhydroxytoluene (BHT) and ethylenediaminetetraacetic acid (EDTA) disodium salt dihydrate and phosphate buffer solution 1.0 M pH 7.4, DMEM, FBS, L-glutamine, penicillin/streptomycin, Griess reagent, L-NAME, and indomethacin were purchased from Sigma Aldrich (Sigma Chemical Co., St. Louis, MO, USA). Cyclosporine A was purchased from Farmalabor srl (Milan, Italy). RAW 264.7 cells were obtained from American Type Culture Collection (ATCC) no. TIB-71, UK. Poloxamer 407, Carbopol 940, soy lectin powder, propylene glycol, isopropyl palmitate, nipagin, propyl paraben, colloidal silica, prunus amygdalus dulcis oil, ethoxydiglycol (Transcutol P). Cellulose acetate membrane (MWCO: 12000–15000Da) was purchased by Medicell International LTD.

2.2 Instruments

FT-IR spectra were measured using a Jasco 4200 IR spectrophotometer with KBr disks. ^{1}H-NMR spectra were recorded on a Bruker VM30 spectrometer; the chemical shifts were expressed as δ-values (ppm) and referred to the solvent. The UV–vis spectra were obtained using a Jasco UV-530 spectrophotometer with quartz cells of 1 cm thickness. Scanning electron microscopy (SEM) analysis was performed with JEOL JSMT 300 A microscope; the surface of the samples was made conductive by deposition of a thin gold layer in a vacuum chamber. Dimensional analysis of nanoparticles was carried out using a Brookhaven 90 Plus Particle Size Analyzer at 25 °C by measuring the autocorrelation function at 90° scattering angle. Sample were freeze-dried using Micro Freeze-drying Modulyo, Edwards. Dermatological formulations were prepared using Citounguator, Triad Scientifics.

2.3 Esterification of naringenin with linolenic acid

Esterification was carried out according to Steglich reaction. In a three necked flask equipped with a reflux condenser and dropping funnel, under stirring, accurately flamed and maintained under nitrogen bubbling, 0.2 g of naringenin (0.73 mmol), 0.288 g of DCC (1.4 mmol) and 0.126 ml of DIPEA (0.72 mmol) and then, after 30 min, 0.223 ml of linolenic acid (0.73 mmol) were dissolved in dry DCM. Then, DMF was added in order to increase the solubility of the compounds. The reaction mixture was kept under magnetic stirring for 24 h covered in foil. DCM was removed under reduced pressure while DMF with several extractions with diethyl ether and distilled water. Sodium sulfate was added to the organic phase, the solution was filtered, diethyl ether was removed under reduced pressure and the product was dried under vacuum obtaining a yellow solid. The compound was characterized through FT-IR and ^{1}H-NMR.

2.4 Preparation of SLNs

SLNs were prepared *via* microemulsion technique according to literature[26]. Briefly, the obtained ester, in the presence or not of cyclosporine A, was melted approximately at 70°C. Meanwhile, a warm aqueous solution of Tween 20, sodium taurocholate and butanol was prepared and added to the melt ester obtaining an O/A microemulsion. This microemulsion was then poured into a flask and kept under magnetic stirring at 2-3 °C in ice bath for 45 min. Then, the two dispersions of empty and loaded nanoparticles were freeze-dried. For loaded SLNs, unloaded drug was removed by filtration. The obtained samples were characterized through dynamic light scattering and scanning electron microscopy.

Ester	Tween 20	Butanol	Sodium taurocholate	Cyclosporine A
0.05 g	0.032 ml	0.012 ml	0.016 g	0.002 g

Scheme 1. Amount of reagents used in SLNs preparation.

2.5 Loading efficiency determination

The loading efficiency of SLNs was determined by UV-Vis spectrometry. SLNs were dissolved in a water methanol solution (1:9) that was sonicated for 15 min at 37 °C in

order to determine the breakage of nanoparticles and consequent drug release. The absorbance of the obtained samples was measured at a fixed wavelength for cyclosporine A (λ=210 nm). The loading efficiency (LE%) is the percentage of loaded drug with respect to the total amount of used drug and is calculated *via* the following equation:

$$LE\% = \frac{Ql}{Qt} x100$$

Where Qt indicates the total amount of drug used and Ql the loaded drug amount. Studies were carried out in duplicate and the results were in agreement with ±5% standard error.

2.6 Preparation of Poloxamer 407-based gel

0.09 g of propylene glycol was solubilized in 6.12 g of distillated water and, then, 1.28 g of Poloxamer 407 was added under vigorous stirring. The obtained gel was left in the refrigerator overnight. Separately, 1 g of soy lecithin was emulsified with 1 g of isopropyl palmitate and left to rest for 24 h. Subsequently 0.004 g of loaded SLNs were suspended in a solution of transcutol P that was mixed with lecithin solution and Poloxamer gel with Citounguator for 2 minutes.

2.7 Preparation of Carbopol-based gel

0.09 g of propylene glycol and 0.1 g of Carbopol were solubilized in 9.29 g of distilled water containing 0.01 g of disodium EDTA. The formation of the gel occurred after the addition of sodium hydroxide (solution 10%) up to pH 6. Subsequently, 0.04 g of loaded SLNs was suspended in a transcutol P solution that was mixed with the gel with Citounguator for 2 minutes.

2.8 Preparation of colloidal silica-based gel

0.01 g of BHT was dissolved in 8.9 g of sweet almond oil and then 0.004 g of loaded SLNs were added to the resulting solution. The obtained mixture was mixed with anhydrous colloidal silica with Citounguator for 4 minutes.

2.9 Preparation of hyaluronic acid and Poloxamer 407-based gel

0.01 g of hyaluronic acid and 0.004 g of loaded SLNs were solubilized in 5 ml of bidistilled water. Then, 3 g of Poloxamer 407 were added under mixing and the resulting gel was sonicated for 1h.

2.10 *In vitro* skin penetration studies

Skin penetration studies were performed (n=8) by using franz diffusion cells apparatus with cellulose acetate membranes and rabbit ear skin for 24 h. The apparatus was maintained at 36.5 °C in order to mimic physiological conditions. Receptor chambers (6.0 ml) were filled with NaCl 0.9% solution containing ethanol (20%) and kept under stirring in order to maintain sink conditions. Unloaded SLNs alone or in dermatological formulations were used as control. At specific time intervals (1 h, 2 h, 4 h, 8 h, 10 h, 24 h) an aliquot (1 ml) of each sample was withdrawn from receptor chambers and replaced with fresh release medium. Samples were analyzed trough UV-Vis spectrophotometry and drug release profiles were expressed as percentage of drug released respect to the total loaded amount in function of time.

2.11 Tape stripping test

After permeation studies, samples were removed from skin surface. Rabbit ear skin were washed 3 times with phosphate buffer (pH= 7.4) and then dried. Subsequently, the stratum corneum was separated from dermal layers (epidermis and dermis) using an adhesive tape (Scotch 845 Book Tape, 3M). Previous studies reported that 15 strips are enough to separate dermal layers[27]. Cyclosporine A was extracted from adhesive tapes by vortexing them with acetonitrile for 2 min. The resulting solution was then filtered with 0.45 µm membrane and the amount of cyclosporine was determined by UV-Vis spectrophotometry. On the other hand, the epidermis-dermis layer was cut into small pieces, vortexed for 5 minutes with 1 ml of acetonitrile and then sonicated for 40 minutes. Subsequently, the resulting solution was filtrated with 0.45 µm membrane and the amount of cyclosporine A was determined by UV-Vis spectrophotometry.

2.12 Malonoaldehyde assay

1 ml of microsomal suspension was added to an ethanolic solution containing 0.07 ml of BHT 0.2%, 3 ml of TCA a 0.5% and 0.5 ml of TBA. The samples were then incubated with the microsomal suspension in a thermostatic bath at 37 °C for 24 h. At specific time intervals (15 min, 30 min, 1h and 24h) the samples were withdrawn, heated at 90 °C and then centrifugated. Subsequently, the thiobarbituric acid-malondialdehyde complex was detected spectrophotometrically at λ=535 nm.

2.13 *In vitro* anti-inflammatory activity evaluation

The anti-inflammatory activity of both empty and loaded SLNs was investigated *in vitro* assessing their ability to inhibit NO production in RAW 264.7 cell line. Dulbecco's modified Eagle's medium (DMEM) supplemented with L-glutamine, fetal bovine serum, and a solution of penicillin and streptomycin (1%, 10% and 1%, respectively) was used as cell medium. Cells were cultured at 37°C under 5% CO_2 and were seeded onto microplates (96 wells, 100,000 cells/well). After 24 h, the medium was removed and fresh medium containing samples at different concentrations and 1 µg/mL LPS were added. After 24 h of incubation, 100 µL of Griess reagent was added in order to evaluate the presence of nitrite, a stable product of NO oxidation. The presence of nitrite was determined spectrophotometrically at λ=490nm. Indomethacin and L-NAME were used as positive controls.

2.14. Statistical analysis

Data are expressed as mean (standard error of the mean of N re- plicates per experiment). Statistical analysis was carried out by Student's t-test using the GraphPad Prism 4 software program. $P < 0.05$ was considered as statistically insignificant.

3. Results and discussion

3.1 Esterification of naringenin with linolenic acid

In order to obtain a lipophilic compound to use in the formulation of SLNs, the alcoholic group of naringenin was functionalized with the carboxylic group of linolenic acid. The esterification was carried out according Steglich reaction by using DCC as crosslinking agent in dry DCM at room temperature (**scheme 2**)[28].

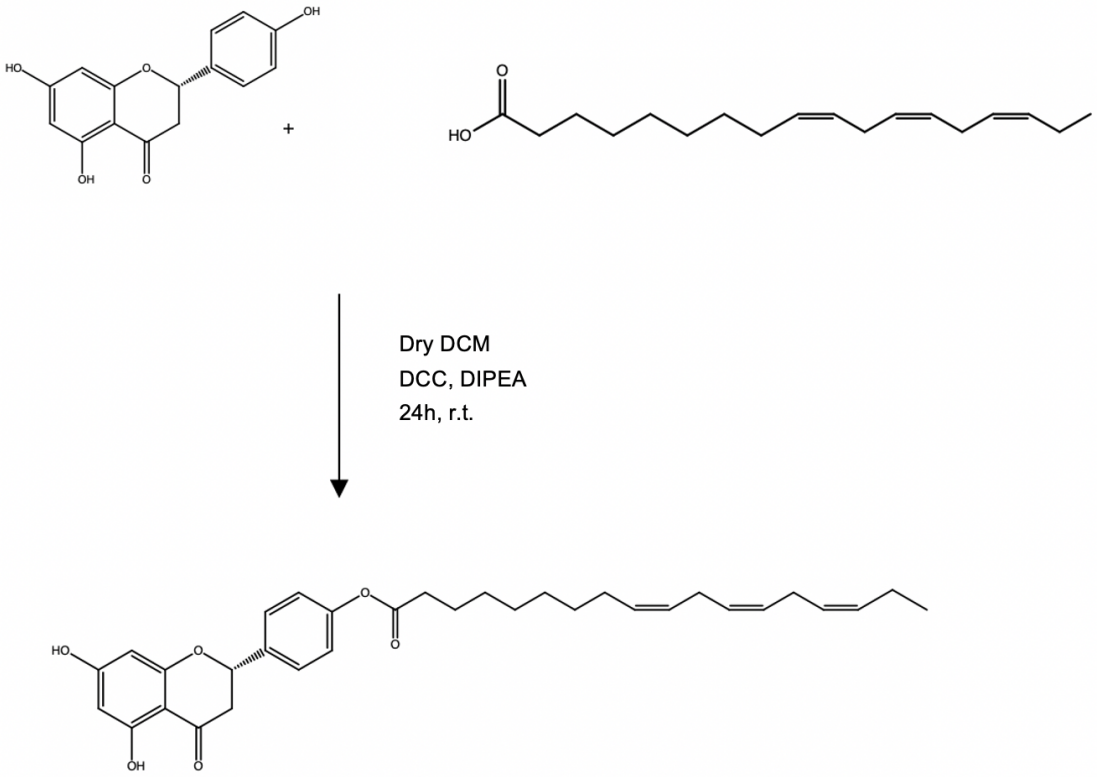

Scheme 2. Schematic representation of the synthetic route of linolenic acid-naringenin ester.

The product formation was confirmed by FT-IR and ^{1}H-NMR spectroscopy.

FT-IR (KBr) v (cm^{-1}): 3550, 3200 (phenolic OH), 3079, 3028 (CH aromatic), 1731(C=O). ^{1}H-NMR (CDCl3): δ 1.09 (3H, t), 1.18-1.64 (8H, m), 1.90-2.15 (5H, m), 2.35-2.62 (4H, m), 2.60-2.68 (4H, m), 4.94 (1H), 5.26-5.48 (6H, m), 6.08-6.11 (2H, d), 7.09 (2H, m), 7.20 (2H, m).

In particular, the FT-IR spectra of the ester (c), naringenin (b) and linolenic acid (a) were compared (**Figure 1**). The spectrum (c) shows a new peak at 1731 cm^{-1}, attributable to the stretching of the C=O of the ester, and peaks at 3079-3028 cm^{-1} and 3550-3200 cm^{-1} corresponding to the stretching vibrations of the phenolic OH and the aromatic CH of naringenin, confirming the successful reaction. Moreover, on the basis of the NMR spectrum, it is possible to hypothesize a monoesterification of one of the two phenolic para-hydroxyl groups of naringenin.

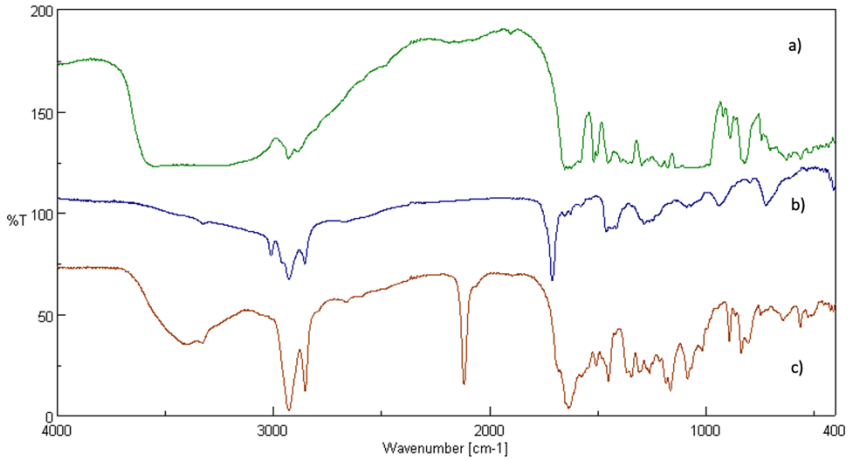

Figure 1. FT-IR spectra of: naringenin(a), linolenic acid (b), linolenic acid-naringenin ester (c)

3.2 Preparation and characterization of SLNs

SLNs based on naringenin and linolenic acid and loaded with cyclosporine were prepared *via* microemulsion technique obtaining an excellent encapsulation efficiency of about 92%[29]; this positive data can be attributable to the high lipophilicity of both Cyclosporine and SLNs. In fact, the encapsulation efficiency depends on several factors such as drug concentration, lipid matrix *etc.*[30].

The obtained SLNs were characterized by morphological and dimensional analyses. DLS data show an average diameter of about 470 nm and PDI of 0.19, which is indicative of a good homogeneity in particle size distribution, and, moreover, confirms cyclosporine encapsulation considering the different size of empty and loaded nanoparticles (**Figure 2**). DLS results were confirmed also by SEM analysis that showed a spherical shape of SLNs (**Figure 2**).

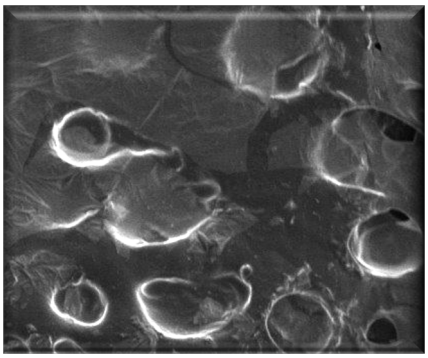

Formulation	Average diameter (nm)	PDI
Empty SLNs	299.9 ±3.1	0.274±0.013
Loaded SLNs	470.0±4.6	0.195±0.047

Figure 2. Photomicrography of loaded SLNs obtained by SEM (on the left), DLS results (on the left).

3.2 Skin permeation studies

3.2.1 *In vitro* permeation studies

In order to have dermatological formulations and further modulate drug release, SLNs were incorporated in several topical vehicles including functional substances such as hyaluronic acid and colloidal silica and gelling agents such as Poloxamer 407 and Carbopol, obtaining gels with a different degree of lipophilicity. These dermatological formulations were subjected to transdermal release studies in order to evaluate their potential application and efficacy in psoriasis treatment.

Drug release profiles were evaluated by using Franz diffusion cells with cellulose acetate membranes or rabbit ear skin. Synthetic membranes, in addition to rabbit ear skin, were used due to the presence of cyclosporine that is characterized by a specific absorbance range (λ=195-215 nm) and, therefore, can interfere with several skin components, such as lipids and proteins, that adsorb at similar wavelengths[31-32]. The presence of skin components in receptor chambers can be attributable to the release medium composition (0.9% NaCl/ethanol 20%), since ethanol can promote phospholipids mobility[33]. Ethanol was added to the release medium since cyclosporine is insoluble in water[34]. To further eliminate the risk of possible interferences, a 12kDa cut-off membrane was used. In fact, the obtained data show, by comparing the release studies carried out using rabbit ear skin and cellulose acetate membranes, absence of significant interferences.

Drug release studies were performed on dermatological formulations at different time intervals (1 h, 2 h, 4 h, 8 h, 10 h, 24 h). The release profiles were determined by UV-Vis spectrometry and expressed as percentage of drug released with respect to the total loaded amount in function of time.

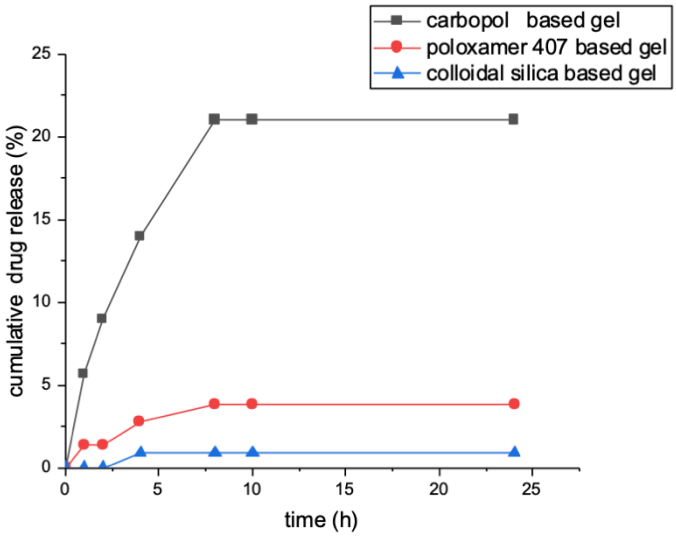

Figure 3. Cyclosporine release profile evaluated within 24 hours by using acetate cellulose membrane. Data are expressed as the mean of two independent experiments.

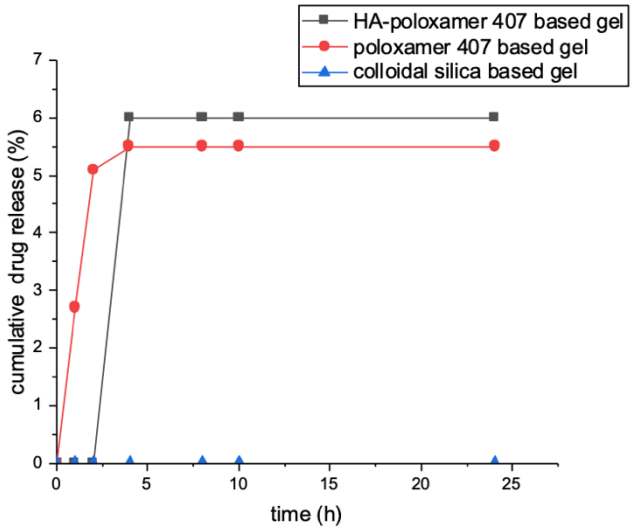

Figure 4. Cyclosporine release profile evaluated within 24 hours by using ear rabbit skin. Data are expressed as the mean of two independent experiments.

Data showed that, with cellulose acetate membrane, cyclosporin A was released within 8 h in quantities ranging from 0.5 to 21% of the total loaded amount from the dermatological formulations containing absorption enhancers. After 8 h, no release was observed. Instead, cyclosporine was not released from SLNs and colloidal silica-based gel within 24 h (**Figure 3**). On the other hand, by using rabbit ear skin, no drug release has been observed except in the case of gels containing absorption promoters, for which only a maximum release of 5% of the loaded drug was reported (**Figure 4**).

A possible rationale for the obtained release profiles, showing no or low transdermal release, can be attributable to the use of SLNs as drug delivery system; in fact, SLNs are excellent drug carriers for dermal delivery, but they show several limitations in transdermal delivery since they tend to remain into superficial skin layers and to not penetrate into the deeper ones[35]. The use of penetration enhancers in dermatological formulations (i.e. propylene glycol and transcutol P) increases the solubility, the permeation rate and the skin retention of cyclosporine, thus leading to a low short-term transdermal release, as observed for the Carbopol and Poloxamer 407 based formulations[36]. Moreover, this release behavior can be explained hypothesizing that propylene glycol, in addition to increase drug solubility in skin layers, may induce skin structural modifications leading to a reduction of the skin barrier properties and an increase of its permeability, as reported in a recent study[37].

However, for all the dermatological formulations tested, no significative concentrations of cyclosporine were found into receptor chambers and, consequently, on the basis of these encouraging results, it is possible to hypothesize that these formulations may reduce or avoid systemic absorption of cyclosporine and, therefore, the occurrence of adverse effects.

3.3.2 Tape stripping test

In order to evaluate the quantity of cyclosporin A released in skin layers, including the stratum corneum, epidermis and dermis, the tape stripping method was performed after permeation studies. The obtained data reported that the amount of drug released within 24 h from the colloidal silica-based gel is negligible in the stratum corneum and approximately equal to 20% in the epidermis-dermis layer, showing a slower release rate compared to the other dermatological formulations tested, probably due to the absence of adsorption enhancers. On the other hand, Poloxamer 407 based gel released, within

10 h, approximately 80% and 15% of the loaded drug in the stratum corneum and epidermis-dermis layer, respectively, showing the most advantageous release profile. This data can be explained by the use, in addition to propylene glycol, of transcutol P as permeation enhancer: it was proven to penetrate into the stratum corneum, thus enhancing drug solubility and retention into the epidermis and decreasing the skin barrier functions[38].

Moreover, in addition to adsorption enhancers, also the nature of the polymeric vehicle was found to influence the release profile; in this regard, Carbopol-based gel showed a slower dermal release kinetic, compared to the Poloxamer-407 based one, with approximately 35% and 25% of the loaded drug released within 24 h, in the stratum corneum and epidermis-dermis layer, respectively. The faster release rate of the Poloxamer 407 based formulation can be attributed to its rapid dissolution in physiological conditions ascribable to the micellar disentanglement that occurs as result of water uptake. According to this, it can be assumed that, in this case, drug release is mainly driven by gel dissolution rather than diffusion[39]. Interestingly, by using Poloxamer 407 in combination with hyaluronic acid, a lower amount of drug was released: 15% in the stratum corneum and 12% in the epidermis-dermis layer after 10 h. Probably, this different release profile can be attributable to an increased viscosity and strength of the gel, resulting in a more crosslinked structure with a consequent slower drug release rate[40]. In fact, the presence of hyaluronic acid could lead to the formation of a densely packed supramolecular structure, thus determining a reduction of the diffusion coefficient of the resulting gel[41]. Beyond this, the reported release behavior can also be caused in part by the retention of SLNs into the gel since, interestingly, recent modelling and experimental studies have shown that hyaluronic acid and phospholipids interact *via* hydrogen bonds and hydrophobic forces, thus leading to strong associations[42].

All the reported data suggest that the type and concentration of the polymeric vehicle, crosslinker, adsorption enhancer and drug are the main determinant of the release kinetics of topical formulations. Furthermore, experimental results indicate a site-specific release of cyclosporine into skin layers, highlighting the therapeutic potential of these dermatological formulations in psoriasis treatment. This release behavior can be explained by the use of SLNs as drug carriers; in fact, given their adhesive properties, SLNs tend to form films on the skin, explicating occlusive properties. Due to this occlusive effect, they enhance skin hydration, by reducing water evaporation, thus increasing drug penetration into skin layers. The occlusion factors are strongly influenced

by several elements such as particle size, crystallinity of the lipid matrix, lipid concentration and mass[43-46].

Cyclosporine release from SLNs is determined by the combination of two different mechanisms: diffusion and lipid degradation[47]. In this regard, a recently reported model for diffusion release from lipid carriers based on Onsager's theory can be considered as putative release mechanism for these delivery platforms[48].

3.4 Evaluation of the antioxidant activity

SLNs and dermatological formulations ability to inhibit lipid peroxidation induced by tert-BOOH, a free radical generator, was examined in microsomal rat liver membrane. The antioxidant activity of the free ester was also investigated in the same conditions. All the samples were found to be able to preserve the antioxidant capacity of the precursor, naringenin, and the most potent activity was exhibited the HA-Poloxamer 407 based formulation; this latter may be attributable to the presence of hyaluronic acid that is also known to exert an antioxidant activity[49]. However, the other formulations, even if not containing antioxidant compounds, were able to preserve, in a dose dependent manner, microsomal membranes from lipid peroxidation induced by tert-BOOH, probably due to the presence of naringenin and linolenic acid based SLNs (**Figure 5**).

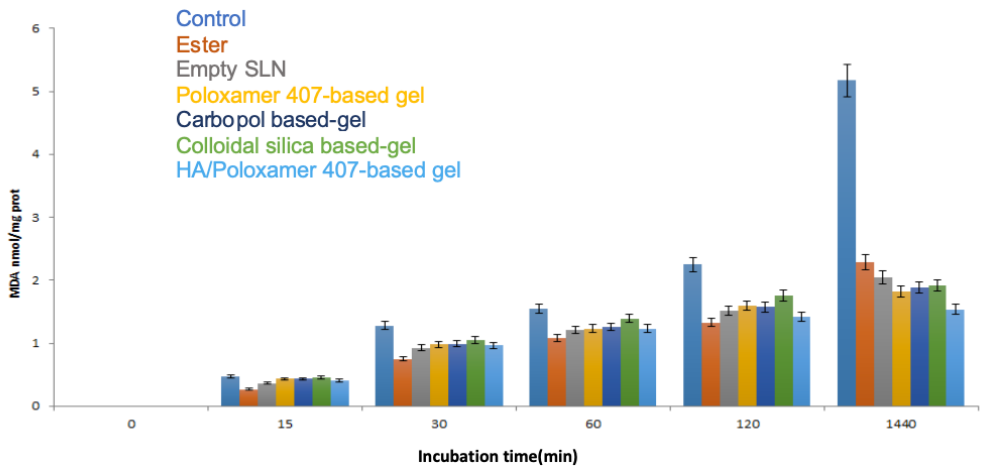

Figure 5. *In vitro* antioxidant activity of the ester, SLNs and dermal formulations. Herein are reported the results obtained from the malonoaldehyde assay.

3.5 Evaluation of anti-inflammatory activity

Inhibition of nitroxide (NO) production by RAW 264.7 murine macrophage cell line, was assessed by quantifying the amount of nitrites, stable oxidized products of NO, after inducing an inflammatory stimulus by E. coli lipopolysaccharide (LPS). Obtained data reported that both loaded and empty SLNs showed inhibitory activity against NO production in macrophages, when stimulated with LPS, with IC_{50} values of 53.78 ± 2.41 and 232.90 ± 11.7 µg/ml, respectively. In particular, loaded SLNs showed to be more active than empty SLNs, exhibiting a higher percentage of inhibition at a lower concentration. The greater anti-inflammatory activity of loaded SLNs is probably due to the presence, in addition to naringenin and linolenic acid, of cyclosporin A which is known to inhibit the production of nitroxide[50].

Interestingly, these results suggest that SLNs, due to the presence of naringenin, linolenic acid and cyclosporine, could exert a synergistic anti-inflammatory activity in reducing the inflammatory state that intervenes in the pathogenesis of psoriasis, turning out to be promising cyclosporine delivery systems for psoriasis treatment.

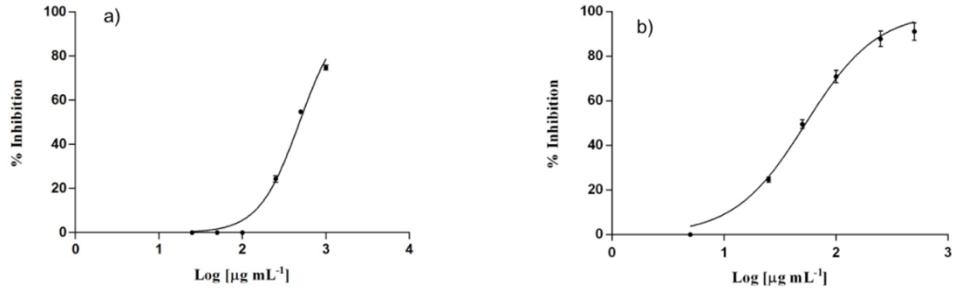

Figure 6. *In vitro* inhibitory activity of empty SLNs (a) and loaded SLNs (b) on NO production.

4. Conclusion

The aim of this work was the design of suitable formulations for cyclosporine topical release in psoriasis treatment. The main objective was to achieve site specific release of cyclosporine to reduce its systemic absorption and, consequently, its side effects. In order to improve dermal penetration, SLNs were used as carriers and naringenin and linolenic acid were chosen as starting materials for nanoparticles design due to their anti-inflammatory activity. SLNs with excellent loading efficiency and suitable size for topical administration were prepared *via* microemulsion technique. In order to have

dermatological formulations and further modulate drug release, SLNs were incorporated in several topical vehicles such as functional substances, like hyaluronic acid and colloidal silica, and gelling agents including Poloxamer 407 and Carbopol, obtaining gels with a different degree of lipophilicity. So, cyclosporine release profiles were evaluated, and *in vitro* data showed a site-specific release in skin layers and a low transdermal release. Furthermore, SLNs exerted potent *in vitro* anti-inflammatory activity turning out to be useful in reducing the inflammatory state that intervenes in the pathogenesis of psoriasis. In conclusion, the obtained results show that these formulations, thanks to their biocompatibility, release profiles, excellent antioxidant and anti-inflammatory activities could be promising formulations for Cyclosporine topical release.

.

References

1. Lowes, M. A., Bowcock, A. M., & Krueger, J. G. (2007). Pathogenesis and therapy of psoriasis. *Nature*, *445*(7130), 866-873.
2. Gottlieb, A. B. (2005). Psoriasis: emerging therapeutic strategies. *Nature reviews Drug discovery*, *4*(1), 19-34.
3. Lebwohl, M. (2005). A clinician's paradigm in the treatment of psoriasis. *Journal of the American Academy of Dermatology*, *53*(1), S59-S69.
4. Greb, J., Goldminz, A., Elder, J., …& (2016). Psoriasis. *Nature primer diseases, 2,16082*
5. Bowcock, A. M., & Krueger, J. G. (2005). Getting under the skin: the immunogenetics of psoriasis. *Nature Reviews Immunology*, *5*(9), 699-711.
6. Armstrong, A. W., & Read, C. (2020). Pathophysiology, clinical presentation, and treatment of psoriasis: a review. *Jama*, *323*(19), 1945-1960.
7. Rizvi, S., Chaudhari, K., Syed, B. A. (2015). The psoriasis drugs market.
8. Azzi, J. R., Sayegh, M. H., & Mallat, S. G. (2013). Calcineurin inhibitors: 40 years later, can't live without…. *The Journal of Immunology*, *191*(12), 5785-5791.
9. Berth-Jones, J. (2005). The use of ciclosporin in psoriasis. *Journal of dermatological treatment*, *16*(5-6), 258-277.
10. De Rie, M. A., Meinardi, M. M., & Bos, J. D. (1991). Lack of efficacy of topical cyclosporin A in atopic dermatitis and allergic contact dermatitis. *Acta dermato-venereologica*, *71*(5), 452-454.
11. Griffiths, C. E. (1990). Systemic and local administration of cyclosporine in the treatment of psoriasis. *Journal of the American Academy of Dermatology*, *23*(6), 1242-1247.
12. Mizoguchi, M., Kawaguchi, K., Ohsuga, Y., Ikari, Y., & Yanagawa, A. (1992). Cyclosporin ointment for psoriasis and atopic dermatitis. *Lancet (British edition)*, *339*(8801).
13. Vena, G. A., & Cassano, N. (2001). Can we still suggest the topical cyclosporin treatment in cutaneous disorders?.
14. Liu, H., Li, S., Wang, Y., Yao, H., & Zhang, Y. (2006). Effect of vehicles and enhancers on the topical delivery of cyclosporin A. *International journal of pharmaceutics*, *311*(1-2), 182-186.

15. Choi, H. K., Flynn, G. L., & Amidon, G. L. (1995). Percutaneous absorption and dermal delivery of cyclosporin A. *Journal of pharmaceutical sciences*, *84*(5), 581-583.
16. Duncan, J. I., Wakeel, R. A., Winfield, A. J., Ormerod, A. D., & Thomson, A. W. (1993). Immunomodulation of psoriasis with a topical cyclosporin A formulation. *Acta dermato-venereologica*, *73*(2), 84-87.
17. Jensen, L. B., Petersson, K., & Nielsen, H. M. (2011). In vitro penetration properties of solid lipid nanoparticles in intact and barrier-impaired skin. *European journal of pharmaceutics and biopharmaceutics*, *79*(1), 68-75.
18. Prow, T. W., Grice, J. E., Lin, L. L., Faye, R., Butler, M., Becker, W., ... & Roberts, M. S. (2011). Nanoparticles and microparticles for skin drug delivery. *Advanced drug delivery reviews*, *63*(6), 470-491.
19. Müller, R. H., Petersen, R. D., Hommoss, A., & Pardeike, J. (2007). Nanostructured lipid carriers (NLC) in cosmetic dermal products. *Advanced drug delivery reviews*, *59*(6), 522-530.
20. Souto, E. B., Baldim, I., Oliveira, W. P., Rao, R., Yadav, N., Gama, F. M., & Mahant, S. (2020). SLN and NLC for topical, dermal, and transdermal drug delivery. *Expert opinion on drug delivery*, *17*(3), 357-377.
21. Salehi, B., Fokou, P. V. T., Sharifi-Rad, M., Zucca, P., Pezzani, R., Martins, N., & Sharifi-Rad, J. (2019). The therapeutic potential of naringenin: a review of clinical trials. *Pharmaceuticals*, *12*(1), 11.
22. Gaggeri, R., Rossi, D., Christodoulou, M. S., Passarella, D., Leoni, F., Azzolina, O., & Collina, S. (2012). Chiral flavanones from Amygdalus lycioides spach: Structural elucidation and identification of TNFalpha inhibitors by bioactivity-guided fractionation. *Molecules*, *17*(2), 1665-1674.
23. Gaggeri, R., Rossi, D., Daglia, M., Leoni, F., Avanzini, M. A., Mantelli, M., ... & Collina, S. (2013). An Eco-Friendly Enantioselective Access to (R)-Naringenin as Inhibitor of Proinflammatory Cytokine Release. *Chemistry & biodiversity*, *10*(8), 1531-1538.
24. Ren, J., & Chung, S. H. (2007). Anti-inflammatory effect of α-linolenic acid and its mode of action through the inhibition of nitric oxide production and inducible nitric oxide synthase gene expression via NF-κB and mitogen-activated protein kinase pathways. *Journal of agricultural and food chemistry*, *55*(13), 5073-5080.
25. Mayser, P., Grimm, H., & Grimminger, F. (2002). n-3 fatty acids in psoriasis. *British Journal of Nutrition*, *87*(S1), S77-S82.

26. Ugazio, E., Cavalli, R., & Gasco, M. R. (2002). Incorporation of cyclosporin A in solid lipid nanoparticles (SLN). *International journal of pharmaceutics*, *241*(2), 341-344.
27. Jain, S., Mistry, M. A., & Swarnakar, N. K. (2011). Enhanced dermal delivery of acyclovir using solid lipid nanoparticles. *Drug delivery and translational research*, *1*(5), 395.
28. Neises, B., & Steglich, W. (1978). Simple method for the esterification of carboxylic acids. *Angewandte Chemie International Edition in English*, *17*(7), 522-524.
29. Bondi, M. L., Fontana, G., Carlisi, B., & Giammona, G. (2003). Preparation and characterization of solid lipid nanoparticles containing cloricromene. *Drug delivery*, *10*(4), 245-250.
30. Souto, E. B., Wissing, S. A., Barbosa, C. M., & Müller, R. H. (2004). Development of a controlled release formulation based on SLN and NLC for topical clotrimazole delivery. *International journal of pharmaceutics*, *278*(1), 71-77.
31. Yee, G. C., Gmur, D. J., & Kennedy, M. S. (1982). Liquid-chromatographic determination of cyclosporine in serum with use of a rapid extraction procedure. *Clinical chemistry*, *28*(11), 2269-2271.
32. Frei, R. W., & Zech, K. (1987). *Selective sample handling and detection in high-performance liquid chromatography*. Elsevier.
33. Verma, D. D., & Fahr, A. (2004). Synergistic penetration enhancement effect of ethanol and phospholipids on the topical delivery of cyclosporin A. *Journal of controlled release*, *97*(1), 55-66.
34. Hamel, A. R., Hubler, F., Carrupt, A., Wenger, R. M., & Mutter, M. (2004). Cyclosporin A prodrugs: design, synthesis and biophysical properties. *The Journal of peptide research*, *63*(2), 147-154.
35. Lauterbach, A., & Müller-Goymann, C. C. (2015). Applications and limitations of lipid nanoparticles in dermal and transdermal drug delivery via the follicular route. *European Journal of Pharmaceutics and Biopharmaceutics*, *97*, 152-163.
36. Haq, A., & Michniak-Kohn, B. (2018). Effects of solvents and penetration enhancers on transdermal delivery of thymoquinone: Permeability and skin deposition study. *Drug delivery*, *25*(1), 1943-1949.
37. Carrer, V., Alonso, C., Pont, M., Zanuy, M., Córdoba, M., Espinosa, S., ... & Coderch, L. (2020). Effect of propylene glycol on the skin penetration of drugs. *Archives of dermatological research*, *312*(5), 337-352.

38. Osborne, D. W., & Musakhanian, J. (2018). Skin penetration and permeation properties of Transcutol®—neat or diluted mixtures. *Aaps Pharmscitech*, *19*(8), 3512-3533.
39. Moore, T., Croy, S., Mallapragada, S., & Pandit, N. (2000). Experimental investigation and mathematical modeling of Pluronic® F127 gel dissolution: drug release in stirred systems. *Journal of Controlled Release*, *67*(2-3), 191-202.
40. Pose-Vilarnovo, B., Rodríguez-Tenreiro, C., dos Santos, J. F. R., Vázquez-Doval, J., Concheiro, A., Alvarez-Lorenzo, C., & Torres-Labandeira, J. J. (2004). Modulating drug release with cyclodextrins in hydroxypropyl methylcellulose gels and tablets. *Journal of controlled release*, *94*(2-3), 351-363.
41. Jung, Y. S., Park, W., Park, H., Lee, D. K., & Na, K. (2017). Thermo-sensitive injectable hydrogel based on the physical mixing of hyaluronic acid and Pluronic F-127 for sustained NSAID delivery. *Carbohydrate polymers*, *156*, 403-408.
42. Dėdinaitė, A., Wieland, D. F., Bełdowski, P., & Claesson, P. M. (2019). Biolubrication synergy: Hyaluronan–Phospholipid interactions at interfaces. *Advances in colloid and interface science*, *274*, 102050.
43. Hamishehkar, H., Same, S., Adibkia, K., Zarza, K., Shokri, J., Taghaee, M., & Kouhsoltani, M. (2015). A comparative histological study on the skin occlusion performance of a cream made of solid lipid nanoparticles and Vaseline. *Research in pharmaceutical sciences*, *10*(5), 378.
44. Puglia, C., Offerta, A., Tirendi, G. G., Tarico, M. S., Curreri, S., Bonina, F., & Perrotta, R. E. (2016). Design of solid lipid nanoparticles for caffeine topical administration. *Drug delivery*, *23*(1), 36-40.
45. Montenegro, L., Parenti, C., Turnaturi, R., & Pasquinucci, L. (2017). Resveratrol-loaded lipid nanocarriers: correlation between in vitro occlusion factor and in vivo skin hydrating effect. *Pharmaceutics*, *9*(4), 58.
46. Wissing, S., Lippacher, A., & Müller, R. (2001). Investigations on the occlusive properties of solid lipid nanoparticles (SLN). *Journal of cosmetic science*, *52*(5), 313-324.
47. Puri, A., Loomis, K., Smith, B., Lee, J. H., Yavlovich, A., Heldman, E., & Blumenthal, R. (2009). Lipid-based nanoparticles as pharmaceutical drug carriers: from concepts to clinic. *Critical Reviews™ in Therapeutic Drug Carrier Systems*, *26*(6).
48. Gadomski, A., Bełdowski, P., Martínez-Balbuena, L., Santamaría-Holek, I., & Pawlak, Z. (2016). Unravelling a self-healing thermo-and hydrodynamic mechanism of transient pore's late-stage closing in vescicles, and related soft matter systems, in

terms of liason between surface-tension and bending effect. *Acta Physica Polonica B*, *47*(5).

49. Ke, C., Sun, L., Qiao, D., Wang, D., & Zeng, X. (2011). Antioxidant acitivity of low molecular weight hyaluronic acid. *Food and chemical toxicology*, *49*(10), 2670-2675.
50. Lima, R., Serone, A. P., Schor, N., & Higa, E. M. S. (2001). Effect of cyclosporin A on nitric oxide production in cultured LLC-PK1 cells. *Renal failure*, *23*(1), 43-52.

SECTION II

INTRODUCTORY PART: "Exploiting Heparan Sulfate Role in Viral Entry for Broad-Spectrum Antivirals Design"

1. Introduction

The ongoing coronavirus pandemic has taught us that viral diseases represent a serious global health threat, leading to catastrophic economic and health consequences.
In the last century, we have experienced several epidemics caused by life-threatening viruses such as Ebola Virus (EBOV), Severe Acute Respiratory Syndrome Coronavirus (SARS-CoV) and Middle East Respiratory Syndrome Coronavirus (MERS-CoV), that have been limited and circumscribed[1,4]. However, unfortunately, in our contemporary society, due to globalization, viral outbreaks can easily spread from one country to another, leading us to change the approach in fighting and managing viral infections. Indeed, in the future, we are likely to face from time to time new and re-emerging viruses, and effective therapeutic strategies need to be found in order to stop possible viral outbreaks.

To date, vaccines remain the best solution to prevent viral infections and eradicate viral pathogens; however, they cannot be considered the only option since their development requires time (even if now approval from health agencies and duration of clinical trials have been shortened) and not always it is a success, like in the case of HIV (Human Immunodeficiency Virus) and Hepatitis C Virus (HCV)[5-6]. Moreover, there are several concerns about vaccines availability worldwide and their efficacy against variants[7]. Therefore, there is an urgent need for novel antiviral drugs in order to control and mitigate viral diseases and buy time before vaccines development and approval.

Current antiviral therapeutics mostly interfere with different steps of viral life cycle such as viral entry, viral DNA or RNA replication and viral enzymes[8]. Most licensed drugs are inhibitors of DNA/RNA polymerases such as nucleoside/nucleotide analogues (i.e. acyclovir and remdesivir), inhibitors of reverse transcriptase (i.e. entecavir and lamivudine) and inhibitors of viral proteases such as peptidomimetics (i.e. lopinavir, ritonavir and boceprevir)[9]. Despite the large and increasing number of emerging viruses, they have been mostly developed following the "one bug-one drug" approach and, consequently, are directed and effective against few and specific viruses like HIV, HCV, Hepatitis B Virus (HBV), Herpes Simplex Virus (HSV) and Influenza Virus[10]. Thus, this

strategy by itself cannot provide an adequate pandemic preparedness as it also emerged from clinical trials of repurposed drugs against Covid-19[11-13]. Finally, another limitation related to this approach is the rapid development of drug resistance, since viral targets can quickly mutate due to error-prone replication mechanisms[14].

Based on these considerations, broad-spectrum antiviral drugs, ideally active against a large number of different viruses families and strains, could represent a new and promising paradigm for managing and controlling viral outbreaks[15]. Despite their genomic and structural differences, the vast majority of current clinically relevant viruses share conserved features providing potential targets for the development of broad-spectrum antivirals. In this context, viral entry is a key and essential step in viruses life-cycle showing commonality, and, therefore, targeting viruses-host cells interactions constitutes a reasonable and promising approach. Inhibiting viral entry has also the advantage to potentially prevent the primary infection and its spread. Furthermore, these mechanisms are unlike to be susceptible to genome mutations thus reducing the possibility of resistance development[16].

Most viruses enter into host cells *via* endocytic or non-endocytic pathways by using receptors located into the cellular membrane[17]. However, viral attachment is not a favored process due to the electrostatic and hydration repulsions occurring between the two biomembranes[18]. Therefore, several viruses employ broadly shared cell-surface associated elements such as glycosaminoglycans and sialic acid as ancillary molecules to enable and facilitate viral entry[19-21]. In this regard, targeting these non-specific interactions can provide solid basis for the development of potential broad-spectrum therapeutics, with respect to the viruses-receptors ones that are more specific. Among them, our attention will be focused on heparan sulfate since it was found to act as common ancillary element, and in rare case as receptor, for different viruses such as HSV, Human Papilloma Virus (HPV), Dengue Virus (DENV), SARS-CoV-2 *etc*[22]. Based on this, in the last few years, several sulfated glycomimetics have been designed and have showed the ability to broadly inhibit viral infections *in* vitro as well *in vivo,* constituting promising candidates[23-24]. The current start-of-art will be illustrated and discussed in the following sections.

2. Heparan Sulfate Proteoglycans: biosynthesis and biological roles

Heparan Sulfate (HS) is a linear polysaccharide formed by repeating disaccharide units composed of sulfated glucosamine and uronic acid (UroA) residues, with various sulfation and epimerization patterns. At cellular level, it is present as heparan sulfate proteoglycans (HPSG) that are composed of a protein core covalently attached to HS polysaccharide chains[25].

HPSG biosynthesis (**Figure 1**) occurs in the lumen of the Golgi apparatus and its first step involves the sequential synthesis and attachment of a tetra-saccharide (xylose, galactose, galactose and glucuronic acid) to a serine residue of a protein core mediated by two O-xylosyltransferases and two galactosyltransferases. This is followed by the addition of a N-acetyl glucosamine (GlcNAc) unit on the terminal residue of the tetra-saccharide linkage, catalyzed by the exostosin glycosyltransferases EXTL2 and EXTL3. This latter allows the elongation of the backbone mediated by two glycosyltransferases (EXT1 and EXT2), responsible of the transfer of GlcNAc and glucuronic acid (GlcA) residues alternatively. Once elongated, the polysaccharide chains are modified by four N-deacetylase/N-sulfotransferases (NDST1-4) that mediate the de-N-acetylation and re-N-sulfation of GlcNAc residues allowing further modifications. Next, epimerization of most GlcA units into IdoA occurs catalyzed by C5-epimerase. Finally, the last step involves several O-sulfation of the polysaccharide chains mediated by three O-sulfotransferases (2-OST, 3-OST and 6-OST)[26]. In particular, a single 2-OST is responsible of the sulfation on the two position of the majority of IdoA and, to a lesser extent, GlcA residues[27]. On the other hand, three isoforms of 6-OST catalyze the sulfation on the 6-OH position of both N-Sulfo-glucosamine and GlcNAc residues, without significant substrate specificity differences[28]. Lastly, 3-OST mediates the sulfation on the 3-OH position of glucosamine residues; currently, seven 3-OST isoforms have been identified and were found to play a key role in the formation of the binding sites for several proteins such as antithrombin and HSV glycoprotein gD[29-31].

Once the biosynthetic process is completed, further modifications may occur mediated by different enzymes such as sheddases, heparanases and 6-O-endosulfatases. The sheddases are a group of enzymes, i.e. matrix metalloproteinases, elastase and cathepsins, targeting the protein core and responsible of the release of HSPGs ectodomains into the extracellular space[26]. On the other hand, heparanase is an endo-β-D-glucuronidase that acts by cleaving polysaccharide chains from the core, thus liberating short bioactive HS fragments extracellularly[32]; moreover, its activity contributes

to the extracellular matrix degradation, determining the release of different HS-binding proteins such as growth factors and chemokine[33]. Interestingly, heparanase was found to be involved in several processes such as inflammation, cancer initiation and progression, and viral infections[34]. In this context, it was identified to act as key enzyme in HSV-1 infection, being upregulated *via* the NF-kB pathway and transferred extracellularly for the degradation of the extracellular matrix where it plays a dual and contrasting role, enhancing viral particles release as well as impairing their entry[35].
Finally, 6-O-endosulfatase, existing as two isoforms SULF1 and SULF2, acts by removing 6-O-sulfate groups with a strong substrate specificity for disaccharides that are mostly located in HS functional domains[35].

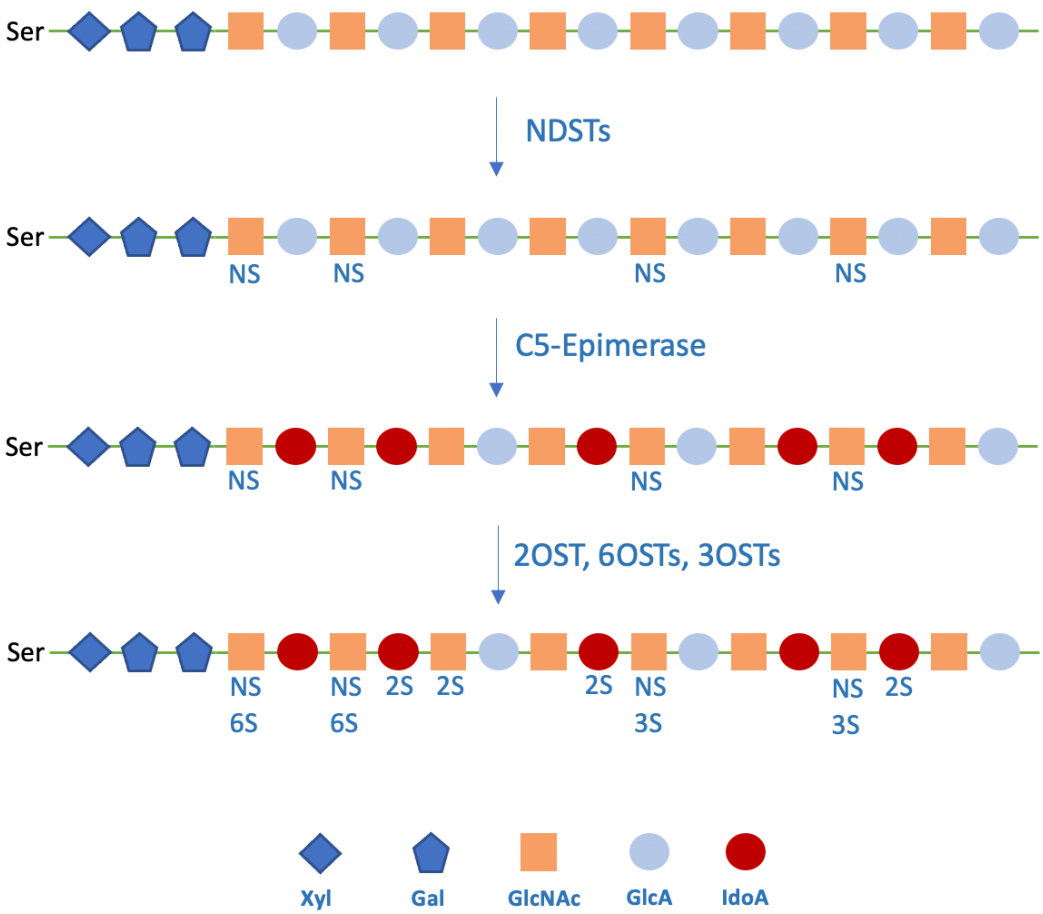

Figure 1. Schematic representation of HSPG synthetic pathway. HS structure is highly variable, and a hypothetical sequence is showed.

Based on the biosynthetic pathway and post-synthetic modifications, HSPG exhibit considerable heterogeneity in terms of structure that is reflected in their wide range of biological roles. In the light of their location, HPSG can be classified as follows: membrane-localized (i.e. glypicans and syndecans), extracellular matrix-localized (i.e. collagen XVIII, perlecan and agrin) and intracellular-localized (i.e. serglycin)[36-37].
Syndecans consist of four members and are type I transmembrane HSPG widely expressed in many tissues. They are formed by a small similar protein core with low homology extracellular domains (that can contain both HS and chondroitin sulfate chains) and conserved transmembrane and cytoplasmatic domains. Syndecans were found to bind to several HS-binding proteins in a selective way[38-39]. On the other hand, glypicans, existing under six isoforms, are highly expressed in mesenchymal and epithelial cells and are covalently linked to the cell membrane through glycosylphosphatidylinositol[40].

HPSG are ubiquitously expressed in nearly all cell types of invertebrate and vertebrate species, carrying out numerous biological roles, extracellularly and intracellularly (**Figure 2**)[41]. Firstly, extracellular HPSG, being important components of the extracellular matrix, contribute to its structural organization and integrity, thus providing adequate support to mechanical stress and cell migration[42]. Moreover, they are implicated in the regulation of solute passage through this barrier[41]. On the other hand, intracellular HSPG are mostly located in secretory vesicles and their major role is to regulate vesicles homeostasis and maturation as well as to store their components and to assist their delivery once secreted[43].

Besides these important functions, HSPG are also involved in relevant biological processes such as cell proliferation and differentiation, inflammation, cancer initiation, angiogenesis, immune response, tissue reparation *etc.*[45-49]. Most of these activities are attributable to cell-surface HSPG, since they bind to several signaling molecules such as growth factors, chemokines and cytokines, preventing their degradation, regulating their activity, and, consequently, important signaling pathways[37,50]. Moreover, in this context, HSPG were found to act as co-receptors and endocytic receptors for diverse biologically active ligands such as cell-penetrating peptides, lipoproteins, growth factors, exosomes and pathogens thus modulating lipid catabolism, infectious diseases and carcinogenesis[51-56]. For example, glypicans were shown to interact with important signaling molecules such as Wnt, Hedgehog and fibroblast growth factor, whereas

syndecans with growth factors, chemokines (i.e. interleukin 8) and viruses (i.e. HIV and HSV)[57-62].

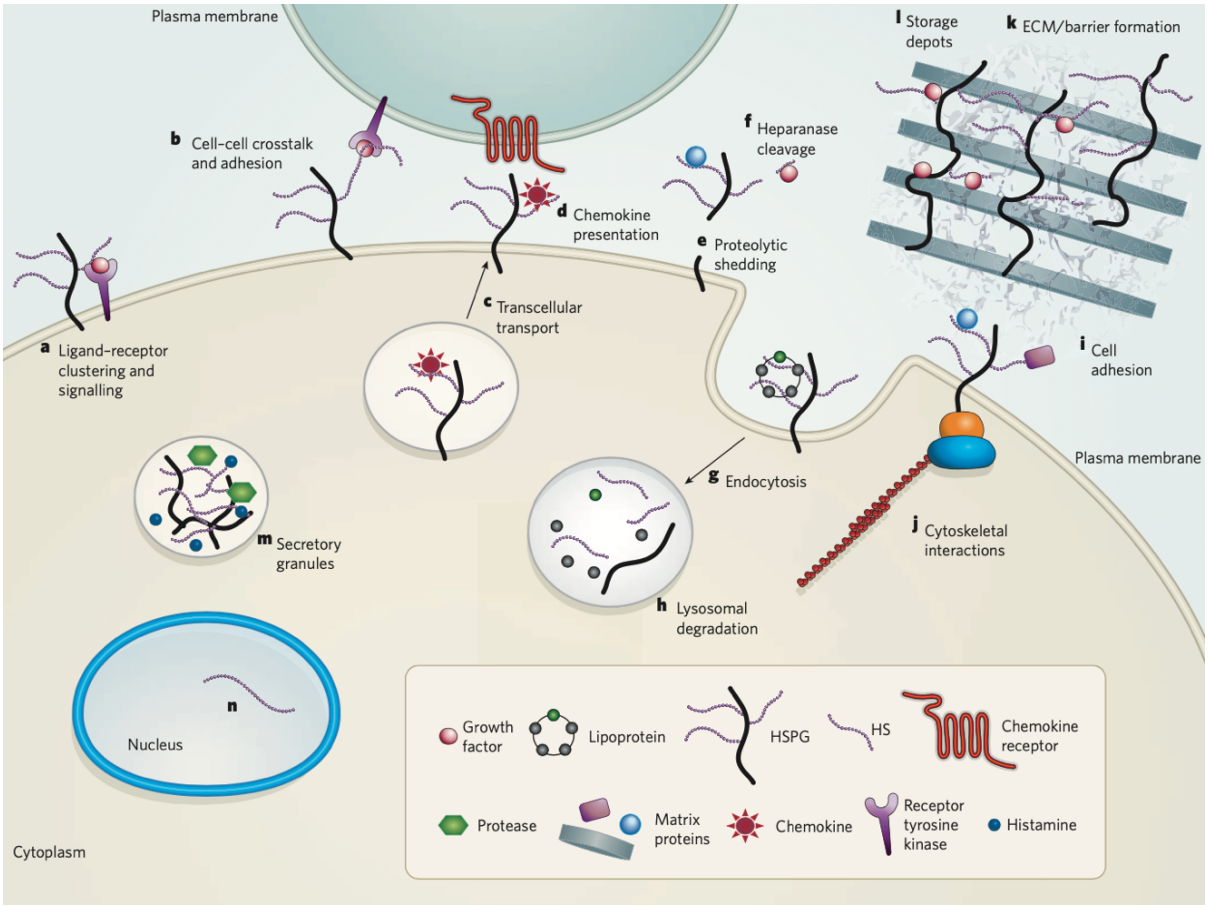

Figure 2. Schematic representation of HSPG extracellular and intracellular roles. HSPG act as co-receptors for several signaling molecules (a) and their receptors (b) both on the same cell and adjacent cells. They are involved in chemokines transcellular transport (c) and presentation (d). Post-synthetic modifications mediated by sheddases and heparinase are responsible of the release of HS fragments and bound ligands in the extracellular space (e-f). Cell-surface HSPG are internalized *via* endocytosis and can undergo lysosomal degradation or be transferred back to the cell surface (g-h). Moreover, they are involved in cell adhesion to the extracellular matrix and interact with the cytoskeleton (i-j). Extracellular HSPG contribute to the structural integrity of the extracellular matrix (k) and act as storage site for signaling molecules (l). Intracellular HSPG are mostly located into secretory granules and regulate vesicles homeostasis and maturation (m). HSPG were also found in the nucleus, but their role is still not known (n)[42]. Reproduced with permission from Springer Nature.

3. Role of Heparan Sulfate Proteoglycans in viral infections

As discussed above, several viruses employ HSPG as ancillary molecules, and in rare case as receptors, for viral entry. For this purpose, they exploit the electrostatic interactions occurring between the basic residues of their envelope glycoproteins or capsid proteins and the negatively charged polysaccharide chains of HSPG to facilitate cellular adsorption and receptor binding by increasing their concentration at the cell-surface [22]. Moreover, beside HSPG, several enzymes involved in their biosynthesis and post-synthetic modifications have showed to influence viral invasion and infection pathogenesis[63-66]. The most medically relevant HSPG dependent viruses will be discussed in this section, describing the current pharmacological treatments, highlighting the recent advances made in the development of glycomimetic agents and exploiting their potential use as broad-spectrum antivirals.

3.1 Herpes Simplex Virus

HSV is a member of the *Herpesviridae* family consisting of enveloped and double-stranded DNA viruses that can cause a wide range of human diseases. Phylogenetically, this family can be classified into three subfamilies: *Alphaherpesvirinae*, *Betaherpesvirinae* and *Gammaherpesvirinae*[67]. HSV-1 and HSV-2 belong to the alpha-group and are among the most prevalent human pathogens, affecting around 60%-90% of current population.

HSV-1 infections mainly involve the orolabial mucosa, while HSV-2 infections the genital region. Their clinical manifestation is variable, ranging from mild symptoms such as oral and genital lesions to severe and life-threatening conditions such as encephalitis and disseminated neonatal infections[68]. Moreover, HSV establishes latency in sensorial neurons, determining chronic latent infections, and, therefore, negatively impacting patients quality of life[69-71].

At present, there are no vaccines available against HSV; in the last years, several candidates (mostly subunit and DNA based) have been developed but unfortunately failed in clinical trials[72]. To date, first-line therapy for HSV is based on the administration of viral DNA polymerase inhibitors such as acyclovir, valaciclovir and famciclovir during first episodes as well as relapses. However, these drugs are not able to eradicate the

viral pathogen and are just used to alleviate symptoms. Moreover, long term treatment can cause drug resistance, in particular among immunocompromised persons[73-75].

As mentioned in the previous section, HSPG were identified to play a key role in HSV attachment to host cells and consequent membrane fusion processes[76]. In this regard, some studies suggest that their presence is not always totally essential, but, anyways, it is associated with more efficient viral penetration and lateral spread[77].

Structurally, HSV is a large virus composed of double stranded DNA genome of about 151 kilobases in length within an icosahedral capsid covered by a tegument that, in its turn, is encapsulated in an envelope[78]. At least 12 glycoproteins form the envelope, and among them, four (gB, gD, gH and gL) are necessarily required for viral entry. The process of infection begins with the initial attachment of viral particles to the cell surface, mediated by the electrostatic interactions occurring between HS chains and gB and gC viral glycoproteins[79]; although gC, unlike gB, is not considered essential for viral entry, it has been observed that its deficiency reduces viral binding[80]. In several cell types, HSV employs a particular attachment method called “viral surfing” that consists in the migration of viral particles to the cell body *via* extracellular filopodia[81].

Following viral attachment, the glycoprotein gD interacts with specific cell surface receptors such as Herpesvirus Entry Mediator, nectin-1 and 3-O-sulfated HS to promote viral fusion. Interestingly, 3-O-sulfated HS was found to act as entry receptor for HSV-1[82]. To confirm this, O’ Donnell *et al.* have demonstrated that the expression of heparan sulfate 3-O-sulfotransferase isoform 2 can trigger HSV-1 entry and cell-to-cell fusion into Chinese hamster ovary K1, a cell line resistant to HSV entry[83]. In this regard, several synthetic 3-O-sulfated HS oligosaccharides have been designed and showed effective inhibition of HSV-1 entry *in vitro*[84-85]. On the other hand, 3-O-sulfated HS does not act as cellular receptor for HSV-2 entry, and it is only involved in viral attachment[86]. Therefore, gD binding to its cellular receptors triggers conformational changes that initiate viral fusion processes mediated by gB and the heterodimer gL and gH[87].

On the basis of these entry mechanisms, at first, naturally occurring polysaccharides structurally similar to HS, including heparin and carrageenan, were investigated as antiherpetic agents and showed effective inhibition of HSV infection in *vitro*[88-89]. However, despite the promising results, several concerns regarding heparin safety have been raised. Thus, in the past years, numerous semi-synthetic and synthetic HS-mimetic polymers have been designed and tested against HSV[90].

Among the different polymeric systems, polyglycerols have emerged as interesting and attractive candidates due to their safety and advantageous pharmacokinetic properties. Recently, various polyglycerol-based scaffolds such as graphene sheets and nanogels have been developed, exhibiting promising and reasonable inhibition profiles against HSV[91-92]. In this context, a study conducted by Pouyan *et al.* is of particular interest, since it investigates the effect of flexibility and molecular architecture on the antiviral activity of sulfated polyglycerols. In particular, four structural different polyglycerol sulfates, including one flexible linear (LPGS), two dendronized ($DenPG_{0.5-1}$) and one hyperbranched (hPGS), were evaluated and compared in terms of inhibition profiles; interestingly, *in vitro* results showed that flexibility is positively correlated with antiviral potency (attributable to the increased contact area), highlighting, moreover, the importance of multivalency (**Figure 3**)[93].

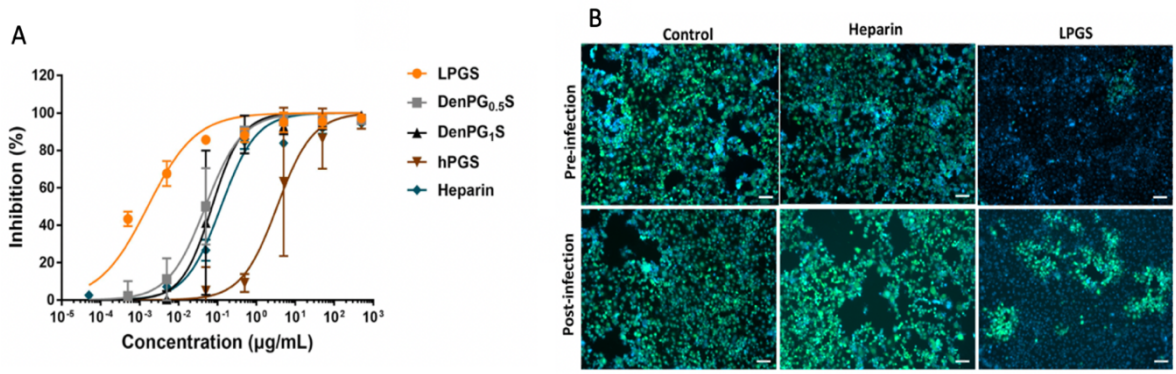

Figure 3. Dose response curves of LPGS, $DenPG_{0.5}S$, $DenPG_1S$, hPGS and heparin against HSV-1 in Vero E6 cells (a). Fluorescent microscopy images of Vero E6 cells infected with HSV-1 and treated with 10 ug/ mL of heparin and LPGS in pre- and post-infection conditions. Total cells are marked blue and infected cells green by the green fluorescent protein (b).[93] Adapted with permission from American Chemical Society.

However, one of the main drawbacks of the use of polymeric scaffolds as therapeutics regards their complex synthesis and heterogeneity. In this regard, as an alternative approach to polymeric systems, Gangji *et al.* designed and proposed an interesting series of small synthetic non-saccharide glycosaminoglycan mimetics with high binding affinity to gD, exhibiting Kd values ranging from 8 to 120 nM. *In vitro*, they reasonably inhibited HSV-1 entry with micromolar IC_{50} values (0.4-1) in HeLa, HFF-1, and VK2/E6E7

cell lines, constituting promising starting candidates, that, however, need to be verified in *in vivo* studies[94]. Another interesting glycomimetic platform was reported by Lee *et al.* that synthetized mesoporous silica nanoparticles functionalized with a hydrophobic glycomimetic ligand (sodium benzene sulfonate) and evaluated their potential efficacy as HSV-1 and HSV-2 entry inhibitors. The use of nanoparticles as scaffolds results to be advantageous since their multivalency and high surface-area-to-volume ratio could optimize and enhance their contact and interactions with viral particles. In fact, the reported results showed that these glycomimetic platforms inhibited significantly both HSV-1 and HSV-1 infection *in vitro*, acting mainly on the early stages such as viral attachment; moreover, a positive correlation between ligand density and antiviral activity was confirmed[95]. On the basis of these data, in a later study, the authors implemented this glycomimetic scaffold loading acyclovir into the mesoporous silica nanoparticles, obtaining an interesting system with a dual mechanism of action, acting on both viral entry and replication[96].

3.2 Human Papilloma Virus

HPV is a member of the *Papillomarividae* family, consisting of small and non-enveloped double stranded DNA viruses. Phylogenetically, this family can be further classified in the following genera: alpha, beta, gamma, mu and nu. To date, more than 200 HPVs have been identified[97].

HPV infects the epithelial cells of oral mucosa, genital mucosa or skin, ranging from asymptomatic infections to malignant lesions. In fact, 14 mucosal HPVs have been classified as high risk and are associated with cervix, vagina, anus and oropharyngeal cancers. Most cervical cancer cases are caused by HPV[98-99]. HPVs are among the most common sexually transmitted viruses and, currently, three vaccines (Gardasil, Gardasil9 and Cervarix) are approved[100]. However, no antiviral drugs are available.

Despite the numerous types, HPVs share the same structural organization, containing a circular double stranded DNA genome of about 8 kilobases in length within a non-enveloped icosahedral capsid formed by 360 molecules of protein L1, which plays a fundamental role in viral entry[101]. As for HSV, HSPG were identified to act as attachment factors for HPV [102]. In this regard, Giroglou *et al.* clearly demonstrated that cell surface HS is essential for HPV-11 and HPV-33 pseudoinfection *in vitro*; in fact, the removal of HS from cell surface, obtained by treating COS-7 cells with heparinase I, determined a

complete inhibition of HPV infection[103]. A similar approach was adopted by Johnson *et al.* to confirm HSPG dependency *in vivo*; in a murine cervicovaginal model, heparinase III treatment significantly inhibited HPV-16, HPV-31 and HPV-5 PsV infection and their cellular and basal attachment[104]. Interestingly, among the different HPSG types, extracellular matrix and cell-surface syndecans were found to be mainly involved in HPV attachment[105]. Moreover, several studies indicate that HSPG processing enzymes, including matrix metalloproteinases and heparinase, promote keratinocytes infection[106-107]. In addition to HSPG, also laminin-5 was proposed as extracellular membrane binding factor, but it resulted to be less involved compared to HSPG[108].

Therefore, virus-HSPG interactions induce conformational changes that lead to L2 proteolytic cleavage mediated by furin. This is followed by the dissociation of viral particles from HSPG and their subsequent binding to a second unknown receptor. In this context, one of the proposed candidates was α6 integrin, however, to date, several steps of HPV entry still remain unclear; in fact, unlike the majority of non-enveloped viruses, its entry seems to be clathrin-, caveolin-, cholesterol- and dynamin- independent[109-111].

As well as for HSV, natural sulfated polysaccharides such as heparin and carrageenan were shown to inhibit viral particles entry and attachment *in vitro* as well *in vivo*[104,112]. Thus, based on these observations, several semi-synthetic and synthetic HS-mimetic polymers have been developed and investigated as anti-HPV agents over the last decades[110]. In this context, particularly interesting is a sulfated chitosan derivative designed and proposed by Gao *et al.* In this study, 3,6-O-sulfated chitosan was prepared and tested *in vitro* against HPV-16 PsV in four different conditions: pretreatment of virus, pretreatment of cells, adsorption and post adsorption. Surprisingly, it inhibited HPV infection in all the conditions (**Figure 4**), hypothesizing a multiple mechanism of action involving not only viral attachment but also later steps; in particular, the authors state that a possible target could be PI3K/Akt/mTOR, a signaling pathway involved in HPV-16 entry, since, in this study, 3,6-O-sulfated chitosan was shown to inhibit the phosphorylation of Akt and mTOR protein[113].

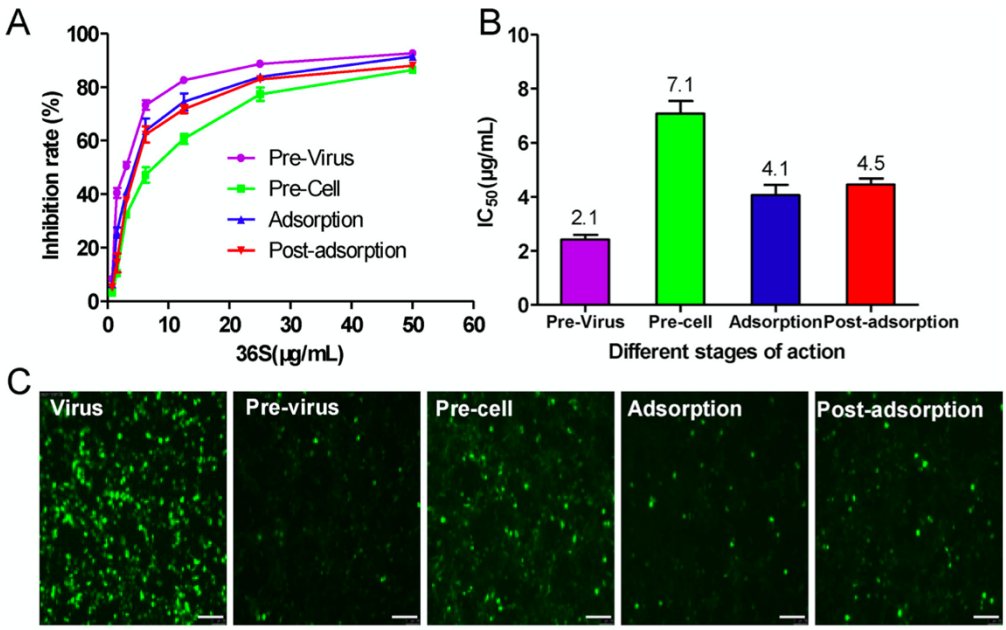

Figure 4. Dose response curves and IC_{50} values of 3,6-O-sulfated chitosan against HPV-16 PsV in 293FT cells tested under four different conditions: pretreatment of virus, pretreatment of cells, adsorption and post adsorption (a-b). Inverted fluorescent microscopy images of 293FT cells infected with HPV-16 PsV and treated under the indicated conditions with 3,6-O-sulfated chitosan (12.5 mg/ml) taken at 72 h p.i. (c)[113]. Reproduced with permission from Elsevier.

Another innovative glycomimetic platform was developed by Lembo *et al.* Herein, heparin based nanoassemblies were obtained *via* the self-association of O-palmitoyl-heparin and α-cyclodextrin, resulting in hexagonal structures comparable to traps for viral particles. Positive results emerged from *in vitro* studies that showed a significative inhibition not only of HPV-16 infection, but also of other different HSPG dependent viruses (HSV-1, HSV-2 and RSV), with micromolar IC_{50} values ranging from 0.42 μg/ml to 2.88 μg/ml. However, one of the main drawbacks of heparin derivatives is their, even if lower, anticoagulant activity, which in this study was found to be positively correlated with the antiviral potency[114]. Therefore, an interesting alternative to heparin derivatives was recently proposed by Soria-Martinez *et al.* In this work, several sulfated glycomimetic polymers with amidoamine or carbon-based backbone were synthetized and exhibited reasonable inhibition profiles, strongly influenced by their structure and length, against several HSPG dependent viruses such as HPV-16, HSV-1 and HSV-2 and Merkel Cell

Polyomavirus. Most importantly, their anti-HPV activity was also confirmed *in vivo*, exerting a prophylactic effect in a murine model for HPV-16 genital infections[115].

3.3 Human Immunodeficiency Virus

HIV is a member of *Retroviridae* family consisting of enveloped single stranded RNA diploid viruses. Two main types of HIV have been identified: HIV-1 and HIV-2. HIV-1 is more pathogenic and common compared to HIV-2. It infects $CD4^+$ T cells, causing their depletion *via* several pathways, and, having, therefore, a considerable impact on the immune system[116-117]. The last stage of HIV infection is acquired immunodeficiency syndrome (AIDS), defined by the occurrence of oncological and infectious complications.

At present, HIV continues still to have a significative impact on global health with over 600.000 deaths and 1.5 million of new infections in 2020, but, surely, it can be considered less severe compared to the past decades[118]. In fact, the development of the antiretroviral therapy (ART) has brought important benefits in the management of HIV infection, considerably improving patients quality of life and life expectancy. ART consists in a combination of anti-HIV drugs (i.e. nucleoside analog reverse transcriptase inhibitors, non-nucleoside analog reverse transcriptase inhibitors and protease inhibitors) and have resulted to be very effective at suppressing viral replication and inducing immune restoration[119-120]. However, HIV-infected adults under ART have an increased risk of cardiovascular, bone and renal diseases[121-123]. Moreover, anti-HIV therapeutics, despite their efficacy, are not curative. In this regard, vaccines represent the only way to eradicate definitely this pathogen, but, unfortunately, there are no licensed vaccines available. The biggest problem faced in their development regards the high mutation rate of HIV[124].

Structurally, HIV is composed of two copies of genomic RNA within a conic capsid enclosed in an envelope formed by the surface enveloped glycoprotein (gp120) and the transmembrane envelope glycoprotein (gp41) organized in “spikes”[125]. In this regard, the surface envelope glycoprotein gp120 was found to play an important role in viral entry, mediating all the attachment processes. HIV entry begins with the attachment of viral particles to cell-surface, which was found to be mediated by different attachment “receptors” such as HSPG, α4β7 integrin and Dendritic Cell Specific ICAM-3-Grabbing Non-integrin[126]. Several studies support HIV dependency on HSPG for its entry into host cells[127]; in this regard, one of the first studies was conducted by Mondor *et al.* and

showed that sulfated polysaccharides, including heparin and dextran sulfate, and cell surface depletion of HS, obtained with heparinase treatment, significantly inhibited HIV-1 infection in HeLa-CD4 cells[128]. Interestingly, among the different HPSG types, cell-surface syndecans were found to be mainly involved in HIV attachment. In fact, in an *in vitro* study conducted by Saphire *et al*. HSPG, in particular syndecans, were shown to be able to succumb to CD4 deficiency, allowing HIV entry in human macrophages[129]. Syndecans role in HIV infection was also supported in another study in which they were identified to act as *in trans* receptors in permissive cells[130].

Following viral attachment, HIV binds to CD4 and undergo conformational changes that lead to the engagement of viral particles to the coreceptors CCR5 and CXCR4 that, in their turn, mediate membrane fusion processes[126]. The V3 loop of gp120 was firstly identified as major HS binding site but later studies recognized also the involvement of V2 and CD4-induced domains[131-132]. Based on these data, it is possible to hypothesize that HSPG are also implicated in other later steps, however their role remains still unclear. In view of these observation, Baleux *et al.* proposed an interesting and innovative strategy, designing a biomimetic platform able to target in parallel both CD4 and HS binding domains. In particular, they synthetized a glycoconjugate consisting in a small CD4 mimetic peptide and a HS dodecamer that was shown to bind with high affinity to the CD4-induced domain of gp120. This latter prevented its interaction with CD4, consequently determining the exposure of the HS binding site, that, in its turn, was blocked by the glycomimetic portion. As result of its mechanism of action, the proposed glycoconjugate exhibited significative inhibition profiles against R5-, X-4 and dual tropic HIV infection *in vitro* with nanomolar ED_{90} values (3-11 nM)[133].

Besides this, as for HSV and HPV, once observed the anti-HIV activity of heparin, several natural occurring and synthetic sulfated polysaccharides such as carrageenan, sulfated derivatives of bacterial glycosaminoglycans *etc.* were evaluated as potential anti-HIV agents[90]. In this regard, particular attention should be given on anionic polymer-based microbicides, such as PRO 2000 and Vivagel (consisting in naphtalenesulfonate polymers), Carraguard (carrageenan based) and Ushercell (cellulose sulfate based) that reached clinical trials but, despite the initial and promising results, unfortunately failed in Phase II/III[134]. These failures have raised several questions that will be discussed in the following paragraphs.

3.4 Respiratory Syncytial Virus

RSV is an enveloped single-stranded RNA virus belonging to the *Paramyxoviridae* family. Based on its genomic features, it can be further classified in two subtypes: A and B. This latter seems to be less pathogenic compared to the A subtype[135]. It is the main causative agent of acute respiratory infection in infants, imposing a significant pediatric burden; in fact, it is estimated to cause 3 million of hospitalizations and 60.000 deaths in young children each year. Besides this, RSV can also cause severe diseases in elderly and high-risk adults[136-137]. To date, despite multiple attempts, there are no licensed vaccines available. The only FDA-approved drugs are Palivizumab, a monoclonal antibody indicated for prophylaxis in high-risk children, and aerosolized ribavirin for treatment[138-139].

Structurally, RSV is composed of single stranded RNA genome of about 15.2 kb in length, enclosed in an envelope formed by G, F and SH surface glycoproteins. The G glycoprotein is mainly involved in attachment processes, while F in membrane fusion[140]. RSV life-cycle starts with the initial attachment of viral particles to the cell-surface, mediated by the interactions occurring between G and diverse attachment factors. In particular, HSPG and the fractalkine receptor CX_3C-chemokine receptor were proposed as ancillary agents[141]. In this regard, a series of *in vitro* studies conducted by Hallak *et al.* not only showed RSV dependency on HSPG but also highlighted the importance of N-Sulfation and the presence of IdoA residues for G-HSPG interactions[142-143]. In particular, the heparin binding site of G was identified in its ectodomain, consisting in a linear sequence of basic amino acids[144]. However, despite its undisputed role in RSV attachment, the glycoprotein G was shown to be not totally essential for viral entry, highlighting a potential role of F-RSV[145]. In this context, also this latter was found to interact with HS *in vitro*, may promoting viral attachment and infectivity[146]. However, it was observed that for viral particles expressing only F, their dependency on HSPG is less pronounced[147].

Although there are several studies suggesting a potential role of HSPG in RSV entry, on the other hand, it is important to report that there are contrasting opinions on their presence on human epithelial airway cells[141]. To date, several steps of RSV entry still remain unclear. Thus, despite the potential role of HS in RSV entry, the scientific community has not really explored HSPG as target for the design of antiviral agents, with respect to other HSPG-dependent viruses.

3.5 Hepatitis C Virus

HCV is a member of the *Flaviviridae* family that consists in enveloped positive-strand RNA viruses. It can cause both acute and chronic infections. Approximately, 70% of infected persons develop chronic hepatitis C that may result in life threatening conditions such as hepatic fibrosis, cirrhosis and hepatocellular cancer[148].

According to WHO, there are currently about 58 million of patients with chronic hepatitis and 1.5 million of new cases each year[149]. At present, despite several attempts, there are no vaccines available[150]. However, fortunately, the introduction of direct-acting antiviral agents has completely revolutionized and improved the pharmacological treatment of HCV. These therapeutics act by targeting the viral enzymes NS3/4A and NS5B (i.e. sofosbuvir and telaprevir) and the non-structural protein NS5A (i.e. ledipasvir), and are usually given in combination, showing high cure rates around 90%[151-152]. However, at present, many cases of HCV infection are not diagnosed and treated. Although direct-acting antivirals proven efficacy, failure is still occurring in a small percentage of patients due to the genetic variability of HCV, and, therefore, the presence of resistant variants and virological breakthrough[153-154]. Thus, the development of broad-spectrum agents could be very beneficial due to the large number of viral subtypes.

Structurally, HCV contains a linear positive-sense single-stranded RNA genome approximately of 9.6 kb in length within an icosahedral capsid enclosed in an envelope formed by two glycoproteins, E1 and E2, organized in spikes[155]. HCV infection begins with the attachment of viral particles to hepatocyte surface; this process involves the envelope glycoproteins E1 and E2, virus-associated apolipoproteins, and several attachment host-factors such as HSPG and LDL receptor[156-158]. Firstly, HSPG dependence of HCV was demonstrated in an *in vitro* study conducted by Barth *et al.* in which was reported that heparin, liver-derived HS and heparinase treatment significantly inhibited HCV entry in HepG2 and MOLT-4 cell lines, identifying a basic amino acids sequence localized in the N-Terminus of E2 as HS binding domain[159].

Interestingly, in addition to E2, also viral ApoE was found to mediate viral attachment *via* interactions with HSPG. In this regard, Lefreve *et al.* clearly demonstrated ApoE role in viral entry and, in particular, a small region rich in basic amino acids located in the RBD was shown to be critical for mediating these interactions. Also in this case, syndecans, primarily syndecan-4, resulted to be mainly involved, and N- and 6-O sulfation required[160-162].

Unfortunately, except some semisynthetic heparin derivatives, to the best of our knowledge, there are no significant studies exploiting this concept for the development of potential antiviral agents[163].

3.6 Severe Acute Respiratory Syndrome Coronavirus 2

SARS-CoV-2 is a large, enveloped single-stranded RNA virus belonging to the *Coronaviridae* family. As is well known, it is the aetiologic agent of the current Covid-19 pandemic. It attacks the respiratory tract and its clinical manifestation is variable, ranging from asymptomatic infections to severe and life-threatening conditions such as interstitial pneumonia, leading, moreover, to multiorgan complications[164-168].

At the beginning of the pandemic, several licensed antiviral therapeutics were repurposed in clinical trials in patients with Covid-19 but resulted to be ineffective, despite the encouraging *in vitro* as well *in vivo* results[11-13, 164]. Therefore, the catastrophic impact of Covid-19 pandemic on global health and society has led to a massive effort by the scientific community to develop effective vaccines and therapeutics. However, unfortunately, to date, there are no new antivirals approved. In this regard, it is worth to mention that Merck & Co. has recently announced the clinical-trial success of molnupiravir, a drug candidate targeting the viral enzyme RNA polymerase[169-170]. On the other hand, incredibly, four effective vaccines have been approved from EMA and FDA, including Comirnaty (Pfizer- BioNTech), Spikevax (Moderna), Vaxzevria (Astrazeneca) and Janssen (Johnson & Johnson). Fortunately, current mass vaccination is giving important and considerable results in fighting the pandemic, significantly reducing infection, hospitalization and mortality rates. However, given the high genetic variability of SARS-CoV-2, several concerns regarding vaccines efficacy against variants are emerging, leading to booster campaigns. In fact, the spread of Delta variant has led to a reduced effectiveness of vaccines in preventing the infection, but, however, protection from hospitalization and death still remains significative[171-173]. On the basis of these considerations, broad-spectrum antivirals, together with vaccines, could represent a fruitful strategy in the fight against potential new-emerging variants.

Structurally, SARS-CoV-2 contains a single-stranded positive sense RNA genome of about 29.9 kb in length, within a capsid formed by the nucleocapsid protein N, encapsulated in an envelope that, in its turn, contains three proteins: the membrane

protein (M), the envelope protein (E) and the spike glycoprotein (S). This latter was identified as key element in viral entry into host cells[174-175].

In the last months, several studies supporting a potential role of HSPG in SARS-CoV-2 entry have been published[176-180]. In this regard, it is worth to mention the model proposed by Clausen *et al.* in which HS is assumed to act as co-attachment factor, enhancing, moreover, the binding of S to its cellular receptor ACE2. Based on docking studies, the HS-binding site may be located in the RBD domain of S, close to the ACE2 binding site[179]. Other studies propose also a HS-binding motif at the S1/S2 site[181]. Regarding HS, 2-O and 6-O-sulfation are considered critical for its interaction with the spike glycoprotein S[22].

Recently, numerous studies demonstrating the inhibitory activity of heparin against SARS-CoV-2 infection and entry have been reported[176,178-179,182]. In this regard, the study conducted by Kwon *et al.* is of particular interest, since it investigates and compares the anti-SARS-CoV-2 activity of different sulfated polysaccharides, previously identified by surface plasmon resonance studies, such as two fucoidans (RPI-27 and RPI-28), non-anticoagulant low molecular weight heparin, chemo-enzymatically synthesized trisulfated (TriS) heparin, and unfractionated USP-heparin. Interestingly, they all inhibited SARS-CoV-2 infection in Vero Cells with IC_{50} values ranging from 0.083 μM (for RPI-127) to 55 μM (for non-anticoagulant low molecular weight heparin)[183]. A detailed study exploiting the effect of the molecular architecture, flexibility, molecular weight and sulfation degree on the anti-SARS-CoV-2 activity of sulfated polymers has been recently reported by Nie *et al.*[184]. In particular, two sulfated polyglycerols with different structure, such as LPGS (linear) and HPGS (hyperbranched), were used as models. Interestingly, the sulfation degree was found to be positively correlated with the antiviral activity, and, moreover, the molecular architecture resulted to be a critical parameter; in fact, LPGS showed a two-fold higher inhibitory activity compared to the corresponding (in terms of sulfation degree and size) hyperbranched form (**Figure 5**). This result may be attributable to the greater flexibility of the linear polymer that results in a greater adaptation and binding to the spike glycoprotein, as it also emerged from affinity studies against the RBD. However, in this study, LPGS was shown to lose its inhibitory effect upon dilution. This observation brings to light one of the major problems faced in the development of supramolecular inhibitors that will be discussed and examined in the next section.

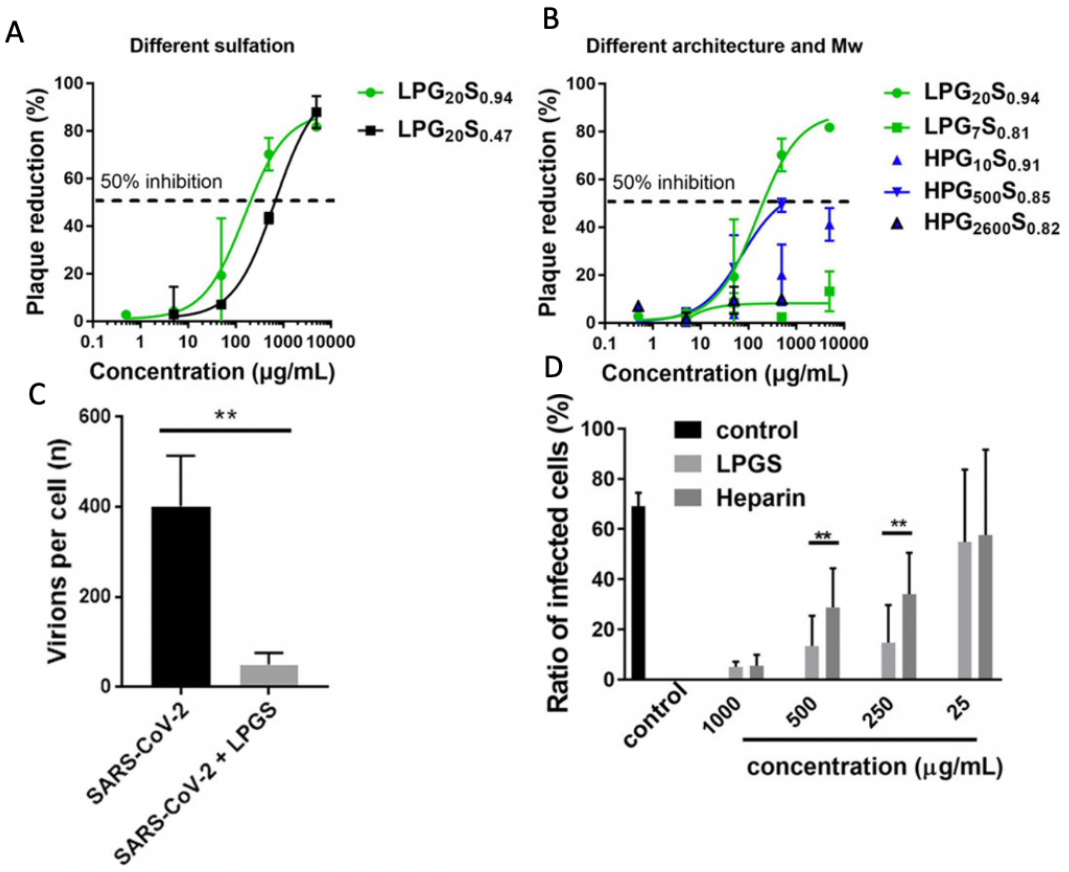

Figure 5. Inhibition profiles of LPGS with different degrees of sulfation (a) and of LPGS and HPGS with different molecular weights (b) against SARS-CoV-2 in Vero E6 cells. Number of viral particles attached to Vero E6 cells infected with SARS-CoV-2 and treated with LPGS obtained from confocal microscopy studies (c). Ratio of infected Vero E6 cells with SARS-CoV-2 after treatment with LPGS or heparin obtained from fluorescent microscopy images[184]. Adapted with permission from Wiley.

4. Glycomimetic virucidal agents: state of the art

Although the concept of HS-mimetic agents as potential broad-spectrum antivirals is promising and reasonable, one of the biggest challenges faced in this approach regards their virustatic, reversible behavior. In fact, they act as competitive binding inhibitors exploiting electrostatic interactions that, however, are by nature reversible and therefore may not be sufficient for an irreversible effect in physiological conditions. Thus, virustatic agents result to be irrelevant from a clinical point of view, since viral particles, once released upon dilution, remain infectious[185]. As evidenced in the previous paragraphs,

the majority of glycomimetic agents was mostly evaluated in terms of their antiviral activity *in vitro* and, consequently, there is a lack of *in vivo* data. Nevertheless, clinical trials of anionic polymer-based microbicides reveled their ineffectiveness in HIV pre-exposure prophylaxis.

In the light of these observations, a virucidal drug, able to irreversibly damage viruses, could represent a fruitful and ideal approach in the treatment of viral infections. However, into this category fall highly toxic agents such as detergents, disinfectants, strong acids *etc.* and, to date, there are no virucidal agents approved for human use. Thus, an ideal virucidal drug should selectively and irreversibly target the virus without damaging its host, keeping the broad-spectrum activity of virustatic agents.

In this context, the innovative concept proposed by Stellacci's group was a notable step forward[186]. They designed a unique glycomimetic platform by coating round shaped gold nanoparticles (AuNPs) with11-mercaptoundecanesulfonic acid (MUS) and 1-octanethiol (OT), a HSPG mimetic and a hydrophobic ligand, respectively. Notably, MUS OT AuNPs exhibited broad-spectrum activity, inhibiting several HSPG-dependent viruses (i.e. HSV-1, HSV-2, HPV-16 and RSV) infection with nanomolar IC_{50} values *in vitro*. Standard dilution assays were performed against HPV-16, RSV, DENV and HSV-2 and revealed their virucidal mechanism of action; on the other hand, AuNPs functionalized with a short sulfonated ligand such as 2-mercaptoethane sulfonic acid (MES) were found to be virustatic, losing their antiviral activity upon dilution with full recovery of the viral infectivity (**Figure 6**). MUS OT AuNPs antiviral efficacy was confirmed *in* ex-vivo studies against HSV-2 in Epi-Vaginal tissues, proving, moreover, their preventive activity. Positive results emerged also from *in vivo* studies: in a murine model with RSV infection, MUS OT AuNPs prevented the spread of the infection to the lungs, circumscribing it to the upper respiratory tract.

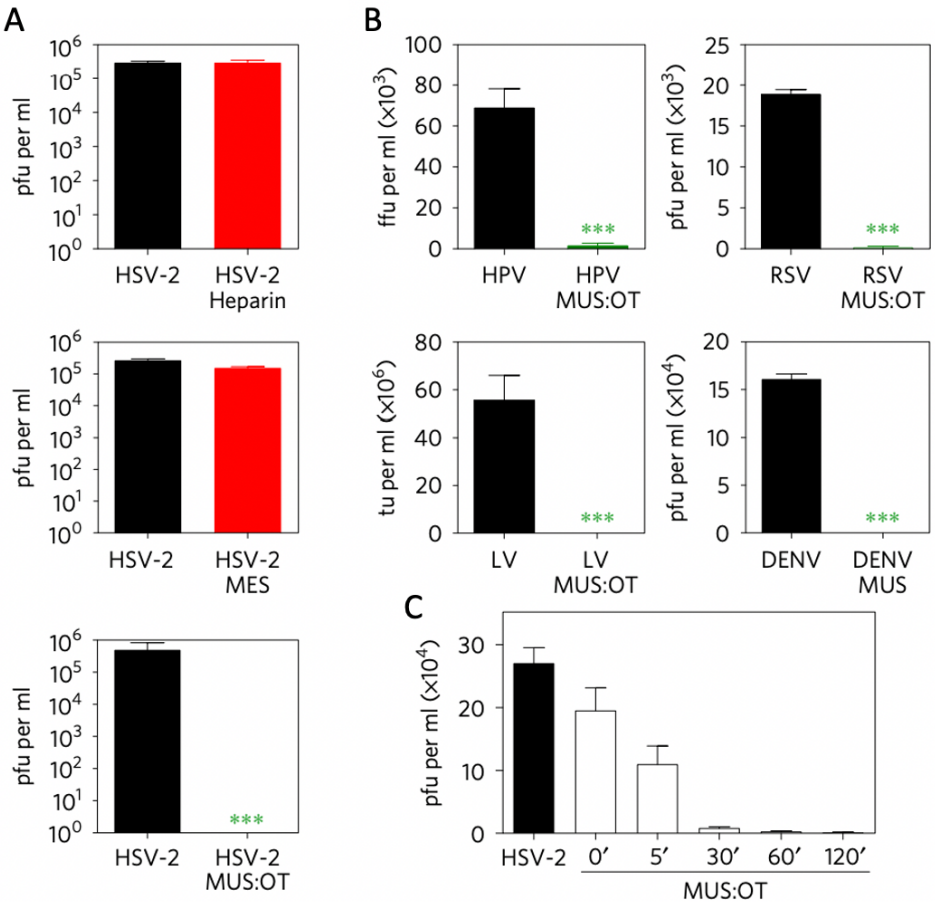

Figure 5. Virucidal assays of MUS:OT AuNPs, MES AuNPs and Heparin against HSV-2 in Vero E6 cells (a). Virucidal assays of MUS:OT AuNPs against DENV, RSV, HPV and LV in Vero E6 cells (b). MUS:OT AuNPs inhibitory activity on HSV-2 in function of time (minutes) (c)[186]. Adapted with permission from Springer Nature.

The introduction of a rigid core and long and hydrophobic linkers allowed to achieve a multivalent, flexible system able to strongly and broadly bind to viral particles, generating mechanical stresses and distortions on the viral capsid/envelope. If strong enough, these latter can lead to a global structural deformation with consequent irreversible viral breakage and deactivation, as also observed in Cryo-TEM studies (**Figure 7**).

These hypotheses were further strengthened in a later study in which beta-cyclodextrin was employed as rigid core instead of AuNPs[188]. Similarly to AuNPs, MUS modified cyclodextrins showed broad-spectrum virucidal activity; moreover, DNA exposure assay was performed and further confirmed the breakage of the viral envelope and capsid induced by MUS cyclodextrins.

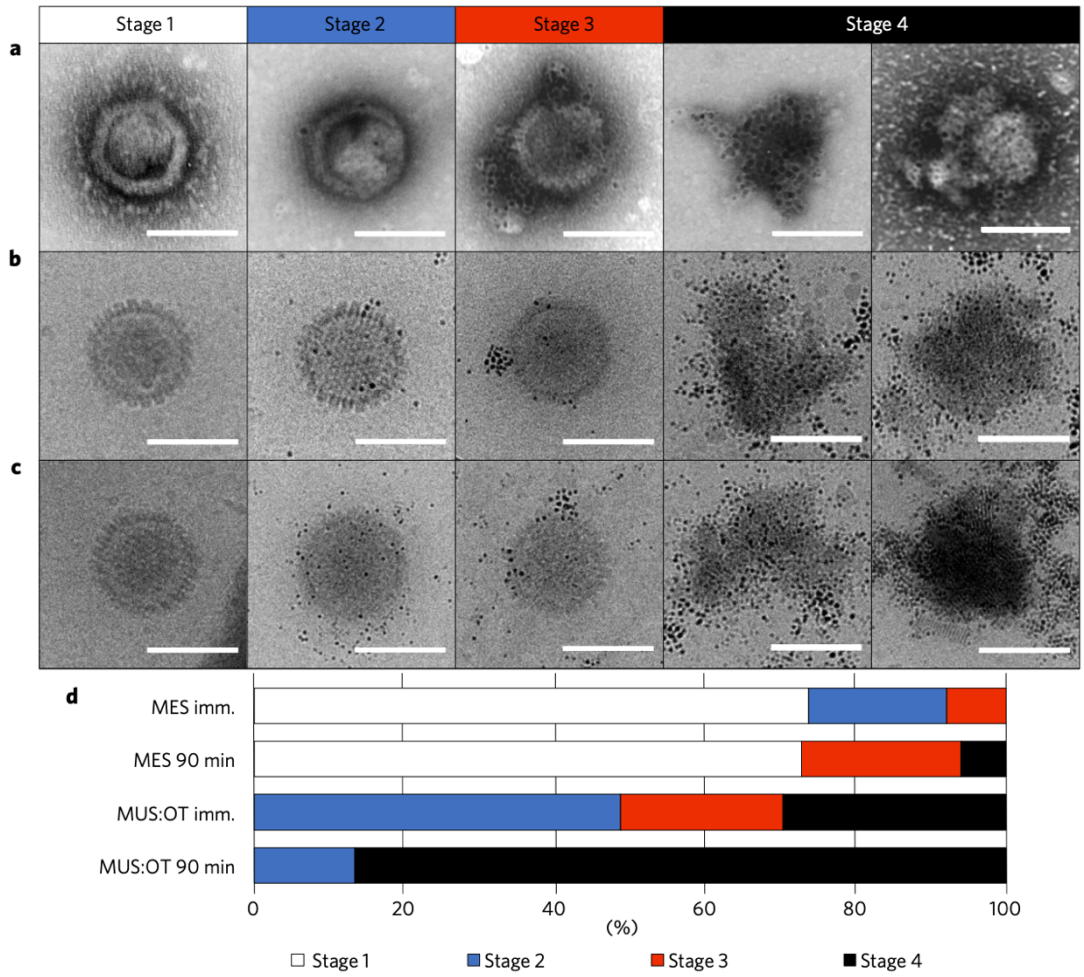

Figure 7. Negative stained transmission electron microscopy (a) and cryo-transmission electron microscopy (b-c) images of viral particles (HSV-2) exposed to MUS:OT AuNPs. In particular, stage 1 shows virus without particles associated; stage 2: virus with some particles associated (mostly isolated); stage 3: clusters of AuNPs associated to the viral particle; stage 4: irreversible deformation of the viral particle with consequent damage and breakage. Percentage of each stage after exposing MES and MUS:OT AuNPs to HSV-2 particles in function of the time (d)[186]. Adapted with permission from Springer Nature.

4.1 Research question and aim of the project

The studies previously performed by Stellacci's group so far show the potential of these HSPG-mimetic systems (AuNPs and cyclodextrins) as broad-spectrum antivirals. In particular, the reported results suggest that the antiviral mechanism of action is correlated with their chemical and structural features; however, an in-depth study is required to clarify important aspects of this approach. Therefore, my research project fits in this context and it aims to unravel their mechanism of action, investigating the

structure-activity relationships and identifying the key parameters required for a virucidal activity. In particular, the effect of the hydrophobicity and flexibility of the ligands, and the type and size of the core is explored. For the first purpose, we chose the length of the sulfonated ligand as parameter to vary and examine, since it is strongly correlated with the flexibility and hydrophobicity. To this end, a library of sulfonated alkanethiols of different length was synthetized and used for the preparation of AuNPs that were characterized in terms of size, molecular weight, ligand density and composition. Thus, their antiviral activity against HSV-2 was evaluated in dose-response and virucidal assays. Based on these results, we decided to study the effect of the presence of a hydrophobic linker (OT) with a “virustatic” sulfonated ligand. Then, to further assess the importance of hydrophobic interactions and evaluate the effect of the core size on the antiviral mechanism of action, we switched to a smaller system, and a series of gold nanoclusters (AuNCs) coated with sulfonated linkers of different length and hydrophilic ligands was synthetized and compared for their inhibitory activity on HSV-2. Finally, to have a complete and comprehensive view on this topic and investigate the effect of the core, the results of a parallel project focused on sulfonated cyclodextrins are reported and a comparative analysis between the different systems is also discussed. Herein, we have chosen HSV-2 as HSPG-dependent virus model.

EXPERIMENTAL PART

1. Materials and Methods

1.1 Materials

11-bromo-1-undecene, 10-bromo-1-decene, 9-bromo-1-nonene, 8-bromo-1-octene, 5-bromo-1-pentene, 4-bromo-1-butene, sodium sulfite, benzyltriethylammonium bromide, thioacetic acid, sodium hydroxide, gold(III) chloride trihydrate, sodium borohydride, L-glutathione reduced, 1-octanethiol, oleylamine (>98%), tetrabutylammonium bromide, acetyl chloride and iodine were purchased from Sigma Aldrich (Schaffhausen, Switzerland). All solvents were HPLC-grade and purchased from Sigma Aldrich (Schaffhausen, Switzerland).

1.2 Instruments

All proton nuclear magnetic resonance (^{1}H-NMR) spectra were recorded using a Bruker Avance III 400 MHz and data analysis was performed with Mestrenova. All mass spectra were obtained by electrospray ionization (ESI) in negative mode using a Xevo G2-S QTOF. UV-Vis spectra were recorded at 25 °C on a Lambda ™ 365 spectrophotometer (PerkinElmer). Thermogravimetric analysis (TGA) was performed with TGA 4000 (PerkinElmer), under N_2 flow heating up from 30 °C to 900 °C at a ramp rate of 10°C/min. Samples were prepared by inserting ~ 5 mg of sample into a ceramic pan. Talos L120C G2 electron microscope operating at 120 kV was used for TEM analysis. Samples were prepared by directly depositing an aliquot of sample into carbon copper grids and dried before imaging. The core size of particles was determined with FIJI (Imagej). Dynamic light scattering analysis was performed with Nano Zetasizer (Malvern) at 25 °C, a scattering angle of 90° and a wavelength of 632.8 nm. Analytical Ultracentrifugation (AUC) analysis was performed on Beckman Optima XLA at 7000 rpm, 20°C and a wavelength of 600 nm. Data analysis was performed with Sedfit. Samples were freeze-dried using ALPHA 1-2 LDplus freeze drier (Kuhner).

1.3 Synthesis of HSPG-mimicking ligands

Herein, a representative example is reported (9-mercaptononane1-sulfonate) but in this work molecules with x=4, 5, 8, 9, 10, 11 were synthetized (MBS, MPS, MOS, MNS, MDS and MUS).

First step, sodium non-8-enesulfonate: in a round bottom flask equipped with a reflux condenser, under stirring, 10.00 g of 9-bromo-1-nonene (48.75 mmol), 12.29 g of sodium sulfite (97.50 mmol) and 20 mg of benzyltriethylammonium bromide were added to a MeOH/H_2O (3:1 ratio) mixture. The reaction was kept at 103°C under stirring for 48 h. The solution became colorless when the reaction was complete. MeOH was removed under reduced pressure while the remaining aqueous phase was extracted with diethyl ether for 6 times (in order to remove unreacted starting material) and, finally, evaporated in a rotary evaporator obtaining a white powder. This latter was then suspended in MeOH or EtOH (depending on the length of the starting material) and filtered with a borosilicate filter for two times in order to remove the inorganic content. At the end, a white solid (yield 80%) was obtained and characterized through ^{1}H-NMR (**Figure 1.1**).
^{1}H-NMR (methanol-d_4): δ 5.76 (m, 1H), 4.90 (m, 2H), 2.73 (t, 2H), 2.02 (m, 2H), 1.74 (m, 2H), 1.29 (m, 8H)

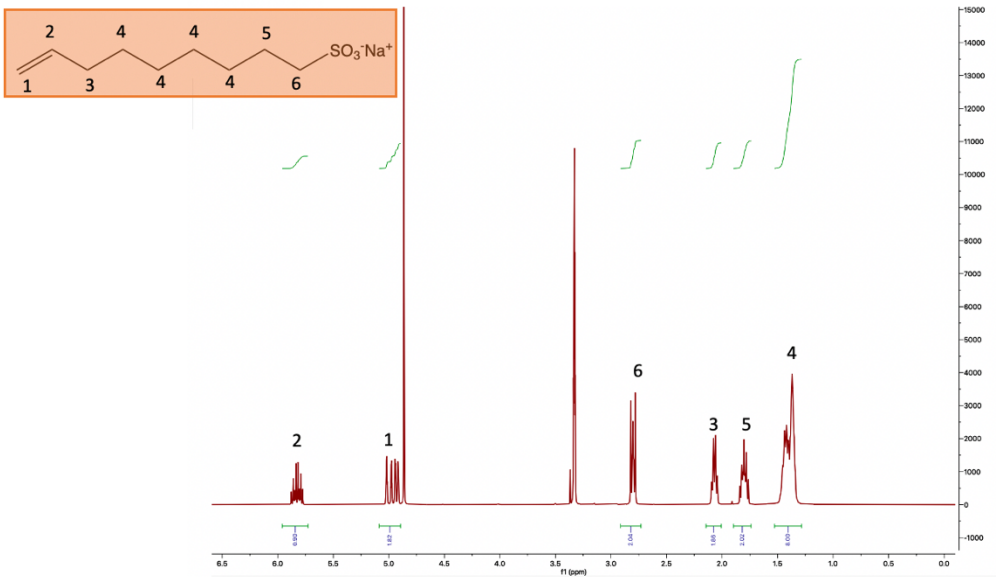

Figure 1.1 ^{1}H-NMR spectrum of sodium non-8-enesulfonate with peak assignment after purification.

Second step, sodium 9-acetylthiononane-1-sulfonate: in a round bottom flask under stirring, 10 g of sodium non-8-enesulfonate (43.80 mmol) and 2.6-time excess of thioacetic acid (6.17 ml, 87.6 mmol) were added to 200 ml of MeOH. The reaction mixture was kept under stirring and UV irradiation for 12 h. Then, the solution was evaporated under reduced pressure obtaining a red powder. This latter was subsequently washed with diethyl ether for 6 times in order to remove unreacted thioacetic acid. The resulting pink powder was then dispersed with ~ 1 g of carbon black in 200 ml of MeOH and purified through filtration. The obtained white powder (yield 72%) was characterized with ^{1}H-NMR (**Figure 1.2**).

^{1}H-NMR (D_2O): δ 2.75(m, 4H), 2.27(s, 3H), 1.57 (m, 2H), 1.40 (m, 2H), 1.13 (m, 10H).

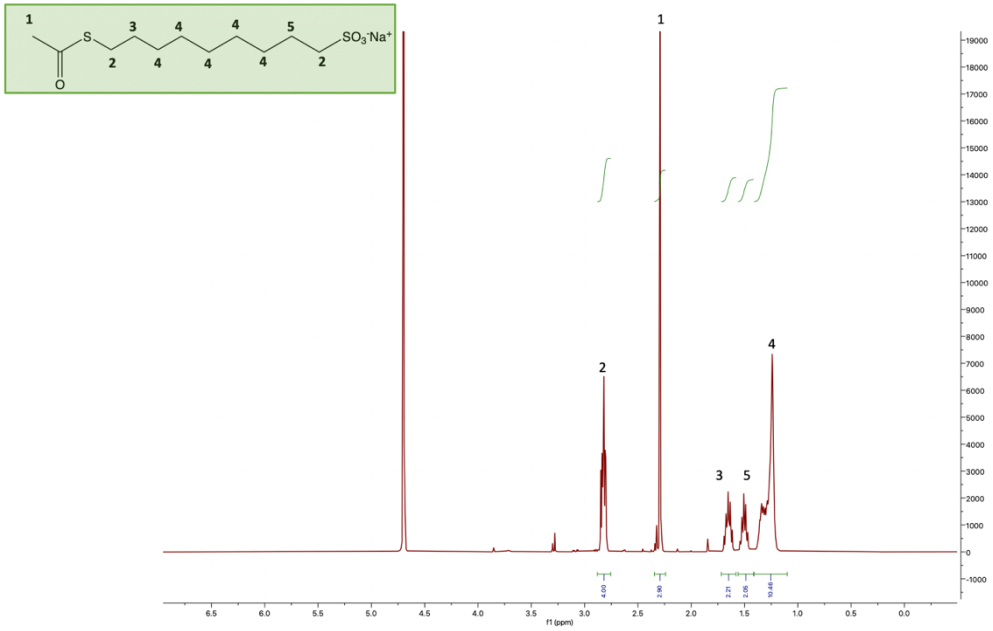

Figure 1.2 ^{1}H-NMR spectrum of sodium 9-acetylthiononane1-sulfonate with peak assignment after purification.

Third step, 9-mercaptononane1-sulfonate: in a round bottom flask, equipped with reflux condenser, under stirring, 6 g of sodium 9-acetylthiononane1-sulfonate was dissolved in 150 ml of 1M HCl. The reaction mixture was kept under stirring at 102 °C for 12 h. Then, 50 ml (1/3 of the starting volume) of 1M NaOH was added to the reaction mixture that was kept at 4°C overnight. The obtained crystals were separated from water with centrifugation (4000 rpm for 5 min) and dried under vacuum. The resulting white powder (yield 45%) was characterized with ^{1}H-NMR (**Figure 1.3**) and mass

spectrometry. NMR (D_2O): δ 2.80(t, 2H), 2.44(t, 2H), 1.59(m, 2H), 1.47(m, 2H), 1.39(m, 2H), 1.13(m, 10H).
Mass spectrum (ESI) found m/z= 239.077; calculated mass=239.37 g/mol.

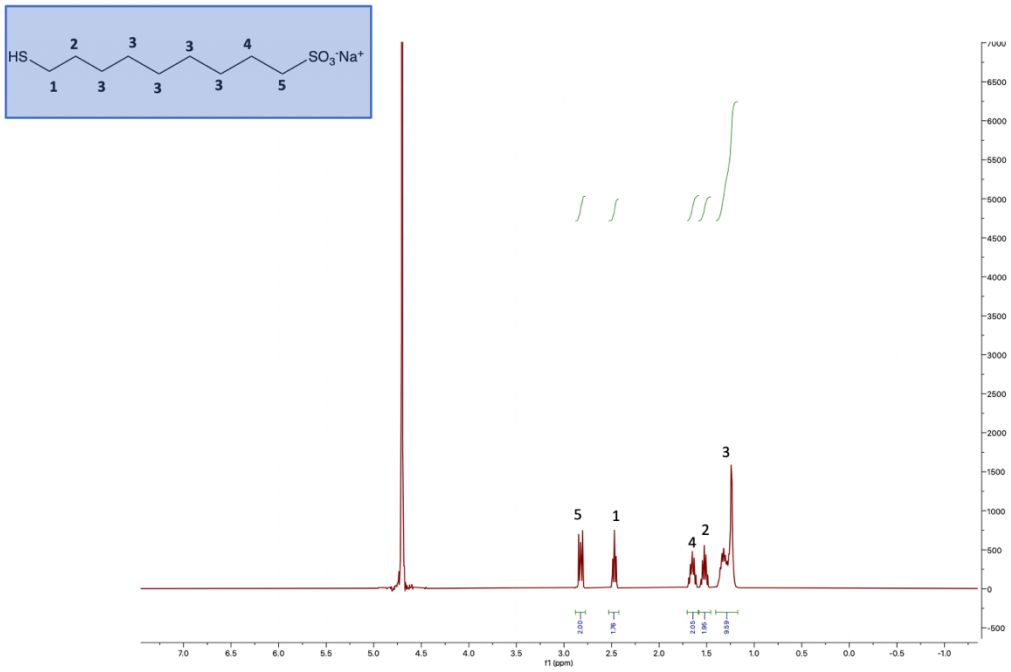

Figure 1.3 ^{1}H-NMR spectrum of 9-mercaptononane1-sulfonate with peak assignment after crystallization.

For shorter ligands (x=4,5) deprotection was performed in MeOH/Acetyl chloride at 70 °C. The volatiles were evaporated, and the inorganic content was removed *via* filtration in MeOH.

1.4 Synthesis of gold nanoparticles

AuNPs were synthetized *via* one phase method[188]. Briefly, in a round bottom flask, 177.2 mg of gold (III) chloride trihydrate (0.45 mmol) was dissolved in 100 ml of EtOH. Meanwhile, 0.45 mmol of the alkanethiol was dissolved in 10 ml of MeOH and added to the reaction mixture that was kept under stirring (900 rpm) for 10 min order to allow the formation of the thiol-gold complex. For bifunctional AuNPs, 0.45 mmol of the desired thiols mixture was dissolved in 10 ml of MeOH before the addition to the gold solution. Then, a filtered, saturated ethanol solution of sodium borohydride was added dropwise to the reaction mixture for about 1 h. The solution was then stirred for a variable time

from 2 to 8 h, depending on the length of the thiol, and subsequently placed in a refrigerator (at 4 °C) overnight. The obtained product was decanted, washed several times (~ 7) with EtOH and dried under vacuum. Subsequently, to completely remove free hydrophilic thiols, AuNPs were dissolved in Milli-Q water and centrifuged at least 8 times using Amicon® Ultra-15 Centrifugal Filters (MWCO 30 kDa). The resulting sample was then suspended in a minimal volume of water and freeze-dried to obtain ~ 100 mg of black powder. AuNPs were characterized through ^{1}H-NMR in order to assess their purity and calculate the ligand ratio. For the first purpose, the sample was prepared by dissolving 5-10 mg of AuNPs in 0.5 ml of D_2O; the resulting ^{1}H-NMR spectrum (**Figure 1.4**) should be free of sharp peaks (indicating the presence of free ligands) and with broad signals, corresponding to the ligands attached to the AuNPs surface.

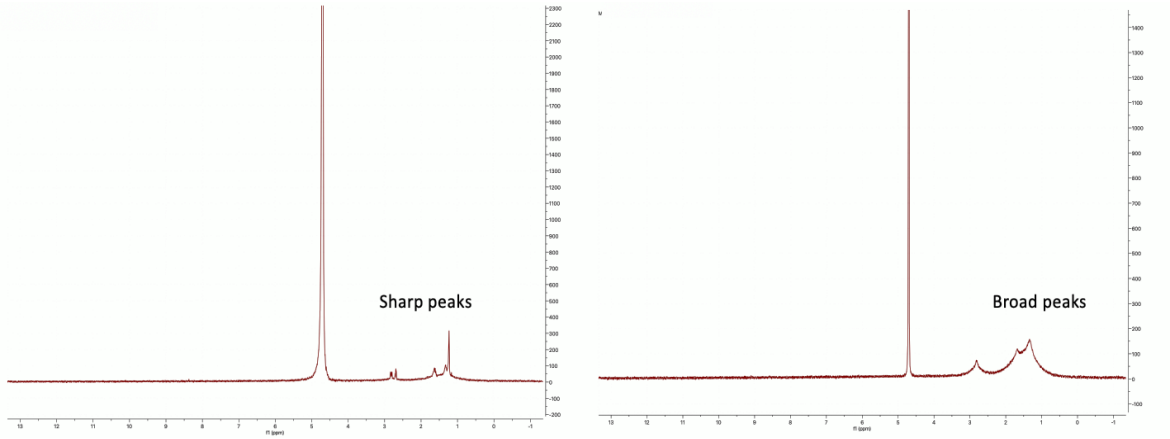

Figure 1.4 A comparison between AuNPs ^{1}H-NMR spectra after EtOH washes (on the left) and after EtOH and water washes (on the right). On the first spectrum are visible sharp peaks corresponding to unbound ligands, while on the second spectrum, the presence of broad peaks is indicative of a “clean” and pure sample.

On the other hand, the ligand ratio was determined by etching AuNPs with iodine. In particular, 5 mg of AuNPs were added to 0.5 ml of iodine methanol-d_4 solution (20 mg/ml) that was subsequently sonicated for 15 min before performing ^{1}H-NMR measurements. In this case, iodine etching was chosen since it did not significantly affect the NMR spectra of our AuNPs (**Figure 1.5**), in contrast to cyanide.

TGA was used to determine the amount of surface-attached ligands coverage on AuNPs. AuNPs were imaged with TEM and AUC analysis was performed to estimate the molecular weight of AuNPs. Moreover, TGA, TEM and ^{1}H-NMR data were used to

calculate the ligand density (LD), which is defined as number of ligands per nm^2, assuming a simple spherical model. It was calculated as follows:

$$LD = \frac{N_{lig}}{A_{tot}}$$

Where

$$N_{lig} = \left[\frac{Mass_{org}}{\frac{(\%_{MXS} \times MW_{MXS}) + (\%_{OT} \times MW_{OT})}{100}}\right] x\, N_{Avogadro}$$

and

$$A_{tot} = N_{part} x A_{part}$$

With

$$A_{part} = 4\pi r^2, \quad V_{part} = \frac{4\pi r^3}{3}, \quad Mass_{part} = V_{part}\, x \rho_{gold}, \quad N_{part} = \frac{Mass_{Au}}{Mass_{part}}$$

A_{part} is the surface area of one particle, V_{part} is the volume of one particle, N_{par} is the number of particles, $Mass_{part}$ is the mass of one particle, $Mass_{Au}$ is the mass of the gold core obtained from TGA analysis, N_{part} is the total number of particles, N_{lig} is the total number of ligands, A_{tot} is the total surface area of particles, $Mass_{org}$ is the total mass of particles ligand shell obtained from TGA analysis, $\%_{MXS}$ is the percentage of the sulfonated ligand extrapolated from NMR spectra and MW is the molecular weight of the ligand (same for OT).

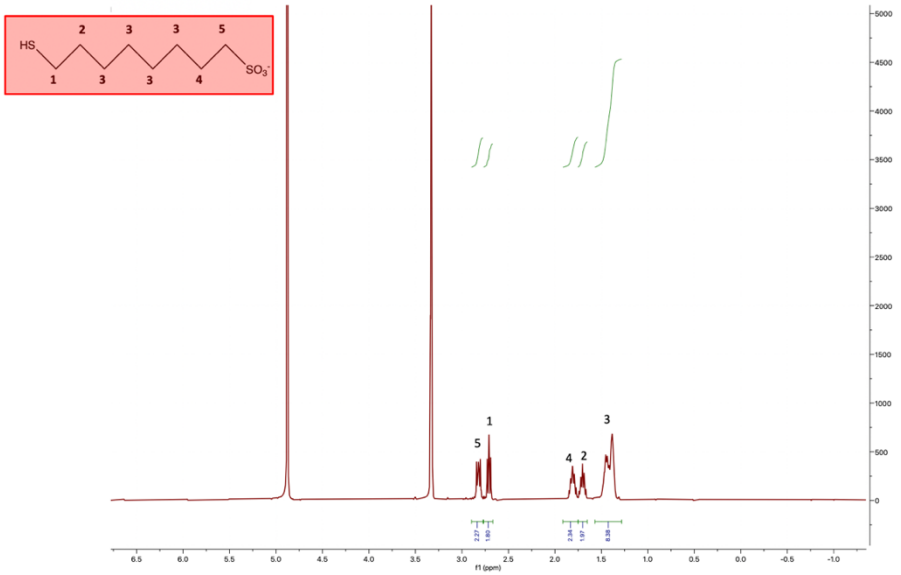

Figure 1.5 ^{1}H-NMR spectrum of MOS AuNPs after I_2 etching in methanol-d_4 with peak assignment. It is clearly shown that peaks integrals and chemical shifts are not significatively influenced by I_2.

1.5 Synthesis of gold nanoclusters

Synthesis and purification of AuNCs followed the published procedure by Loynachan *et al.* with some modifications[189]. Herein is reported the synthetic procedure for 1:1 GSH:MXS ratio, but different proportions were also tested. Briefly, 0.75 ml of fresh MXS aqueous solution (20 mM) and 0.75 ml of fresh GSH aqueous solution (20 mM) were added to 7.50 ml of Milli-Q water and mixed together. Subsequently, 1 ml of $HAuCl_4$ aqueous solution (20 mM) was added to the reaction mixture that was kept at 70 °C under stirring (700 rpm) for 20 h. Firstly, the solution turned from pale yellow to transparent, indicating the transition from Au (III) to Au (I), and then to more intense yellow due to subsequent reduction to Au (0). The obtained product was washed several times with water using Amicon® Ultra-15 Centrifugal Filters (MWCO 10 kDa). The resulting sample was then suspended in a minimal volume of water and freeze-dried to obtain ~ 10 mg of yellow powder. AuNCs were imaged with TEM and DLS analysis was performed to determine their hydrodynamic diameter; in this case, the number distribution was taken into consideration. The ligand ratio was estimated through ^{1}H-NMR. In particular, 5 mg of AuNCs was dissolved in 0.4 ml of D_2O and the relaxation time and the number of scans were set to 7.5 s and 128, respectively. TGA was used to determine the amount of surface-attached ligand coverage on AuNCs and therefore the organic content.

1.6 Cells and Virus

Vero cells (clone E6) were maintained in Dulbecco's modified Eagle's medium (DMEM), supplemented with heat-inactivated 10% FBS and 1% penicillin/streptomycin (Sigma-Aldrich) at 37°C in an atmosphere of 5% CO_2. HSV-2 was propagated and titrated on Vero cells with plaque assays.

1.7 Dose-response assay

The inhibitory effect on HSV-2 infection was evaluated by a plaque reduction assay. Vero cells (100.000 cells *per* well) were plated 24 h before in 24 well-plates. Increasing concentrations of the compounds were mixed and incubated with HSV-2 at 37 °C for 1 h. *The* mixture was then added to cells and incubated for another hour at 37 °C. Subsequently, the mixture was aspirated, the cells were washed and free medium with

methylcellulose was added. After 24 h incubation, the cells were fixed, treated with crystal violet 0.1% and the formed plaques were counted. The infectivity was calculated as follows:

$$\boldsymbol{Infectivity}\ (\%) = \frac{\boldsymbol{Number\ of\ plaques\ (sample)}}{\boldsymbol{Number\ of\ plaques\ (control)}}\ \boldsymbol{x\ 100}$$

The experiment was conducted in duplicate for two times, and the mean value was considered for each concentration. The concentrations that produced 50% and 99% reduction in plaque formation, EC_{50} and EC_{99} values, were calculated using GraphPad Prism.

1.8 Virucidal assay

Vero E6 cells were seeded 24 h before the experiment in 96-well plates in order to have 10^4 cells *per* well. HSV-2 (PFU 10^6) was mixed with each sample at its EC_{99} value and incubated for 1 h at 37 °C. Subsequently, the mixture was added to the cells and serial dilutions were performed. After 1 h incubation, the virus inoculum was removed, the cells were washed, treated with fresh medium with methylcellulose and, subsequently, incubated for 24 h. Then, the cells were fixed, treated with crystal violet 0.1% and the formed plaques were counted. The viral treater was calculated in the control wells.

2. Results and Discussion

2.1 Design of HSPG mimetic platforms: synthesis and characterization

2.1.1 Synthesis of HSPG-mimicking ligands

In this study we systematically investigate the structure-activity relationships of the HSPG-mimicking AuNPs previously developed in our group (chapter 4) identifying the key parameters required for the virucidal activity that should be taken in consideration for their rational design. Firstly, we decided to study the effect of the hydrophobicity and flexibility of the sulfonated ligand; to this end, the length of the aliphatic chain was chosen as eligible parameter to vary and examine, since it is positively correlated with the two considered factors.

A library of sulfonated alkanethiols was synthetized following a three steps route (**Figure 2**):

- Sulfonation of the bromo derivative *via* Strecker reaction with sodium sulfite;
- UV-mediated thiol-ene click reaction;
- Deacetylation of thioacetate under acid conditions.

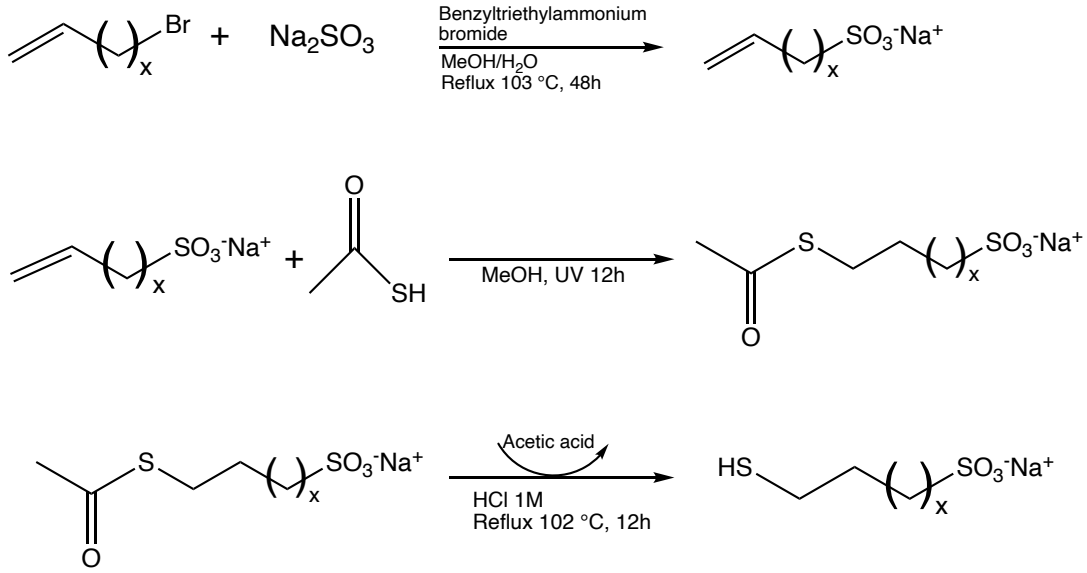

Figure 2. Schematic representation of HPSG-mimicking ligands synthetic route. In this work, molecules with x=4,5,8,9,10,11 were synthetized.

The final product was purified through crystallization under acid conditions in order to avoid the formation of disulfides, obtaining pure, water and methanol-soluble sulfonated ligands that can be easily used for AuNPs and AuNCs preparation. In fact, thiols act as strong stabilizers in AuNPs formation since the sulfur-gold bonds can prevent crystallites agglomeration minimizing the Van Der Waals interactions[190]. Consequently, the purity of the thiol is a key parameter for AuNPs quality and size; for example, a high inorganic content, which is a typical consequence of this deprotection step, was found to be correlated with the formation of highly polydisperse, large, and irregular particles.

However, this deprotection strategy in HCl could not be adopted for shorter ligands (x=4-5), since several problems were faced in their crystallization. Perhaps for their high water solubility or tendency to form disulfides, they were not able to crystalize in the reported conditions even with the use of a nonsolvent. For these reasons, in this case, the deprotection was performed under inert conditions (in order to avoid air oxidation of thiols) using acetyl chloride/methanol, followed by the evaporation of volatiles and the removal of the inorganic content through filtration in MeOH[191]. The suitability of this deprotection method was confirmed with ^{1}H-NMR and mass spectrometry. Herein, is reported the ^{1}H-NMR spectrum of 5-mercaptopentane-1-sulfonate (**Figure 2.1**) that shows the absence of disulfides derivatives and the overall purity of our target molecule (D_2O): 2.79 (t, 2H), 2.46 (t, 2H) 1.62 (m, 2H), 1.58 (m, 2H), 1.38 (m, 2H).

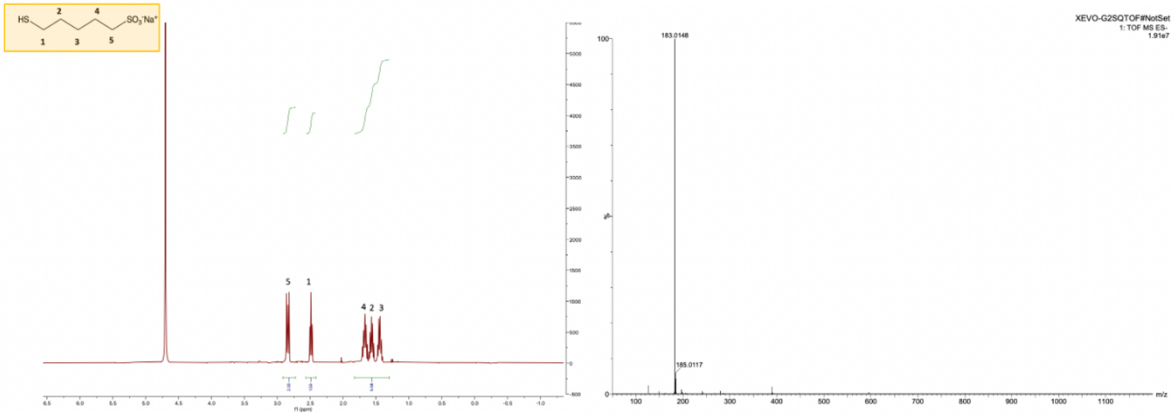

Figure 2.1 Mass and ^{1}H-NMR spectrum of 5-mercaptopentane-1-sulfonate with peak assignment after deprotection with acetyl chloride-methanol.

2.1.2 Synthesis and characterization of gold nanoparticles

Given the interest in investigating the structure-activity relationships of our system, we aimed to find a controlled approach for AuNPs synthesis that would have allowed us to obtain comparable particles in terms of crucial parameters including size and ligand density, ensuring, therefore, a rational study on their antiviral mechanism of action. In the past decades, various methods for AuNPs synthesis have been developed. The most common routes are based on the use of $HAuCl_4$ as gold precursor and $NaBH_4$, tetrabutylammonium bromide, and trisodium citrate as reducing agents[192-194]. In this context, it is worth to mention the two-phase approach proposed by Brust and Schriffin, that represent a milestone of alkanethiol-functionalized AuNPs synthesis[195]. However, the majority of these methods are limited to hydrophobic thiols and non-polar solvents.

Ligand exchange represents a viable strategy to obtain hydrophilic AuNPs; in particular, it consists in a two-steps process: firstly AuNPs are synthetized with a weak capping agent (such as oleylamine, cetrimonium bromide, citrate *etc*.) and subsequently are mixed with the desired ligand so that it will displace the weakly coordinating one[196]. In this regard, the study conducted by Yang *et al.* is of particular interest since they reported a two-phase place exchange protocol that allows to obtain monodisperse AuNPs functionalized with a wide library of thiolated molecules including MUS[197]. At first, in this project, this method was followed, however several drawbacks and problems have emerged and led us to change the synthetic approach. In fact, this process mostly depends on the binding affinity of the capping agents, and, therefore, a complete replacement is not always obtained. In our case, with long ligands such as MUS and MDS, we managed to achieve a complete phase exchange; however, by decreasing the length of the thiol, the lengthy aliphatic chains of oleylamine make their displacement thermodynamically and kinetically unfavorable, resulting in bifunctional AuNPs. Moreover, with short alkyl chains (MBS and MPS), ligand exchange was not successfully achieved even by increasing the temperature, using a large excess of thiols, varying the pH *etc.* Thus, due to their high toxicity, oleylamine residues could have precluded AuNPs use for biomedical applications.

On the basis of these considerations, a direct one-phase synthetic approach, reproducible and controlled, was preferred. In fact, the presented procedure was found to be advantageous for the study of crucial design parameters since it gave us a reasonable control over particles ligand density, ensuring a rational comparison of the resulting AuNPs in the antiviral assays. The adopted one phase method is based on the

reduction of $AuCl_4^-$ by a large excess of $NaBH_4$ in EtOH (**Figure 2.2**); the gold-to-thiol ratio, the rate of $NaBH_4$ addition, the reaction time and the purity of the thiols were found to play a key role in AuNPs formation.

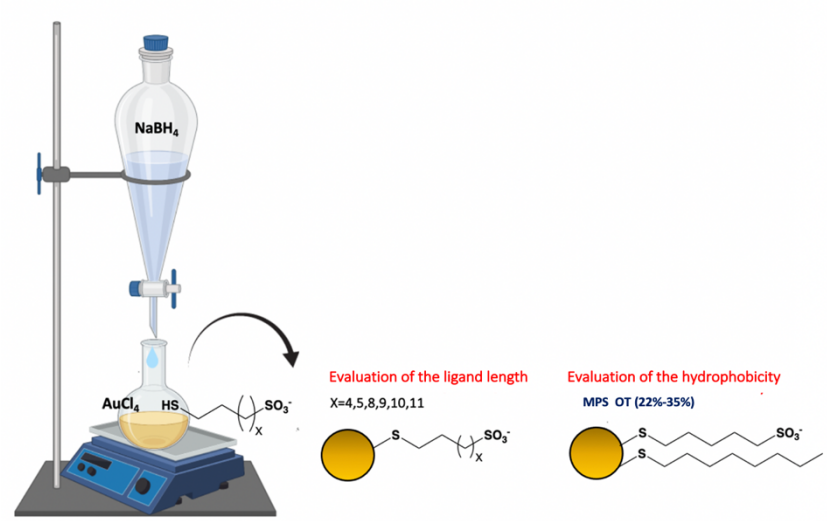

Figure 2.2 Schematic representation of the adopted one phase method for our AuNPs library synthesis.

Through a detailed physicochemical characterization of AuNPs, that has served as the backbone of this work, the parameters that allowed us to achieve the best compromise in terms of size, stability and ligand density were established. In particular, TEM and AUC were adopted for dimensional and morphological analysis and in **table 1** are reported the estimated core size values of our AuNPs library.

Sample	Length	D_m (nm)TEM	D_{core}(nm)AUC
MBS AuNPs	4	2.283 ± 0.664	2.4
MPS AuNPs	5	2.955 ± 0.980	2.7
MOS AuNPs	8	2.490 ± 1.060	2.4
MNS AuNPs	9	2.684 ± 0.999	2.7
MDS AuNPs	10	3.056 ± 1.025	3.1
MUS AuNPs	11	3.573 ± 1.007	3.8
MPS OT (22%) AuNPs	5;8	2.460 ± 0.993	2.7
MPS OT (35%) AuNPs	5;8	2.310 ± 0.841	2.8

Table 1. AuNPs estimated core size with TEM and AUC. The core size of particles was determined with FIJI (Imagej) for TEM, while AUC data were analyzed with Sedfit.

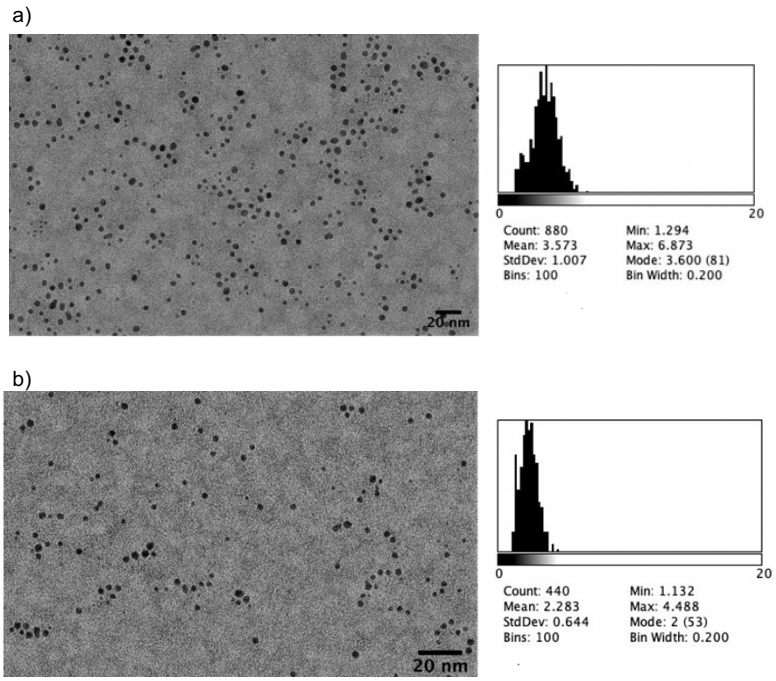

Figure 2.3 TEM images and size distribution histograms of MUS AuNPs (a) and MBS AuNPs (b) obtained with ImageJ; scale bar 20 nm.

As it can be seen, AuNPs core size and size distribution are in part influenced by the choice of the thiol, and a positive correlation with the length of the ligand was found; moreover, a small percentage of "seed clusters" can be observed. Bigger particles can be obtained by increasing the gold-to-thiol ratio and consequently the nucleation intensity; however, they result to be unstable and tend to aggregate due to a lower surface coverage. Therefore, we can assume that the aliphatic chain has a substantial impact on the stabilization and the surface energy of the particles. The reason of this correlation between the core size, the growth kinetic and the length of the ligand is still unclear, but several factors such as entropy, conformation, solubility and pH are likely to play a key role. Surely, longer ligands require more free volume on AuNPs surface and are associated with a higher stabilization energy[198-199]; moreover, in this regard, is worth to mention that with longer alkanethiols, a higher percentage of Au(0) species was found at the beginning of particles formation process[200]. In the light of these observations, a systematic study involving different ligands is very challenging, and the optimal results are here reported and were achieved by keeping a fixed thiol-to-gold ratio (1:1), increasing the reaction time with the decrease of the length of the ligand, since for MPS and MBS slower growth kinetics were observed. Moreover, the obtained AuNPs showed high solubility in water and good colloidal stability over one month.

On the other hand, AuNPs chemical composition was quantified by a combination of TGA and ^{1}H-NMR analyses. TGA was used to determinate the amount of surface-attached ligands on AuNPs. It measures the weight loss in function of time and, therefore, results to be suitable for estimating AuNPs organic content. In detail, TGA data are presented in **table 2** and are expressed in terms of weight loss percentage. The organic surface coverage burns before 700 °C and was found to range from 11 to 17% of particles total weight. Overall, we can assume that this parameter is not significantly affected by the choice of the ligand, since its variation can be attributed to the different molecular weights. Moreover, in this case, these data cannot be considered strictly quantitative due to the polydispersity of the samples; however, they allow us to adequately estimate, together with TEM and ^{1}H-NMR data, the ligand density. Notably, we managed to achieve a similar ligand density by adopting the same gold-to-thiol ratio, ensuring a rational and controlled study on the effect of the length and the hydrophobicity of the ligand on the antiviral mechanism of action.

Sample	Organic content%	Ligand density (nm^2)
MBS AuNPs	10.68%	3.33
MPS AuNPs	12.50%	4.66
MOS AuNPs	16.18%	4.43
MNS AuNPs	16.52%	4.39
MDS AuNPs	17.95%	5.44
MUS AuNPs	17.12%	5.70
MPS OT (22%) AuNPs	12.35%	4.04
MPS OT (35%) AuNPs	11.67%	3.20

Table 2. AuNPs organic content percentage obtained from TGA analysis and estimated ligand density.

Beyond this, TGA data were also exploited for determining the ligand ratio of the bifunctional AuNPs, since the two ligands decompose at different temperature. Herein, are reported the TGA graphs of MPS AuNPs alone or covered with OT (**Figure 2.4**)

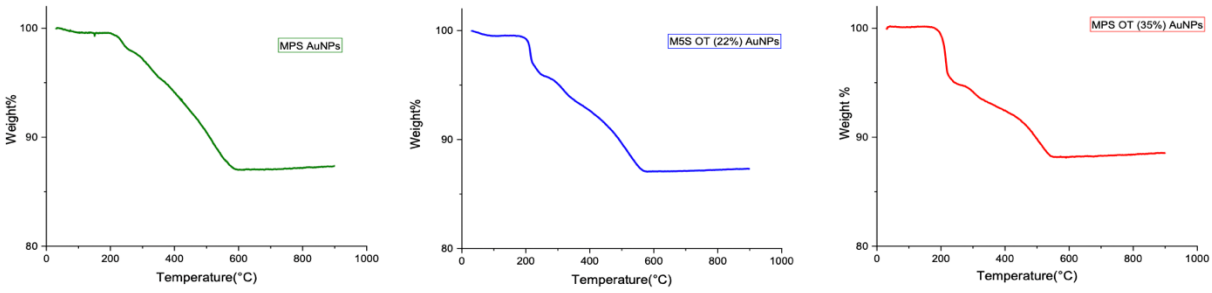

Figure 2.4 TGA results of MPS, MPS OT(22%) and MPS OT(35%) AuNPs. TGA analysis was performed under N_2 flow heating up from 30 °C to 900 °C at a ramp rate of 10°C/min.

In particular, we can distinguish two different losses in mass: the first one around 200-220 °C, corresponding to OT, and the second one approximately from 250 °C to 550 °C corresponding to MPS. Moreover, comparing the two graphs of MPS OT AuNPs, it is clear a distinct difference in the OT composition; in detail, the estimated values were ~ 20% and 40%, which resulted to be overall in agreement with those extrapolated from ^{1}H-NMR. In fact, in order to avoid eventual overlapping effects of the thermal decomposition of the two ligands, their actual ratio was also determined by ^{1}H-NMR. Herein, we adopted iodine etching since it did not affect the NMR spectra of our thiol-capped AuNPs (as reported in the materials and method section). Alternatively, cyanide etching or thermal decomposition may be also employed. In detail, in **figure 2.5** are shown the spectra of OT, MPS, and MPS OT AuNPs after etching in methanol-d_4: for MPS, the CH_2 groups next to -SH and SO_3^- (2.51 ppm, 2.84 ppm) were considered, while for OT the terminal methyl group (0.83 ppm). As it can be seen, the adjacent two peaks (2.63-2.94 ppm) were integrated together (I_2), and the OT % was calculated normalizing the first peak (corresponding to the methyl group of OT) to three and subtracting the contribute of the two OT protons:

$$OT\ \% = \frac{1}{\left(\frac{I_2 - 2}{4}\right) + 1}$$

The calculated OT content was around 22% and 35% for a feeding ratio of 33% and 55%, respectively. Based on these data, it is possible to conclude that the actual ligand ratio does not perfectly match with the molar ratio adopted for the synthesis, and the

observed trend indicates that the OT content results to be approximately 10%-20% less, but, anyways, a positive correlation can be found.

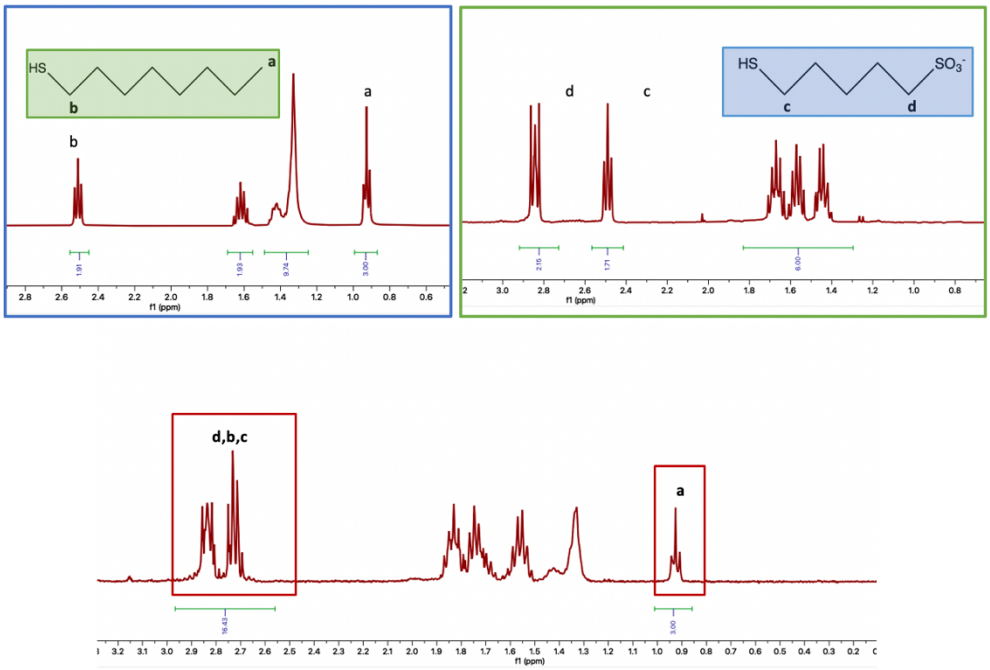

Figure 2.5 ^{1}H-NMR spectra of OT, MPS and MPS OT AuNPs (feeding ratio 66-33%) in methanol-d_4. Herein, the peaks considered for the calculation of the OT% are highlighted.

2.1.3 Synthesis and characterization of gold nanoclusters

As a secondary project, a smaller system consisting in a series of AuNCs coated with our ligands library was synthetized in order assess the importance of hydrophobic interactions and evaluate the effect of the core size on the antiviral mechanism of action. In the last years, AuNCs have attracted a growing interest in many areas such as sensing, catalysis, optics *etc;* interestingly, they show a "molecule like" behavior, serving as a bridge between AuNPs and small molecules[201-203].

To date, several synthetic protocols have been developed and, herein, we adopted a one pot method in which glutathione (glu, cys, gly), a biocompatible hydrophilic ligand, serves as both reducing and capping agent and AuNCs were prepared by using a fixed gold to thiol ratio and thiol to thiol ratio of 1.5 and 1, respectively. The reaction was performed in water at 70°C and, firstly, the solution turned from pale yellow to transparent, indicating the transition from Au (III) to Au (I) induced by the thiols, and then,

to more intense yellow due to subsequent reduction to Au (0) favored by the elevated reaction temperature. The obtained AuNCs resulted to be fluorescent, and their absorption spectra did not show the surface plasmon resonance peak typical of AuNPs around 520 nm (**Figure 2.6**).

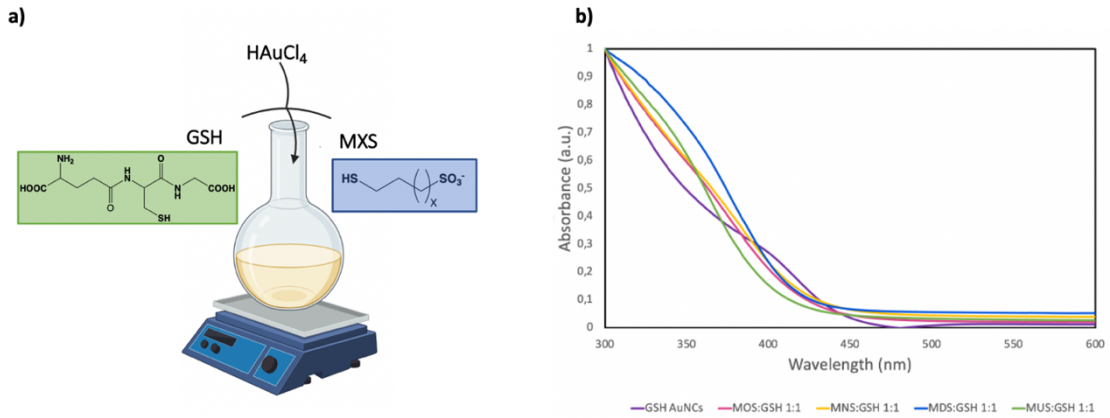

Figure 2.6 Schematic representation of the adopted one pot method for AuNCs synthesis (a); UV-Vis spectra of our AuNCs library (b).

To evaluate if the synthesis of our AuNCs was successfully achieved with all the ligands, DLS and TEM analyses were performed and their core size, hydrodynamic diameter, size distribution and shape were evaluated (**Figure 2.7**). The obtained DLS results show that the presence of an amphiphilic ligand (i.e. MUS) is associated with an increase of the hydrodynamic diameter (compared to GSH alone) and, moreover, a positive correlation between the length of the ligand and the mean diameter can be noted; however, TEM results indicate that all the samples have overall a similar core size of ~ 1.4 nm with a narrow size distribution and, consequently, the observed correlation can be attributable to a larger hydration shell. In this regard, it is important to consider that the imaging analysis software has a limit of resolution and, therefore, the obtained results cannot be considered strictly accurate (< 1 nm).

a)

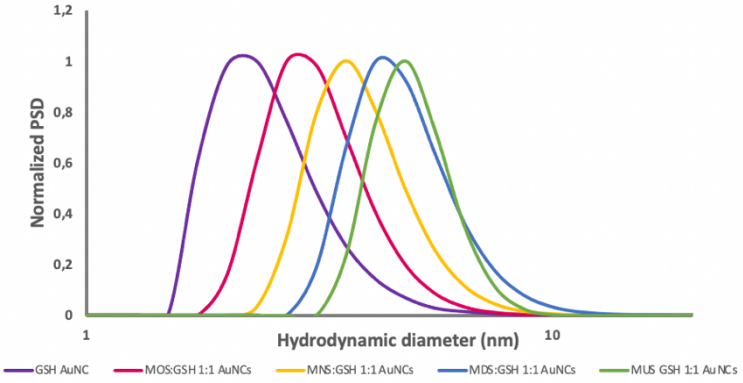

b)

Sample	d_h(nm)
ALL GSH	2.50±0.78
MOS:GSH 1:1	3.22±0.88
MNS:GSH 1:1	4.00±1.06
MDS:GSH 1:1	4.93±1.37
MUS:GSH 1:1	5.08±1.00

c)

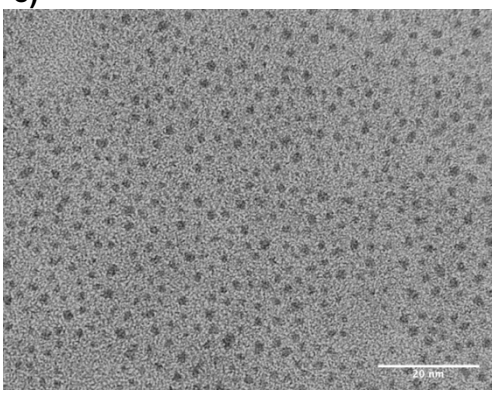

d)

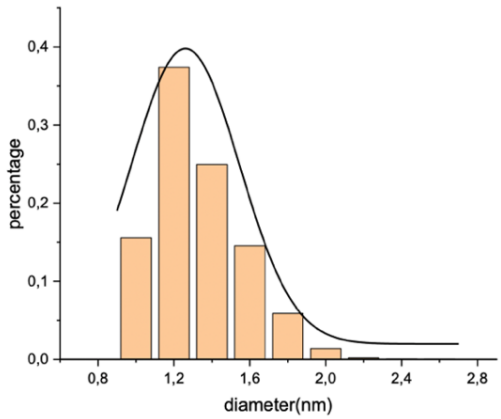

Figure 2.7 Normalized particles size distribution in terms of hydrodynamic diameter of our AuNCs library in PBS (a) (DLS measurements were performed in triplicate) and the calculated mean values are reported in the adjacent table (b). TEM micrograph (b) and particle size distribution histogram of MNS GSH 1:1 AuNCs(c), scale bar 20 nm.

On the other hand, in order to evaluate if the used thiol-to-thiol ratio dictates the ligand composition on the AuNCs surface and, therefore, to calculate the actual ligand ratio, ^{1}H-NMR analysis was performed. In particular, in this case, it was estimated integrating the peaks after the deconvolution of the spectrum with a Gaussian Lorentzian fit and the corresponding values are reported in **table 3**. Overall, the obtained results show a rough agreement between the feeding ratio and the actual ligand composition, with a slight decrease of the MXS percentage for shorter ligands, confirming the same trend observed for AuNPs.

Sample	GSH%	MXS%
MOS:GSH 1:1 AuNCs	49	51
MNS:GSH 1:1 AuNCs	47	53
MDS:GSH 1:1 AuNCs	42	58
MUS:GSH 1:1 AuNCs	39	61

Table 3. Estimated ligand percentage values of the AuNCs library from ^{1}H-NMR analysis.

2.2 Evaluation of the antiviral mechanism of action

In the previous chapters, we reported the synthesis and the characterization of two different types of AuNPs: monoligand, capped with various sulfonated alkanethiols of different length (4,5,8,9,10,11), and biligand, functionalized with a short sulfonated ligand (MPS) and the hydrophobic linker OT. The systematic study on their antiviral mechanism of action will be presented in this section, investigating first the effect of the length of the HSPG-mimicking ligand, and then of the presence of the hydrophobic OT. To have a complete and comprehensive view on this topic and explore the effect of the core, the results of a parallel project focused on sulfonated cyclodextrins will be reported and a comparative analysis between the two different systems will be also presented. Finally, to further assess the importance of hydrophobic interactions and evaluate the effect of the core size, we will discuss the antiviral activity of the designed AuNCs. Herein, we used HSV-2 as HSPG-dependent virus model.

2.2.1 Effect of the length of the ligand

To evaluate the anti-HSV-2 activity of our monoligand AuNPs, dose-response assays were firstly performed, pre-treating each sample with HSV-2 1 h before adding this mixture to the cells. In **figure 2.8** are showed the resulting dose response curves and in **table 4** the respective EC_{50} values.

All the samples significantly inhibited HSV-2 infection with nanomolar EC_{50} values; in detail, a slight decrease of this latter with the increase of the length of the aliphatic chain can be observed, however this trend can be considered negligible since this parameter could be affected by several factors such as viral titer, human error, cells *etc.* Therefore, we can assume that all the samples have approximately a similar inhibitory activity.

Sample	Length	EC_{50} (μg/ml)	EC_{50} (μM)
MBS AuNPs	4	2.051 (1.767-2.375)	0.018
MPS AuNPs	5	1.677 (1.340-2.094)	0.012
MOS AuNPs	8	1.063 (0.810-1.388)	0.0099
MNS AuNPs	9	0.784 (0.605-1.018)	0.0040
MDS AuNPs	10	0.865 (0.708-1.057)	0.0030
MUS AuNPs	11	1.030 (0.756-1.396)	0.0021

Table 4. Inhibitory activity of monoligand AuNPs against HSV-2. 50% effective concentration (EC_{50}) values were calculated with GraphPad Prism. The molecular weight of AuNPs was estimated with AUC.

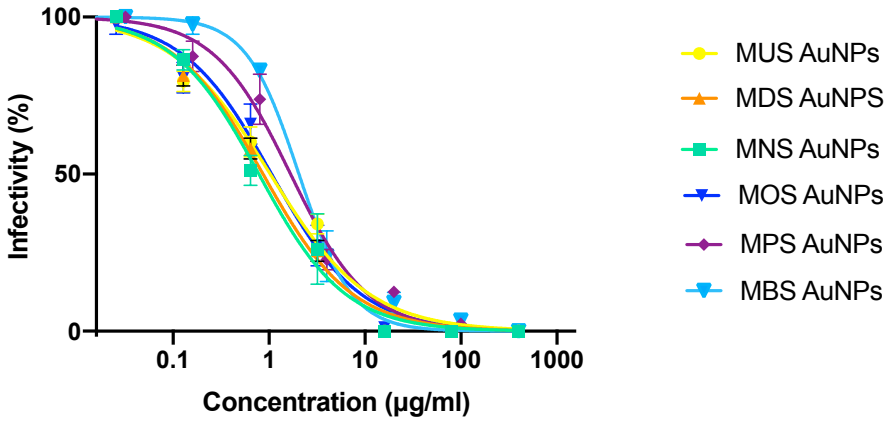

Figure 2.8 Dose response curves of monoligand AuNPs against HSV-2. The virus was pre-mixed with increasing concentration of the compound for 1 h at 37 °C and then added to cells.

On the other hand, a completely different trend was found for cyclodextrins: in **figure 2.9** are reported the dose reponse curves of cyclodextrins functionalized with 7-11 carbon sulfonated alkyl chains, synthetized and tested in our group. As it can be seen, the inhibitory activity decreases with the length of the aliphatic chain, and a significant difference can be observed from CDS8. The reasons for this particular behaviour are still not known, but the different core, spatial conformation and solubility may play a key role. In particular, we have noted that by switching the core of the system, the solubility changes. In fact, while the alkanethiols capped AuNPs exhibit a similar solubility in the aqueous medium, for the functionalized cyclodextrins this parameter was found to be influenced by the length of the aliphatic chain. On the basis of this consideration, it is

possible to hypothesize that these solubility variations could determine changes in the binding free energy ($\Delta G = G_{bound} - G_{solution}$); therefore, given their lower water solubility, longer aliphatic chains functionalized cyclodextrins may be associated with a higher binding constant, and, consequently, lower EC_{50} values. In fact, the binding free energy is related to the binding constant (K_B) *via* the following equation:

$$\Delta G = -RTlnK_B$$

where R is the universal gas constant and T the temperauture in Kelvin. Conversely, alkanethiols capped AuNPs should have a similar binding affinity towards viral particles ascribable to their comparable water solubility. Thus, in the light of these observations it can be concluded that the electrostatic interactions occurring between the sulfonate groups of AuNPs and the basic amino acids of viral proteins could represent the main driving force for AuNPs recognizing and binding to viral particles.

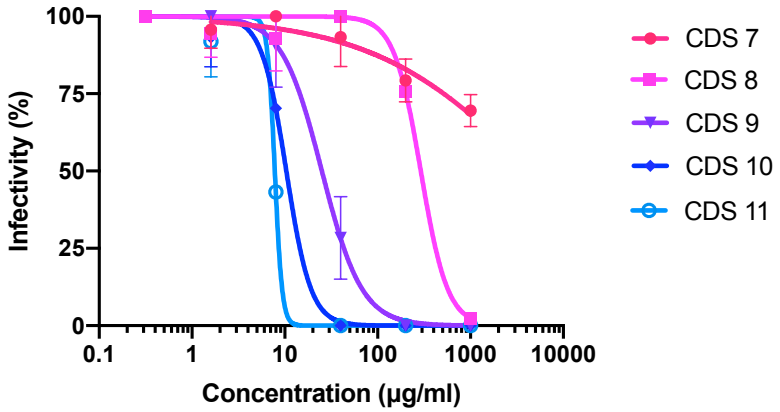

Figure 2.9 Dose response curves of functionalized cyclodextrins against HSV-2. The virus was pre-mixed with increasing concentration of the compound for 1 h at 37 °C and then added to cells.

As reported in the previous section, several sulfonated materials have shown inhibitory activity against HSV-2 infection; however, this effect was found to be virustatic, reversible upon dilution. Therefore, our compounds were then evaluated for their mechanism of action. To this end, a virucidal test was performed: in detail, it consists in the pre-treatment of the virus with the compound at its EC_{99} for 1 h at 37 °C, followed by the addition of this mixture to cells, performing serial dilutions (**Figure 2.10**). A compound is considered virucidal if it causes a reduction of at least 2 log unit in the viral titer.

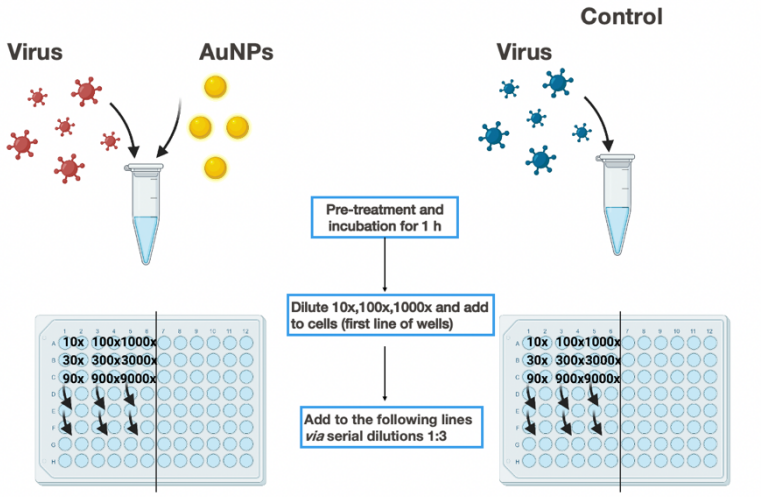

Figure 2.10 Schematic representation of the performed virucidal assay. HSV-2 (PFU 10^6) was pre-incubated with AuNPs for 1 h, the resulting mixture was diluted and added to cells, performing serial dilutions.

In **figure 2.11** are reported the results of the performed virucidal assays: the AuNPs functionalized with short aliphatic chains, such as MBS and MPS, resulted to be virustatic with almost full recovery of viral infectivity, whereas the particles functionalized with long ligands (starting from MOS) showed a virucidal mechanism, without a significant recovery of infectivity upon dilution.

Based on the molecular dynamics simulations previously performed on MUS AuNPs and HPV-16 capsid, we can assume that this virustatic activity observed for the shorter ligands can be ascribed to their lower flexibility[186]; in fact, the presence of a flexible linker could enhance the multivalent capability of AuNPs by increasing the contacts and binding chances to viral particles. Moreover, given its flexibility, this system can easily adapt to its substrate overcoming the limitations arising from steric hindrance[204]. On the other hand, AuNPs coated with less flexible linkers such as MPS and MBS establish a lower number of Coulomb contacts with viral particles; therefore, they may not be able to lead to the development of a fast multivalent binding capable, in its turn, of generating strong forces on the capsid and, consequently, its breakage, as it was observed for MUS AuNPs.

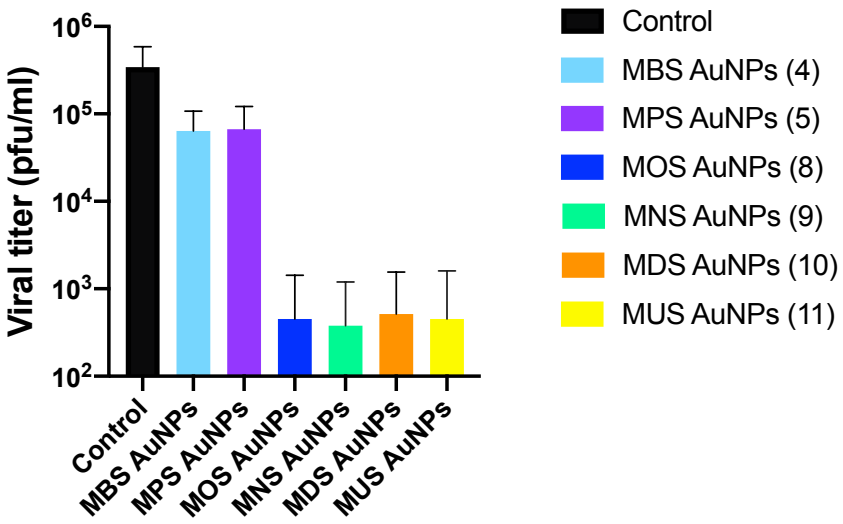

Figure 2.11 Virucidal activity of monoligand AuNPs. Each compound was pre-treated with the virus (PFU ~10^6) and incubated for 1 h at 37 °C. Then, the mixture was added to Vero E6 cells performing serial dilution. The control without sample was used for calculating the viral titer on the base of the number of formed plaques.

Furthermore, interestingly, the obtained data indicate that all the virucidal AuNPs exerted a similar effect despite the different length of the ligand, suggesting that a minimum length is required for a virucidal mechanism of action, without significantly affecting the antiviral potency. These results are in agreement with the model proposed by Kane regarding the thermodynamic behind the influence of the length of the linker in multivalent systems; in particular, it is assumed that for long and flexible ligands, their binding free energy weakly depends on their length[205].

Despite all the alkanethiol capped AuNPs exhibited a great inhibitory effect, there are significative differences in their antiviral mechanism of action. On the other hand, in **figure 2.12** are reported the results of the virucidal assay performed on functionalized cyclodextrins. As we can see, in this case, unlike AuNPs, the minimum chain length required for an irreversible effect is 9, and a weaker inhibitory activity is associated with a virustatic mechanism of action.

However, beyond these considerations, indeed, another important role is played by the hydrophobic interactions, and it will be discussed in the following section.

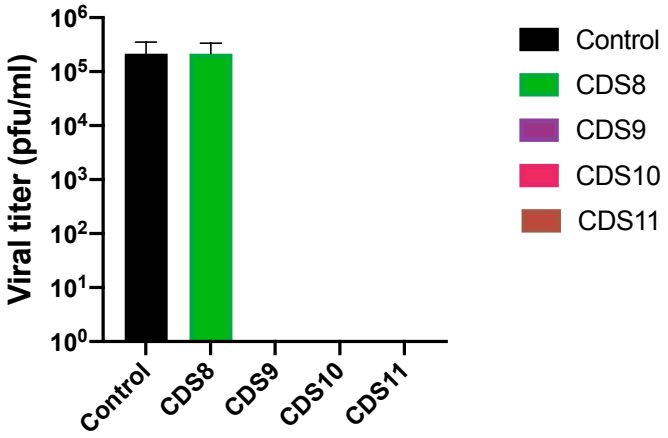

Figure 2.12 Virucidal activity of functionalized cyclodextrins. Each compound was pre-treated with the virus (PFU ~10^6) and incubated for 1 h at 37 °C. Then, the mixture was added to Vero E6 cells performing serial dilution. The control without sample was used for calculating the viral titer on the base of the number of formed plaques.

2.2.2 Effect of the hydrophobicity

Based on the results reported in the previous paragraph showing that short alkyl chains (MPS-MBS) are associated with a virustatic activity, we synthetized MPS OT AuNPs (with increasing content of OT, 22%-35%) in order to evaluate the effect and the importance of hydrophobicity for a virucidal mechanism of action.

Dose response curves against HSV-2 are reported in **figure 2.13**, and in **table 5** the respective EC_{50} values, in comparison with MPS AuNPs.

Sample	EC_{50} (μg/ml)	EC_{50} (μM)
MPS AuNPs	1.677 (1.340-2.094)	0.012
MPS OT (22%) AuNPS	0.081 (0.067-0.097)	0.00044
MPS OT (34%) AuNPs	0.180 (0.140-0.231)	0.00085

Table 5. Inhibitory activity of MPS and MPS OT AuNPs against HSV-2. 50% effective concentration (EC_{50}) values were calculated with GraphPad Prism. The molecular weight of AuNPs was estimated with AUC.

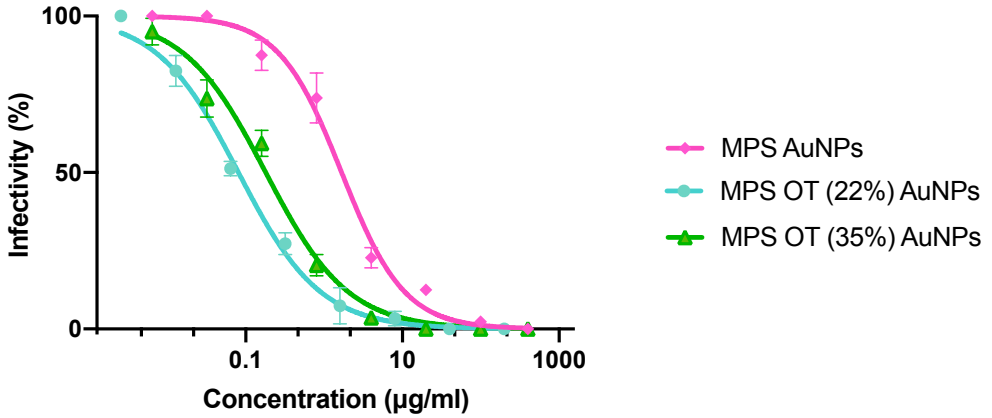

Figure 2.13 Dose response curves of MPS and MPS OT AuNPs against HSV-2. The virus was pre-mixed with increasing concentration of the compound for 1 h at 37 °C and then added to cells.

The conjugation with OT leads to an enhanced inhibitory activity, however, as previously discussed, this difference should not be considered strictly significative since the EC_{50} value can be influenced by several parameters such as the viral titer, competency of cells *etc.* In this case, we can hypothesize that with respect to hydrophilic linkers, OT should pay a lower entropic penalty in the aqueous environment and, therefore, the binding process may be driven by a more negative energy of binding with consequent lower dissociation constant and EC_{50} values.

The compounds were then evaluated for their mechanism of action and the virucidal assay was performed; in **figure 2.14** are reported the results together with the monoligand AuNPs. It is clearly shown that the presence of OT strongly improves the antiviral activity of MPS AuNPs, switching their mechanism of action from virustatic to virucidal. In fact, MPS AuNPs are associated with a less than one log reduction in the viral titer, whereas MPS OT (22%) and MPS OT (35%) lead to a 2.5 log and almost 4 log reduction, respectively, indicating a positive correlation between the antiviral potency and the hydrophobic content.

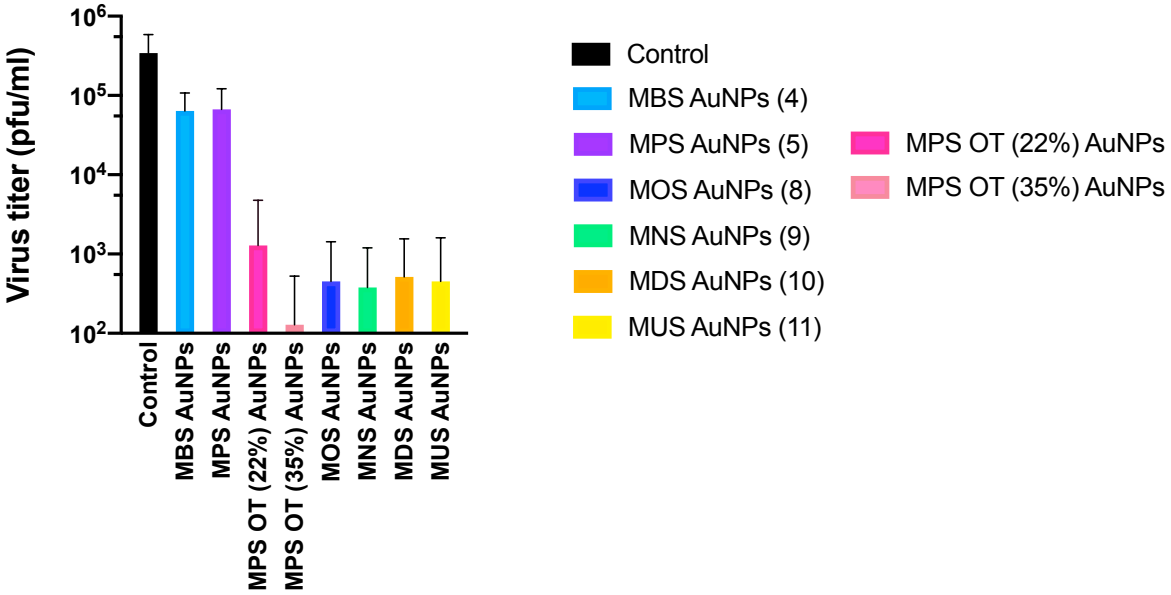

Figure 2.14 Comparison between the virucidal activity of MPS OT AuNPs and monoligand AuNPs. Each compound was pre-treated with the virus (PFU ~10^6) and incubated for 1 h at 37 °C. Then, the mixture was added to Vero E6 cells performing serial dilution. The control without sample was used for calculating the viral titer on the base of the number of formed plaques.

The obtained results highlight the importance of the hydrophobic interactions for a virucidal mechanism of action, clearly demonstrating that this latter can also be achieved with a short HSPG-mimicking ligand, if a hydrophobic linker is present. In fact, in addition to the electrostatic interactions that are essential for AuNPs binding to viral particles, the presence of a hydrophobic ligand such as OT can further increase the contacts with the viral proteins by interacting with their hydrophobic portions; consequently, the lower number of coulombic contacts ascribable to less flexible ligands can be compensated and a multivalent and more stable binding can be established, leading to stronger mechanical stresses and distortions on the viral capsid/envelope[186].

2.2.3 Antiviral activity of gold nanoclusters

To further assess the importance of hydrophobic interactions and evaluate the effect of the core size on the antiviral mechanism of action, the synthetized library of AuNCs was tested against HSV-2. In **figure 2.15** are reported the dose response curves determined *via* a plaque reduction assay, and in **table 6** the respective EC_{50} values.

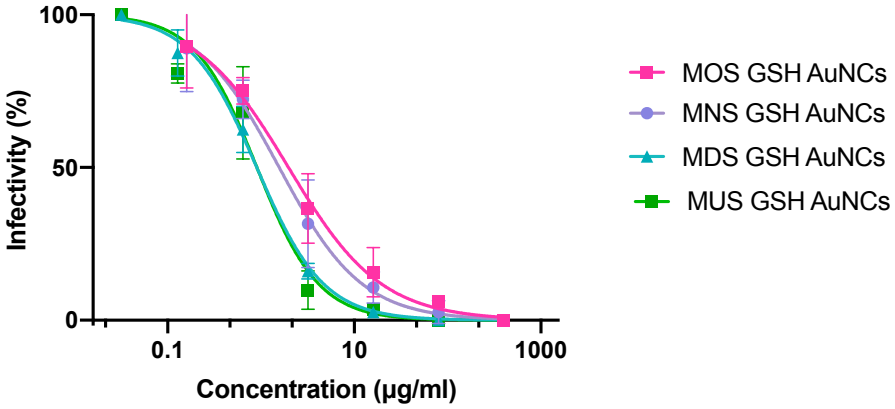

Figure 2.15 Dose response curves of MXS GSH AuNCs against HSV-2. The virus was pre-mixed with increasing concentration of the compound for 1 h at 37 °C and then added to cells.

Sample	Length	EC_{50}(µg/ml)
MOS GSH AuNCs	8	1.974 (1.397-2.801)
MNS GSH AuNCs	9	1.569 (1.108-2.230)
MDS GSH AuNCs	10	0.902 (0.765-1.065)
MUS GSH AuNCs	11	0.905 (0.637-1.252)

Table 6. Antiviral activity of MXS GSH AuNCs against HSV-2. 50% effective concentration (EC_{50}) values were calculated with GraphPad Prism.

The obtained data further confirmed the importance of the presence of the sulfonate group for AuNPs recognizing and binding to viral particles. In fact, as expected, all the samples greatly inhibited HSV-2 infection *in vitro,* showing a similar trend as that observed for AuNPs, even if with a weaker activity, ascribable to a lower sulfonate density and contact area.

On the other hand, different results emerged from the virucidal assay (**Figure 2.16**). In this case, the experiment was performed in two different conditions: one hour and three hour incubation after pre-treating the virus with AuNCs.

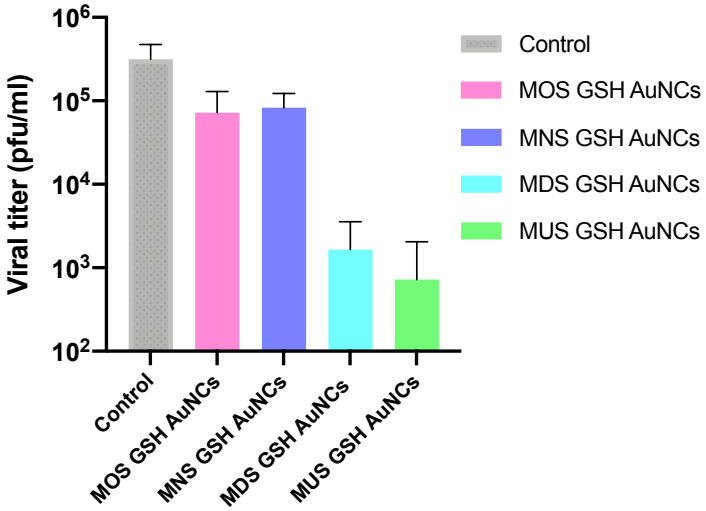

Figure 2.16 Virucidal activity of MXS GSH AuNCs. Each compound was pre-treated with the virus (PFU ~10^6) and incubated for 1 h at 37 °C. Then, the mixture was added to Vero E6 cells performing serial dilution. The control without sample was used for calculating the viral titer on the base of the number of formed plaques.

As it can be seen, interestingly, we found that for long alkyl chains (MDS and MUS) the virucidal activity was not much affected by the presence of GSH and the size of the core, whereas a trend reversal was observed for shorter ligands (MOS and MNS), in comparison with the corresponding AuNPs. Moreover, the same results were obtained by increasing the pre-treatment incubation time from 1 to 3 h. These data clearly confirm that the chemical features of the ligand are strongly correlated with the antiviral mechanism of action. In fact, we can suppose that GSH acts oppositely to OT; therefore, MOS and MNS, being less flexible and hydrophobic, may require a lower GSH content to develop a strong multivalent binding and exert an irreversible effect. Moreover, the hydrophilic GSH may to lead a higher dissociation constant in the aqueous medium. Beyond this, based on the virucidal data reported for the three different systems, we can hypothesize that the cut-off length required for an irreversible effect may be correlated with the size of the core, but a more detailed study is indeed required.

3. Conclusions

In this study, we have demonstrated that the antiviral mechanism of action of sulfonated ligand coated AuNPs is strongly influenced by their chemical structure. Our aim was to rationally design HSPG mimicking platforms in order to evaluate the effect of the flexibility

and hydrophobicity of the linkers and identify the structural parameters required for a virucidal effect. Therefore, we successfully synthetized AuNPs capped with sulfonated alkanethiols of different length *via* one phase method, obtaining a similar ligand density. In dose-response assays, all the samples inhibited HSV-2 infection with nanomolar EC_{50} values, without significant differences. However, the performed virucidal assays reveled that the AuNPs with short chain length exerted a reversible inhibitory effect, with almost full recovery of viral infectivity upon dilution, whereas the elongation of the aliphatic chain was associated with an irreversible inhibition; moreover, it was noted that the antiviral potency of the virucidal samples was not significantly affected by the length of the alkyl chain. On the other hand, we found that the presence of a hydrophobic ligand such as OT could switch the antiviral mechanism of action of the virustatic AuNPs from reversible to irreversible, and a positive correlation between the OT content and the virucidal effect was observed.

On the basis of these considerations, we can conclude that the presence of sulfonate groups is essential for AuNPs recognizing and binding to viral particles; however, these electrostatic interactions may be not strong enough to lead to an irreversible effect. Therefore, the flexibility and the hydrophobicity of the linkers were found to play a key role, enhancing the contacts between our HSPG mimicking system and viral particles. This latter allowed the development of a strong, multivalent binding with consequent capsid rupture.

This work opens the doors to a rational design of novel virucidal agents, unravelling their mechanism of action and identifying the structural and chemical features essential for a virucidal effect. Future studies will be addressed to understand if these structure-activity relationships can be translatable to other HSPG-dependent viruses or they differ in some aspects.

References

1. Jacob, S. T., Crozier, I., Fischer, W. A., Hewlett, A., Kraft, C. S., de La Vega, M. A., ... & Kuhn, J. H. (2020). Ebola virus disease. *Nature reviews Disease primers*, *6*(1), 1-31.
2. WHO website. Available online: https://www.who.int/news/item/25-06-2020-10th-ebola-outbreak-in-the-democratic-republic-of-the-congo-declared-over-vigilance-against-flare-ups-and-support-for-survivors-must-continue
3. De Wit, E., Van Doremalen, N., Falzarano, D., & Munster, V. J. (2016). SARS and MERS: recent insights into emerging coronaviruses. *Nature Reviews Microbiology*, *14*(8), 523-534.
4. Reperant, L. A., & Osterhaus, A. D. (2017). AIDS, Avian flu, SARS, MERS, Ebola, Zika… what next?. *Vaccine*, *35*(35), 4470-4474.
5. Vasan, S., & Pitisuttithum, P. (2021). Vaccine development lessons between HIV and COVID-19. *The Lancet Infectious Diseases*, *21*(6), 759-761.
6. Hartlage, A. S., & Kapoor, A. (2021). Hepatitis C Virus Vaccine Research: Time to Put Up or Shut Up. *Viruses*, *13*(8), 1596
7. Plotkin, S. A. (2005). Vaccines: past, present and future. *Nature medicine*, *11*(4), S5-S11.
8. Lou, Z., Sun, Y., & Rao, Z. (2014). Current progress in antiviral strategies. *Trends in pharmacological sciences*, *35*(2), 86-102.
9. De Clercq, E., & Li, G. (2016). Approved antiviral drugs over the past 50 years. *Clinical microbiology reviews*, *29*(3), 695-747.
10. Bekerman, E., & Einav, S. (2015). Combating emerging viral threats. *Science*, *348*(6232), 282-283.
11. Ader, F., Bouscambert-Duchamp, M., Hites, M., Peiffer-Smadja, N., Poissy, J., Belhadi, D., ... & Braz, S. (2021). Remdesivir plus standard of care versus standard of care alone for the treatment of patients admitted to hospital with COVID-19 (DisCoVeRy): a phase 3, randomised, controlled, open-label trial. *The Lancet Infectious Disease*
12. Reis, G., Silva, E. A. D. S. M., Silva, D. C. M., Thabane, L., Singh, G., Park, J. J., ... & TOGETHER Investigators. (2021). Effect of Early Treatment With Hydroxychloroquine or Lopinavir and Ritonavir on Risk of Hospitalization Among

Patients With COVID-19: The TOGETHER Randomized Clinical Trial. *JAMA network open*, *4*(4), e216468-e216468.

13. Tong, S., Su, Y., Yu, Y., Wu, C., Chen, J., Wang, S., & Jiang, J. (2020). Ribavirin therapy for severe COVID-19: a retrospective cohort study. *International journal of antimicrobial agents*, *56*(3), 106114.
14. De Clercq, E. (2007). The design of drugs for HIV and HCV. *Nature reviews Drug discovery*, *6*(12), 1001-1018.
15. Cho, N. J., & Glenn, J. S. (2020). Materials science approaches in the development of broad-spectrum antiviral therapies. *Nature Materials*, *19*(8), 813-816.
16. Vigant, F., Santos, N. C., & Lee, B. (2015). Broad-spectrum antivirals against viral fusion. *Nature Reviews Microbiology*, *13*(7), 426-437.
17. Dimitrov, D. S. (2004). Virus entry: molecular mechanisms and biomedical applications. *Nature Reviews Microbiology*, *2*(2), 109-122.
18. Schneck, E., Sedlmeier, F., & Netz, R. R. (2012). Hydration repulsion between biomembranes results from an interplay of dehydration and depolarization. *Proceedings of the National Academy of Sciences*, *109*(36), 14405-14409.
19. Taube, S., Jiang, M., & Wobus, C. E. (2010). Glycosphingolipids as receptors for non-enveloped viruses. *Viruses*, *2*(4), 1011-1049.
20. Heida, R., Bhide, Y. C., Gasbarri, M., Kocabiyik, Ö., Stellacci, F., Huckriede, A. L., ... & Frijlink, H. W. (2020). Advances in the development of entry inhibitors for sialic-acid-targeting viruses. *Drug Discovery Today*.
21. Shi, D., Sheng, A., & Chi, L. (2021). Glycosaminoglycan-protein interactions and their roles in human disease. *Frontiers in Molecular Biosciences*, *8*.
22. De Pasquale, V., Quiccione, M. S., Tafuri, S., Avallone, L., & Pavone, L. M. (2021). Heparan Sulfate Proteoglycans in Viral Infection and Treatment: A Special Focus on SARS-CoV-2. *International Journal of Molecular Sciences*, *22*(12), 6574
23. Cagno, V., Tseligka, E. D., Jones, S. T., & Tapparel, C. (2019). Heparan sulfate proteoglycans and viral attachment: true receptors or adaptation bias?. *Viruses*, *11*(7), 596.
24. Weiss, R. J., Esko, J. D., & Tor, Y. (2017). Targeting heparin and heparan sulfate protein interactions. *Organic & biomolecular chemistry*, *15*(27), 5656-5668.
25. Simon Davis, D. A., & Parish, C. R. (2013). Heparan sulfate: a ubiquitous glycosaminoglycan with multiple roles in immunity. *Frontiers in immunology*, *4*, 470.

26. Annaval, T., Wild, R., Crétinon, Y., Sadir, R., Vivès, R. R., & Lortat-Jacob, H. (2020). Heparan sulfate proteoglycans biosynthesis and post synthesis mechanisms combine few enzymes and few core proteins to generate extensive structural and functional diversity. *Molecules*, *25*(18), 4215.
27. Multhaupt, H. A., & Couchman, J. R. (2012). Heparan sulfate biosynthesis: methods for investigation of the heparanosome. *Journal of Histochemistry & Cytochemistry*, *60*(12), 908-915.
28. Jemth, P., Smeds, E., Do, A. T., Habuchi, H., Kimata, K., Lindahl, U., & Kusche-Gullberg, M. (2003). Oligosaccharide library-based assessment of heparan sulfate 6-O-sulfotransferase substrate specificity. *Journal of Biological Chemistry*, *278*(27), 24371-24376.
29. Kaltenbach, D. D., Jaishankar, D., Hao, M., Beer, J. C., Volin, M. V., Desai, U. R., & Tiwari, V. (2018). Sulfotransferase and heparanase: remodeling engines in promoting virus infection and disease development. *Frontiers in pharmacology*, *9*, 1315.
30. Moon, A. F., Edavettal, S. C., Krahn, J. M., Munoz, E. M., Negishi, M., Linhardt, R. J., ... & Pedersen, L. C. (2004). Structural analysis of the sulfotransferase (3-o-sulfotransferase isoform 3) involved in the biosynthesis of an entry receptor for herpes simplex virus 1. *Journal of Biological Chemistry*, *279*(43), 45185-45193.
31. Chen, J., & Liu, J. (2005). Characterization of the structure of antithrombin-binding heparan sulfate generated by heparan sulfate 3-O-sulfotransferase 5. *Biochimica et Biophysica Acta (BBA)-General Subjects*, *1725*(2), 190-200.
32. Koganti, R., Suryawanshi, R., & Shukla, D. (2020). Heparanase, cell signaling, and viral infections. *Cellular and Molecular Life Sciences*, 1-19.
33. Masola, V., Bellin, G., Gambaro, G., & Onisto, M. (2018). Heparanase: A multitasking protein involved in extracellular matrix (ECM) remodeling and intracellular events. *Cells*, *7*(12), 236.
34. Hadigal, S. R., Agelidis, A. M., Karasneh, G. A., Antoine, T. E., Yakoub, A. M., Ramani, V. C., ... & Shukla, D. (2015). Heparanase is a host enzyme required for herpes simplex virus-1 release from cells. *Nature communications*, *6*(1), 1-11.
35. Vivès, R. R., Seffouh, A., & Lortat-Jacob, H. (2014). Post-synthetic regulation of HS structure: the yin and yang of the sulfs in cancer. *Frontiers in oncology*, *3*, 331.
36. Karamanos, N. K., Piperigkou, Z., Theocharis, A. D., Watanabe, H., Franchi, M., Baud, S., ... & Iozzo, R. V. (2018). Proteoglycan chemical diversity drives

multifunctional cell regulation and therapeutics. *Chemical reviews*, *118*(18), 9152-9232.

37. Sarrazin, S., Lamanna, W. C., & Esko, J. D. (2011). Heparan sulfate proteoglycans. *Cold Spring Harbor perspectives in biology*, *3*(7), a004952.
38. Gondelaud, F., & Ricard-Blum, S. (2019). Structures and interactions of syndecans. *The FEBS journal*, *286*(15), 2994-3007.
39. Park, P. W. (2018). Isolation and functional analysis of syndecans. *Methods in cell biology*, *143*, 317-333.
40. Iozzo, R. V., & Schaefer, L. (2015). Proteoglycan form and function: a comprehensive nomenclature of proteoglycans. *Matrix biology*, *42*, 11-55
41. Bishop, J. R., Schuksz, M., & Esko, J. D. (2007). Heparan sulphate proteoglycans fine-tune mammalian physiology. *Nature*, *446*(7139), 1030-1037.
42. Karamanos, N. K., Theocharis, A. D., Piperigkou, Z., Manou, D., Passi, A., Skandalis, S. S., ... & Onisto, M. (2021). A guide to the composition and functions of the extracellular matrix. *FEBS J*.
43. Kolset, S. O., & Pejler, G. (2011). Serglycin: a structural and functional chameleon with wide impact on immune cells. *The journal of Immunology*, *187*(10), 4927-4933.
44. Tumova, S., Woods, A., & Couchman, J. R. (2000). Heparan sulfate proteoglycans on the cell surface: versatile coordinators of cellular functions. *The international journal of biochemistry & cell biology*, *32*(3), 269-288.
45. Onyeisi, J. O. S., Ferreira, B. Z. F., Nader, H. B., & Lopes, C. C. (2020). Heparan sulfate proteoglycans as targets for cancer therapy: A review. *Cancer Biology & Therapy*, *21*(12), 1087-1094.
46. Nagarajan, A., Malvi, P., & Wajapeyee, N. (2018). Heparan sulfate and heparan sulfate proteoglycans in cancer initiation and progression. *Frontiers in endocrinology*, *9*, 483.
47. Collins, L. E., & Troeberg, L. (2019). Heparan sulfate as a regulator of inflammation and immunity. *Journal of leukocyte biology*, *105*(1), 81-92.
48. Schwartz, N. B., & Domowicz, M. S. (2018). Proteoglycans in brain development and pathogenesis. *FEBS letters*, *592*(23), 3791-3805.
49. Papy-Garcia, D., & Albanese, P. (2017). Heparan sulfate proteoglycans as key regulators of the mesenchymal niche of hematopoietic stem cells. *Glycoconjugate journal*, *34*(3), 377-391.

50. Li, J. P., & Kusche-Gullberg, M. (2016). Heparan sulfate: biosynthesis, structure, and function. *International review of cell and molecular biology*, *325*, 215-273.
51. Christianson, H. C., & Belting, M. (2014). Heparan sulfate proteoglycan as a cell-surface endocytosis receptor. *Matrix Biology*, *35*, 51-55.
52. Kawaguchi, Y., Takeuchi, T., Kuwata, K., Chiba, J., Hatanaka, Y., Nakase, I., & Futaki, S. (2016). Syndecan-4 is a receptor for clathrin-mediated endocytosis of arginine-rich cell-penetrating peptides. *Bioconjugate chemistry*, *27*(4), 1119-1130.
53. Park, H., Kim, M., Kim, H. J., Lee, Y., Seo, Y., Pham, C. D., ... & Kwon, M. H. (2017). Heparan sulfate proteoglycans (HSPGs) and chondroitin sulfate proteoglycans (CSPGs) function as endocytic receptors for an internalizing anti-nucleic acid antibody. *Scientific reports*, *7*(1), 1-15.
54. Joshi, B. S., & Zuhorn, I. S. (2021). Heparan sulfate proteoglycan-mediated dynamin-dependent transport of neural stem cell exosomes in an in vitro blood–brain barrier model. *European Journal of Neuroscience*, *53*(3), 706-719.
55. Bartlett, A. H., & Park, P. W. (2011). Heparan sulfate proteoglycans in infection. In *Glycans in Diseases and Therapeutics* (pp. 31-62). Springer, Berlin, Heidelberg.
56. Xie, M., & Li, J. P. (2019). Heparan sulfate proteoglycan–a common receptor for diverse cytokines. *Cellular signalling*, *54*, 115-121
57. McGough, I. J., Vecchia, L., Bishop, B., Malinauskas, T., Beckett, K., Joshi, D., ... & Vincent, J. P. (2020). Glypicans shield the Wnt lipid moiety to enable signalling at a distance. *Nature*, *585*(7823), 85-90.
58. Kolluri, A., & Ho, M. (2019). The role of glypican-3 in regulating Wnt, YAP, and hedgehog in liver cancer. *Frontiers in oncology*, *9*, 708.
59. Filmus, J., & Capurro, M. (2014). The role of glypicans in Hedgehog signaling. *Matrix Biology*, *35*, 248-252.
60. Latko, M., Czyrek, A., Porębska, N., Kucińska, M., Otlewski, J., Zakrzewska, M., & Opaliński, Ł. (2019). Cross-talk between fibroblast growth factor receptors and other cell surface proteins. *Cells*, *8*(5), 455.
61. Bacsa, S., Karasneh, G., Dosa, S., Liu, J., Valyi-Nagy, T., & Shukla, D. (2011). Syndecan-1 and syndecan-2 play key roles in herpes simplex virus type-1 infection. *The Journal of general virology*, *92*(Pt 4), 733.
62. de Witte, L., Bobardt, M., Chatterji, U., Degeest, G., David, G., Geijtenbeek, T. B., & Gallay, P. (2007). Syndecan-3 is a dendritic cell-specific attachment receptor for HIV-1. *Proceedings of the National Academy of Sciences*, *104*(49), 19464-19469.

63. Hadigal, S., Koganti, R., Yadavalli, T., Agelidis, A., Suryawanshi, R., & Shukla, D. (2020). Heparanase-regulated syndecan-1 shedding facilitates herpes simplex virus 1 egress. *Journal of virology*, *94*(6), e01672-19.
64. Thakkar, N., Yadavalli, T., Jaishankar, D., & Shukla, D. (2017). Emerging roles of heparanase in viral pathogenesis. *Pathogens*, *6*(3), 43.
65. Mitra, D., Hasan, M. H., Bates, J. T., Bierdeman, M. A., Ederer, D. R., Parmar, R. C., ... & Tandon, R. (2021). The degree of polymerization and sulfation patterns in heparan sulfate are critical determinants of cytomegalovirus entry into host cells. *PLoS pathogens*, *17*(8), e1009803.
66. Zhang, Z., Liu, X., Chen, J., Su, H., Luo, Q., Ye, J., ... & Huang, A. (2010). Heparin sulphate D-glucosaminyl 3-O-sulfotransferase 3B1 plays a role in HBV replication. *Virology*, *406*(2), 280-285.
67. Roizmann, B., Desrosiers, R. C., Fleckenstein, B., Lopez, C., Minson, A. C., & Studdert, M. J. (1992). The familyHerpesviridae: an update. *Archives of virology*, *123*(3-4), 425-449.
68. Jiang, Y. C., Feng, H., Lin, Y. C., & Guo, X. R. (2016). New strategies against drug resistance to herpes simplex virus. *International journal of oral science*, *8*(1), 1-6
69. Margolis, T. P., Imai, Y., Yang, L., Vallas, V., & Krause, P. R. (2007). Herpes simplex virus type 2 (HSV-2) establishes latent infection in a different population of ganglionic neurons than HSV-1: role of latency-associated transcripts. *Journal of virology*, *81*(4), 1872-1878.
70. Maroui, M. A., Callé, A., Cohen, C., Streichenberger, N., Texier, P., Takissian, J., ... & Lomonte, P. (2016). Latency entry of herpes simplex virus 1 is determined by the interaction of its genome with the nuclear environment. *PLoS pathogens*, *12*(9), e1005834
71. Sawtell, N. M., & Thompson, R. L. (2020). Alphaherpesvirus Latency and Reactivation with a Focus on Herpes Simplex Virus. *Current Issues in Molecular Biology*, *41*(1), 267-356.
72. Xu, X., Zhang, Y., & Li, Q. (2019). Characteristics of herpes simplex virus infection and pathogenesis suggest a strategy for vaccine development. *Reviews in medical virology*, *29*(4), e2054
73. Sadowski, L. A., Upadhyay, R., Greeley, Z. W., & Margulies, B. J. (2021). Current drugs to treat infections with herpes simplex viruses-1 and-2. *Viruses*, *13*(7), 1228.
74. Tenser, R. B., & Tenser, R. B. (2021). Acyclovir resistant HSV in immunocompromised patients.

75. Piret, J., & Boivin, G. (2011). Resistance of herpes simplex viruses to nucleoside analogues: mechanisms, prevalence, and management. *Antimicrobial agents and chemotherapy*, *55*(2), 459-472.
76. O'Donnell, C. D., & Shukla, D. (2008). The importance of heparan sulfate in herpesvirus infection. *Virologica sinica*, *23*(6), 383-393.
77. Pertel, P. E., Fridberg, A., Parish, M. L., & Spear, P. G. (2001). Cell fusion induced by herpes simplex virus glycoproteins gB, gD, and gH-gL requires a gD receptor but not necessarily heparan sulfate. *Virology*, *279*(1), 313-324.
78. Whitley, R. J., & Roizman, B. (2001). Herpes simplex virus infections. *The lancet*, *357*(9267), 1513-1518.
79. Madavaraju, K., Koganti, R., Volety, I., Yadavalli, T., & Shukla, D. (2021). Herpes simplex virus cell entry mechanisms: an update. *Frontiers in Cellular and Infection Microbiology*, *10*, 852.
80. Laquerre, S., Argnani, R., Anderson, D. B., Zucchini, S., Manservigi, R., & Glorioso, J. C. (1998). Heparan sulfate proteoglycan binding by herpes simplex virus type 1 glycoproteins B and C, which differ in their contributions to virus attachment, penetration, and cell-to-cell spread. *Journal of virology*, *72*(7), 6119-6130.
81. Agelidis, A. M., & Shukla, D. (2015). Cell entry mechanisms of HSV: what we have learned in recent years. *Future virology*, *10*(10), 1145-1154.
82. Connolly, S. A., Jardetzky, T. S., & Longnecker, R. (2021). The structural basis of herpesvirus entry. *Nature reviews Microbiology*, *19*(2), 110-121.
83. O'Donnell, C. D., Tiwari, V., Oh, M. J., & Shukla, D. (2006). A role for heparan sulfate 3-O-sulfotransferase isoform 2 in herpes simplex virus type 1 entry and spread. *Virology*, *346*(2), 452-459.
84. Copeland, R., Balasubramaniam, A., Tiwari, V., Zhang, F., Bridges, A., Linhardt, R. J., ... & Liu, J. (2008). Using a 3-O-sulfated heparin octasaccharide to inhibit the entry of herpes simplex virus type 1. *Biochemistry*, *47*(21), 5774-5783.
85. Hu, Y. P., Lin, S. Y., Huang, C. Y., Zulueta, M. M. L., Liu, J. Y., Chang, W., & Hung, S. C. (2011). Synthesis of 3-O-sulfonated heparan sulfate octasaccharides that inhibit the herpes simplex virus type 1 host–cell interaction. *Nature chemistry*, *3*(7), 557-563.
86. Shukla, D., & Spear, P. G. (2001). Herpesviruses and heparan sulfate: an intimate relationship in aid of viral entry. *The Journal of clinical investigation*, *108*(4), 503-510.

87. Jambunathan, N., Clark, C. M., Musarrat, F., Chouljenko, V. N., Rudd, J., & Kousoulas, K. G. (2021). Two Sides to Every Story: Herpes Simplex Type-1 Viral Glycoproteins gB, gD, gH/gL, gK, and Cellular Receptors Function as Key Players in Membrane Fusion. *Viruses*, *13*(9), 1849.
88. Gonzalez, M. E., Alarcón, B., & Carrasco, L. (1987). Polysaccharides as antiviral agents: antiviral activity of carrageenan. *Antimicrobial agents and chemotherapy*, *31*(9), 1388-1393
89. Nahmias, A. J., & Kibrick, S. (1964). Inhibitory effect of heparin on herpes simplex virus. *Journal of Bacteriology*, *87*(5), 1060-106
90. Bianculli, R. H., Mase, J. D., & Schulz, M. D. (2020). Antiviral polymers: Past approaches and future possibilities. *Macromolecules*, *53*(21), 9158-9186.
91. Dey, P., Bergmann, T., Cuellar-Camacho, J. L., Ehrmann, S., Chowdhury, M. S., Zhang, M., ... & Azab, W. (2018). Multivalent flexible nanogels exhibit broad-spectrum antiviral activity by blocking virus entry. *ACS nano*, *12*(7), 6429-6442.
92. Donskyi, I. S., Azab, W., Cuellar-Camacho, J. L., Guday, G., Lippitz, A., Unger, W. E., ... & Haag, R. (2019). Functionalized nanographene sheets with high antiviral activity through synergistic electrostatic and hydrophobic interactions. *Nanoscale*, *11*(34), 15804-15809.
93. Pouyan, P., Nie, C., Bhatia, S., Wedepohl, S., Achazi, K., Osterrieder, N., & Haag, R. (2021). Inhibition of Herpes Simplex Virus Type 1 Attachment and Infection by Sulfated Polyglycerols with Different Architectures. *Biomacromolecules*, *22*(4), 1545-1554.
94. Gangji, R. N., Sankaranarayanan, N. V., Elste, J., Al-Horani, R. A., Afosah, D. K., Joshi, R., ... & Desai, U. R. (2018). Inhibition of herpes simplex virus-1 entry into human cells by nonsaccharide glycosaminoglycan mimetics. *ACS medicinal chemistry letters*, *9*(8), 797-802.
95. Lee, E. C., Davis-Poynter, N., Nguyen, C. T., Peters, A. A., Monteith, G. R., Strounina, E., ... & Ross, B. P. (2016). GAG mimetic functionalised solid and mesoporous silica nanoparticles as viral entry inhibitors of herpes simplex type 1 and type 2 viruses. *Nanoscale*, *8*(36), 16192-16196.
96. Lee, E. C., Nguyen, C. T., Strounina, E., Davis-Poynter, N., & Ross, B. P. (2018). Structure–activity relationships of GAG mimetic-functionalized mesoporous silica nanoparticles and evaluation of acyclovir-loaded antiviral nanoparticles with dual mechanisms of action. *ACS omega*, *3*(2), 1689-1699.

97. Chen, Z., Schiffman, M., Herrero, R., DeSalle, R., Anastos, K., Segondy, M., ... & Burk, R. D. (2018). Classification and evolution of human papillomavirus genome variants: Alpha-5 (HPV26, 51, 69, 82), Alpha-6 (HPV30, 53, 56, 66), Alpha-11 (HPV34, 73), Alpha-13 (HPV54) and Alpha-3 (HPV61). *Virology*, *516*, 86-101.
98. Gheit, T. (2019). Mucosal and cutaneous human papillomavirus infections and cancer biology. *Frontiers in Oncology*, *9*, 355
99. https://www.who.int/news-room/fact-sheets/detail/human-papillomavirus-(hpv)-and-cervical-cancer
100. European commission website. Available online: ihttps://ec.europa.eu/health/vaccination/hpv_en
101. Doorbar, J., Egawa, N., Griffin, H., Kranjec, C., & Murakami, I. (2015). Human papillomavirus molecular biology and disease association. *Reviews in medical virology*, *25*, 2-23.
102. Horvath, C. A., Boulet, G. A., Renoux, V. M., Delvenne, P. O., & Bogers, J. P. J. (2010). Mechanisms of cell entry by human papillomaviruses: an overview. *Virology journal*, *7*(1), 1-7.
103. Giroglou, T., Florin, L., Schäfer, F., Streeck, R. E., & Sapp, M. (2001). Human papillomavirus infection requires cell surface heparan sulfate. *Journal of virology*, *75*(3), 1565-1570.
104. Johnson, K. M., Kines, R. C., Roberts, J. N., Lowy, D. R., Schiller, J. T., & Day, P. M. (2009). Role of heparan sulfate in attachment to and infection of the murine female genital tract by human papillomavirus. *Journal of virology*, *83*(5), 2067-2074.
105. Shafti-Keramat, S., Handisurya, A., Kriehuber, E., Meneguzzi, G., Slupetzky, K., & Kirnbauer, R. (2003). Different Heparan Sulfate Proteoglycans Serve as Cellular Receptors for Human Papillomaviruses. *Journal of virology*, *77*(24), 13125-13135.
106. Surviladze, Z., Sterkand, R. T., & Ozbun, M. A. (2015). Interaction of human papillomavirus type 16 particles with heparan sulfate and syndecan-1 molecules in the keratinocyte extracellular matrix plays an active role in infection. *The Journal of general virology*, *96*(Pt 8), 2232.
107. Surviladze, Z., Dziduszko, A., & Ozbun, M. A. (2012). Essential roles for soluble virion-associated heparan sulfonated proteoglycans and growth factors in human papillomavirus infections. *PLoS pathogens*, *8*(2), e1002519.
108. Culp, T. D., Budgeon, L. R., Marinkovich, M. P., Meneguzzi, G., & Christensen, N. D. (2006). Keratinocyte-secreted laminin 5 can function as a transient receptor for

human papillomaviruses by binding virions and transferring them to adjacent cells. *Journal of virology*, *80*(18), 8940-8950.

109. Raff, A. B., Woodham, A. W., Raff, L. M., Skeate, J. G., Yan, L., Da Silva, D. M., ... & Kast, W. M. (2013). The evolving field of human papillomavirus receptor research: a review of binding and entry. *Journal of virology*, *87*(11), 6062-6072.
110. Carse, S., Bergant, M., & Schäfer, G. (2021). Advances in Targeting HPV Infection as Potential Alternative Prophylactic Means. *International journal of molecular sciences*, *22*(4), 2201.
111. Ozbun, M. A., & Campos, S. K. (2021). The long and winding road: human papillomavirus entry and subcellular trafficking. *Current Opinion in Virology*, *50*, 76-86.
112. Buck, C. B., Thompson, C. D., Roberts, J. N., Müller, M., Lowy, D. R., & Schiller, J. T. (2006). Carrageenan is a potent inhibitor of papillomavirus infection. *PLoS pathogens*, *2*(7), e69.
113. Gao, Y., Liu, W., Wang, W., Zhang, X., & Zhao, X. (2018). The inhibitory effects and mechanisms of 3, 6-O-sulfated chitosan against human papillomavirus infection. *Carbohydrate polymers*, *198*, 329-338.
114. Lembo, D., Donalisio, M., Laine, C., Cagno, V., Civra, A., Bianchini, E. P., ... & Bouchemal, K. (2014). Auto-associative heparin nanoassemblies: A biomimetic platform against the heparan sulfate-dependent viruses HSV-1, HSV-2, HPV-16 and RSV. *European Journal of Pharmaceutics and Biopharmaceutics*, *88*(1), 275-282.
115. Soria-Martinez, L., Bauer, S., Giesler, M., Schelhaas, S., Materlik, J., Janus, K., ... & Schelhaas, M. (2020). Prophylactic antiviral activity of sulfated glycomimetic oligomers and polymers. *Journal of the American Chemical Society*, *142*(11), 5252-5265.
116. Deeks, S. G., Overbaugh, J., Phillips, A., & Buchbinder, S. (2015). HIV infection. *Nature reviews Disease primers*, *1*(1), 1-22.
117. Alimonti, J. B., Ball, T. B., & Fowke, K. R. (2003). Mechanisms of CD4+ T lymphocyte cell death in human immunodeficiency virus infection and AIDS. *Journal of general Virology*, *84*(7), 1649-1661.
118. WHO website. Available online: https://www.who.int/news-room/fact-sheets/detail/hiv-aids
119. Fauci, A. S., & Folkers, G. K. (2012). Toward an AIDS-free generation. *Jama*, *308*(4), 343-344.

120. Volberding, P. A., & Deeks, S. G. (2010). Antiretroviral therapy and management of HIV infection. *The Lancet*, *376*(9734), 49-62.
121. Laurence, J., Elhadad, S., & Ahamed, J. (2018). HIV-associated cardiovascular disease: importance of platelet activation and cardiac fibrosis in the setting of specific antiretroviral therapies. *Open Heart*, *5*(2), e000823.
122. Compston, J. (2016). HIV infection and bone disease. *Journal of internal medicine*, *280*(4), 350-358.
123. Calza, L. (2012). Renal toxicity associated with antiretroviral therapy. *HIV clinical trials*, *13*(4), 189-211.
124. Ng'uni, T., Chasara, C., & Ndhlovu, Z. M. (2020). Major scientific hurdles in HIV vaccine development: Historical perspective and future directions. *Frontiers in Immunology*, *11*, 2761.
125. Zhu, P., Liu, J., Bess, J., Chertova, E., Lifson, J. D., Grisé, H., ... & Roux, K. H. (2006). Distribution and three-dimensional structure of AIDS virus envelope spikes. *Nature*, *441*(7095), 847-852.
126. Wilen, C. B., Tilton, J. C., & Doms, R. W. (2012). HIV: cell binding and entry. *Cold Spring Harbor perspectives in medicine*, *2*(8), a006866.
127. Connell, B. J., & Lortat-Jacob, H. (2013). Human immunodeficiency virus and heparan sulfate: from attachment to entry inhibition. *Frontiers in immunology*, *4*, 385.
128. Mondor, I., Ugolini, S., & Sattentau, Q. J. (1998). Human immunodeficiency virus type 1 attachment to HeLa CD4 cells is CD4 independent and gp120 dependent and requires cell surface heparans. *Journal of virology*, *72*(5), 3623-3634.
129. Saphire, A. C., Bobardt, M. D., Zhang, Z., David, G., & Gallay, P. A. (2001). Syndecans serve as attachment receptors for human immunodeficiency virus type 1 on macrophages. *Journal of virology*, *75*(19), 9187-9200.
130. Bobardt, M. D., Saphire, A. C., Hung, H. C., Yu, X., Van der Schueren, B., Zhang, Z., ... & Gallay, P. A. (2003). Syndecan captures, protects, and transmits HIV to T lymphocytes. *Immunity*, *18*(1), 27-39.
131. Vivès, R. R., Imberty, A., Sattentau, Q. J., & Lortat-Jacob, H. (2005). Heparan sulfate targets the HIV-1 envelope glycoprotein gp120 coreceptor binding site. *Journal of Biological Chemistry*, *280*(22), 21353-21357
132. Crublet, E., Andrieu, J. P., Vivès, R. R., & Lortat-Jacob, H. (2008). The HIV-1 envelope glycoprotein gp120 features four heparan sulfate binding domains,

including the co-receptor binding site. *Journal of Biological Chemistry*, *283*(22), 15193-15200.

133. Baleux, F., Loureiro-Morais, L., Hersant, Y., Clayette, P., Arenzana-Seisdedos, F., Bonnaffé, D., & Lortat-Jacob, H. (2009). A synthetic CD4–heparan sulfate glycoconjugate inhibits CCR5 and CXCR4 HIV-1 attachment and entry. *Nature chemical biology*, *5*(10), 743-748.
134. Pirrone, V., Wigdahl, B., & Krebs, F. C. (2011). The rise and fall of polyanionic inhibitors of the human immunodeficiency virus type 1. *Antiviral research*, *90*(3), 168-182.
135. Collins, P. L., Fearns, R., & Graham, B. S. (2013). Respiratory syncytial virus: virology, reverse genetics, and pathogenesis of disease. *Challenges and opportunities for respiratory syncytial virus vaccines*, 3-38.
136. Andeweg, S. P., Schepp, R. M., van de Kassteele, J., Mollema, L., Berbers, G. A., & van Boven, M. (2021). Population-based serology reveals risk factors for RSV infection in children younger than 5 years. *Scientific reports*, *11*(1), 1-8.
137. Bianchini, S., Silvestri, E., Argentiero, A., Fainardi, V., Pisi, G., & Esposito, S. (2020). Role of Respiratory Syncytial Virus in Pediatric Pneumonia. *Microorganisms*, *8*(12), 2048.
138. Saravolatz, L. D., Empey, K. M., Peebles Jr, R. S., & Kolls, J. K. (2010). Pharmacologic advances in the treatment and prevention of respiratory syncytial virus. *Clinical Infectious Diseases*, *50*(9), 1258-1267.
139. Mazur, N. I., Higgins, D., Nunes, M. C., Melero, J. A., Langedijk, A. C., Horsley, N., ... & Foundation, R. S. V. N. R. (2018). The respiratory syncytial virus vaccine landscape: lessons from the graveyard and promising candidates. *The Lancet Infectious Diseases*, *18*(10), e295-e311.
140. Eiland, L. S. (2009). Respiratory syncytial virus: diagnosis, treatment and prevention. *The Journal of Pediatric Pharmacology and Therapeutics*, *14*(2), 75-85.
141. Battles, M. B., & McLellan, J. S. (2019). Respiratory syncytial virus entry and how to block it. *Nature Reviews Microbiology*, *17*(4), 233-245.
142. Hallak, L. K., Spillmann, D., Collins, P. L., & Peeples, M. E. (2000). Glycosaminoglycan sulfation requirements for respiratory syncytial virus infection. *Journal of virology*, *74*(22), 10508-10513.

143. Hallak, L. K., Collins, P. L., Knudson, W., & Peeples, M. E. (2000). Iduronic acid-containing glycosaminoglycans on target cells are required for efficient respiratory syncytial virus infection. *Virology*, *271*(2), 264-27
144. Feldman, S. A., Hendry, R. M., & Beeler, J. A. (1999). Identification of a linear heparin binding domain for human respiratory syncytial virus attachment glycoprotein G. *Journal of virology*, *73*(8), 6610-6617.
145. Karron, R. A., Buonagurio, D. A., Georgiu, A. F., Whitehead, S. S., Adamus, J. E., Clements-Mann, M. L., ... & Sidhu, M. S. (1997). Respiratory syncytial virus (RSV) SH and G proteins are not essential for viral replication in vitro: clinical evaluation and molecular characterization of a cold-passaged, attenuated RSV subgroup B mutant. *Proceedings of the National Academy of Sciences*, *94*(25), 13961-13966.
146. Feldman, S. A., Audet, S., & Beeler, J. A. (2000). The fusion glycoprotein of human respiratory syncytial virus facilitates virus attachment and infectivity via an interaction with cellular heparan sulfate. *Journal of Virology*, *74*(14), 6442-6447.
147. Techaarpornkul, S., Collins, P. L., & Peeples, M. E. (2002). Respiratory syncytial virus with the fusion protein as its only viral glycoprotein is less dependent on cellular glycosaminoglycans for attachment than complete virus. *Virology*, *294*(2), 296-304.
148. Manns, M. P., Buti, M., Gane, E. D., Pawlotsky, J. M., Razavi, H., Terrault, N., & Younossi, Z. (2017). Hepatitis C virus infection. *Nature reviews Disease primers*, *3*(1), 1-19.
149. WHO website. Available online: https://www.who.int/news-room/fact-sheets/detail/hepatitis-c
150. Hepatology, T. L. G. (2021). The hunt for a vaccine for hepatitis C virus continues.
151. Li, G., & De Clercq, E. (2017). Current therapy for chronic hepatitis C: The role of direct-acting antivirals. *Antiviral research*, *142*, 83-122.
152. Zając, M., Muszalska, I., Sobczak, A., Dadej, A., Tomczak, S., & Jelińska, A. (2019). Hepatitis C–New drugs and treatment prospects. *European journal of medicinal chemistry*, *165*, 225-249.
153. Sarrazin, C. (2016). The importance of resistance to direct antiviral drugs in HCV infection in clinical practice. *Journal of hepatology*, *64*(2), 486-504.
154. Li, D. K., & Chung, R. T. (2019). Overview of direct-acting antiviral drugs and drug resistance of hepatitis C virus. *Hepatitis C Virus Protocols*, 3-32.
155. Morozov, V. A., & Lagaye, S. (2018). Hepatitis C virus: Morphogenesis, infection and therapy. *World journal of hepatology*, *10*(2), 186.

156. Zeisel, M. B., Felmlee, D. J., & Baumert, T. F. (2013). Hepatitis C virus entry. *Hepatitis C virus: from molecular virology to antiviral therapy*, 87-112.
157. Alazard-Dany, N., Denolly, S., Boson, B., & Cosset, F. L. (2019). Overview of HCV life cycle with a special focus on current and possible future antiviral targets. *Viruses*, *11*(1), 30.
158. Colpitts, C. C., Tsai, P. L., & Zeisel, M. B. (2020). Hepatitis C virus entry: an intriguingly complex and highly regulated process. *International journal of molecular sciences*, *21*(6), 2091.
159. Barth, H., Schäfer, C., Adah, M. I., Zhang, F., Linhardt, R. J., Toyoda, H., ... & Baumert, T. F. (2003). Cellular binding of hepatitis C virus envelope glycoprotein E2 requires cell surface heparan sulfate. *Journal of Biological Chemistry*, *278*(42), 41003-41012.
160. Jiang, J., Cun, W., Wu, X., Shi, Q., Tang, H., & Luo, G. (2012). Hepatitis C virus attachment mediated by apolipoprotein E binding to cell surface heparan sulfate. *Journal of virology*, *86*(13), 7256-7267.
161. Lefèvre, M., Felmlee, D. J., Parnot, M., Baumert, T. F., & Schuster, C. (2014). Syndecan 4 is involved in mediating HCV entry through interaction with lipoviral particle-associated apolipoprotein E. *PloS one*, *9*(4), e95550.
162. Xu, Y., Martinez, P., Séron, K., Luo, G., Allain, F., Dubuisson, J., & Belouzard, S. (2015). Characterization of hepatitis C virus interaction with heparan sulfate proteoglycans. *Journal of virology*, *89*(7), 3846-3858.
163. Basu, A., Kanda, T., Beyene, A., Saito, K., Meyer, K., & Ray, R. (2007). Sulfated homologues of heparin inhibit hepatitis C virus entry into mammalian cells. *Journal of virology*, *81*(8), 3933-3941.
164. Servidio, C., & Stellacci, F. (2021). Therapeutic approaches against coronaviruses acute respiratory syndrome. *Pharmacology Research & Perspectives*, *9*(1), e00691.
165. Raghu, G., & Wilson, K. C. (2020). COVID-19 interstitial pneumonia: monitoring the clinical course in survivors. *The Lancet Respiratory Medicine*, *8*(9), 839-842.
166. Long, B., Brady, W. J., Koyfman, A., & Gottlieb, M. (2020). Cardiovascular complications in COVID-19. *The American journal of emergency medicine*, *38*(7), 1504-1507.
167. Gu, X., & Cao, B. (2021). In-hospital complications associated with COVID-19. *The Lancet*, *398*(10296), 188-190.

168. Del Rio, C., Collins, L. F., & Malani, P. (2020). Long-term health consequences of COVID-19. *Jama*, *324*(17), 1723-1724.
169. https://www.nature.com/articles/d41586-021-02783-1
170. Malone, B., & Campbell, E. A. (2021). Molnupiravir: coding for catastrophe. *Nature Structural & Molecular Biology*, *28*(9), 706-708.
171. Harvey, W. T., Carabelli, A. M., Jackson, B., Gupta, R. K., Thomson, E. C., Harrison, E. M., ... & Robertson, D. L. (2021). SARS-CoV-2 variants, spike mutations and immune escape. *Nature Reviews Microbiology*, *19*(7), 409-424.
172. Farinholt, T., Doddapaneni, H., Qin, X., Menon, V., Meng, Q., Metcalf, G., ... & Petrosino, J. (2021). Transmission event of SARS-CoV-2 Delta variant reveals multiple vaccine breakthrough infections. *BMC medicine*, *19*(1), 1-6.
173. Chemaitelly, H., Tang, P., Hasan, M. R., AlMukdad, S., Yassine, H. M., Benslimane, F. M., ... & Abu-Raddad, L. J. (2021). Waning of BNT162b2 vaccine protection against SARS-CoV-2 infection in Qatar. *New England Journal of Medicine*.
174. Yang, H., & Rao, Z. (2021). Structural biology of SARS-CoV-2 and implications for therapeutic development. *Nature Reviews Microbiology*, 1-16.
175. Jackson, C. B., Farzan, M., Chen, B., & Choe, H. (2021). Mechanisms of SARS-CoV-2 entry into cells. *Nature Reviews Molecular Cell Biology*, 1-18.
176. Zhang, Q., Chen, C. Z., Swaroop, M., Xu, M., Wang, L., Lee, J., ... & Ye, Y. (2020). Heparan sulfate assists SARS-CoV-2 in cell entry and can be targeted by approved drugs in vitro. *Cell discovery*, *6*(1), 1-14.
177. Hudák, A., Letoha, A., Szilák, L., & Letoha, T. (2021). Contribution of syndecans to the cellular entry of SARS-CoV-2. *International journal of molecular sciences*, *22*(10), 5336.
178. Liu, L., Chopra, P., Li, X., Bouwman, K. M., Tompkins, S. M., Wolfert, M. A., ... & Boons, G. J. (2021). Heparan sulfate proteoglycans as attachment factor for SARS-CoV-2. *ACS Central Science*.
179. Clausen, T. M., Sandoval, D. R., Spliid, C. B., Pihl, J., Perrett, H. R., Painter, C. D., ... & Esko, J. D. (2020). SARS-CoV-2 infection depends on cellular heparan sulfate and ACE2. *Cell*, *183*(4), 1043-1057.
180. Yue, J., Jin, W., Yang, H., Faulkner, J., Song, X., Qiu, H., ... & Wang, L. (2021). Heparan sulfate facilitates spike protein-mediated SARS-CoV-2 host cell invasion and contributes to increased infection of SARS-CoV-2 G614 mutant and in lung cancer. *Frontiers in Molecular Biosciences*, *8*.

181. Kim, S. Y., Jin, W., Sood, A., Montgomery, D. W., Grant, O. C., Fuster, M. M., ... & Linhardt, R. J. (2020). Characterization of heparin and severe acute respiratory syndrome-related coronavirus 2 (SARS-CoV-2) spike glycoprotein binding interactions. *Antiviral research*, *181*, 104873.
182. Tandon, R., Sharp, J. S., Zhang, F., Pomin, V. H., Ashpole, N. M., Mitra, D., ... & Linhardt, R. J. (2020). Effective inhibition of SARS-CoV-2 entry by heparin and enoxaparin derivatives. *Journal of virology*, *95*(3), e01987-20.
183. Kwon, P. S., Oh, H., Kwon, S. J., Jin, W., Zhang, F., Fraser, K., ... & Dordick, J. S. (2020). Sulfated polysaccharides effectively inhibit SARS-CoV-2 in vitro. *Cell discovery*, *6*(1), 1-4.
184. Nie, C., Pouyan, P., Lauster, D., Trimpert, J., Kerkhoff, Y., Szekeres, G. P., ... & Haag, R. (2021). Polysulfates Block SARS-CoV-2 Uptake through Electrostatic Interactions. *Angewandte Chemie International Edition*, *60*(29), 15870-15878.
185. Zelikin, A. N., & Stellacci, F. (2021). Broad-Spectrum Antiviral Agents Based on Multivalent Inhibitors of Viral Infectivity. *Advanced Healthcare Materials*, *10*(6), 2001433.
186. Cagno, V., Andreozzi, P., D'Alicarnasso, M., Silva, P. J., Mueller, M., Galloux, M., ... & Stellacci, F. (2018). Broad-spectrum non-toxic antiviral nanoparticles with a virucidal inhibition mechanism. *Nature materials*, *17*(2), 195-203
187. Jones, S. T., Cagno, V., Janeček, M., Ortiz, D., Gasilova, N., Piret, J., ... & Tapparel, C. (2020). Modified cyclodextrins as broad-spectrum antivirals. *Science advances*, *6*(5), eaax9318.
188. Uzun, O., Hu, Y., Verma, A., Chen, S., Centrone, A., & Stellacci, F. (2008). Water-soluble amphiphilic gold nanoparticles with structured ligand shells. *Chemical communications*, (2), 196-198.
189. Loynachan, C. N., Soleimany, A. P., Dudani, J. S., Lin, Y., Najer, A., Bekdemir, A., ... & Stevens, M. M. (2019). Renal clearable catalytic gold nanoclusters for in vivo disease monitoring. *Nature nanotechnology*, *14*(9), 883-890.
190. Chen, X., Wei, M., Jiang, S., & Förster, S. (2019). Two growth mechanisms of thiol-capped gold nanoparticles controlled by ligand chemistry. *Langmuir*, *35*(37), 12130-12138.
191. Tewari, N., Nizar, H., Mane, A., George, V., & Prasad, M. (2006). Deacetylation of thioacetate using acetyl chloride in methanol. *Synthetic communications*, *36*(13), 1911-1914.

192. Yeh, Y. C., Creran, B., & Rotello, V. M. (2012). Gold nanoparticles: preparation, properties, and applications in bionanotechnology. *Nanoscale*, *4*(6), 1871-1880.
193. Sardar, R., Funston, A. M., Mulvaney, P., & Murray, R. W. (2009). Gold nanoparticles: past, present, and future. *Langmuir*, *25*(24), 13840-13851.
194. Elahi, N., Kamali, M., & Baghersad, M. H. (2018). Recent biomedical applications of gold nanoparticles: A review. *Talanta*, *184*, 537-556.
195. Brust, M., Walker, M., Bethell, D., Schiffrin, D. J., & Whyman, R. (1994). Synthesis of thiol-derivatised gold nanoparticles in a two-phase liquid–liquid system. *Journal of the Chemical Society, Chemical Communications*, (7), 801-802.
196. Zhou, S., Huo, D., Goines, S., Yang, T. H., Lyu, Z., Zhao, M., ... & Xia, Y. (2018). Enabling complete ligand exchange on the surface of gold nanocrystals through the deposition and then etching of silver. *Journal of the American Chemical Society*, *140*(38), 11898-11901
197. Yang, Y., Serrano, L. A., & Guldin, S. (2018). A versatile AuNP synthetic platform for decoupled control of size and surface composition. *Langmuir*, *34*(23), 6820-6826.
198. Schadt, M. J., Cheung, W., Luo, J., & Zhong, C. J. (2006). Molecularly tuned size selectivity in thermal processing of gold nanoparticles. *Chemistry of materials*, *18*(22), 5147-5149.
199. Tambasco, M., Kumar, S. K., & Szleifer, I. (2008). Quantitatively modeling the equilibrium properties of thiol-decorated gold nanoparticles. *Langmuir*, *24*(16), 8448-8451.
200. Koerner, H., MacCuspie, R. I., Park, K., & Vaia, R. A. (2012). In situ UV/Vis, SAXS, and TEM study of single-phase gold nanoparticle growth. *Chemistry of Materials*, *24*(6), 981-995
201. Zhou, M., Zeng, C., Li, Q., Higaki, T., & Jin, R. (2019). Gold nanoclusters: Bridging gold complexes and plasmonic nanoparticles in photophysical properties. *Nanomaterials*, *9*(7), 933.
202. iu, M., Tang, F., Yang, Z., Xu, J., & Yang, X. (2019). Recent progress on gold-nanocluster-based fluorescent probe for environmental analysis and biological sensing. *Journal of analytical methods in chemistry*, *2019*.
203. He, Z., Shu, T., Su, L., & Zhang, X. (2019). Strategies of luminescent gold nanoclusters for chemo-/bio-sensing. *Molecules*, *24*(17), 3045.

204. Bhatia, S., Camacho, L. C., & Haag, R. (2016). Pathogen inhibition by multivalent ligand architectures. *Journal of the American Chemical Society*, *138*(28), 8654-8666.

205. Kane, R. S. (2010). Thermodynamics of multivalent interactions: influence of the linker. *Langmuir*, *26*(11), 8636-8640.

[redacted] APPENDIX

ABSTRACT

(Italian version)

Negli ultimi anni un crescente interesse è stato rivolto verso nuove tecnologie per lo sviluppo di soluzioni terapeutiche efficaci. In tale contesto si inquadra il presente lavoro di tesi focalizzato sulla progettazione di sistemi innovativi per applicazioni biomedicali quali *drug delivery* e *drug discovery*. A tale scopo, una particolare attenzione è stata rivolta ad approcci bioispirati per lo sviluppo di materiali intelligenti multifunzionali adatti ad interagire adeguatamente con sistemi biologici. La natura costituisce una fonte d'ispirazione per scienziati e studiosi, offrendo esempi di strutture eleganti e complesse. Traslare questi principi nel design di sistemi ingegnerizzati rappresenta una strategia promettente con un enorme potenzialità in campo farmaceutico.

Il presente elaborato è suddiviso in due sezioni. La prima sezione è incentrata sullo sviluppo di formulazioni farmaceutiche per il rilascio sito-specifico di farmaci nella terapia antitumorale e per il trattamento topico di malattie dermatologiche. In particolare, nel primo capitolo viene presentata la progettazione e la caratterizzazione di un idrogel termo-responsivo multifunzionale per il rilascio controllato e selettivo di un farmaco chemioterapico quale il cisplatino. Le caratteristiche chimico-fisiche favorevoli e l'effetto antineoplastico in linee cellulari di carcinoma ovarico, anche cisplatino resistente, hanno evidenziato le grandi potenzialità di questo sistema per la chemioterapia intraperitoneale. Nel capitolo II viene invece presentato un approccio innovativo per la preparazione di formulazioni topiche per il rilascio della ciclosporina A nel trattamento della psoriasi. In particolare, nanoparticelle lipidiche solide basate su due sostanze bioattive quali la naringenina e l'acido linoleico sono state usate come *carriers* e incorporate in gel a differente grado di lipofilicità utilizzando sostanze funzionali quali la silice colloidale e l'acido ialuronico e agenti gelificanti come il Poloxamer 407 e il Carbopol. Risultati promettenti sono stati ottenuti dagli studi di rilascio dermici e transdermici; inoltre, le formulazioni hanno mostrato una buona attività antiossidante e antinfiammatoria che potrebbe risultare estremamente utile nel trattamento della psoriasi.

La seconda sezione è invece incentrata sulla progettazione di antivirali ad ampio spettro sfruttando il ruolo svolto dall'eparan solfato nelle infezioni virali. In particolare, viene presentata una strategia innovativa per il design di agenti multivalenti virucidi consistente nell'utilizzo di nanoparticelle d'oro funzionalizzate con ligandi mimanti l'eparan solfato.

In questo lavoro, una particolare attenzione è stata rivolta allo studio delle relazioni struttura-attività di questi sistemi e all'identificazione delle caratteristiche strutturali richieste per un'attività virucida. A tal fine, è stato valutato l'effetto della flessibilità, lunghezza e idrofobicità dei ligandi, e delle dimensioni e tipologia di *core*. I risultati ottenuti hanno permesso di capire e studiare al meglio il loro meccanismo d'azione, ponendo delle basi solide per la progettazione e lo sviluppo razionale di composti virucidi.

LIST OF PUBLICATIONS

Serini S., Cassano R., Bruni M., Servidio C., Calviello G., Trombino S., Characterization of a hyaluronic acid- and folic acid- based hydrogel for cisplatin delivery: antineoplastic effect in human ovarian cancer cell in vitro. *International journal of pharmaceutics* (2021), 606,120899.

Cassano R., Servidio C., Trombino S., Biomaterials for drugs nose-brain transport: a new therapeutic approach for neurological diseases. *Molecules* (2021), 14(7):1802.

Servidio C., Stellacci F., Therapeutic approaches against coronaviruses acute respiratory syndrome. *Pharmacology Research & Perspectives* (2021), 9(1): e00691.

Trombino S., Servidio C., Laganà A.S., Conforti F., Marrelli M., Cassano R., Viscosified solid lipid nanoparticles based on naringenin and linolenic acid for the release of cyclosporine a on the skin. *Molecules* (2020), 25(15): 3535.

Cassano R., De Amicis F., Servidio C., Curcio F., Trombino S., Preparation, characterization and in vitro evaluation of resveratol loaded nanospheres potentially useful for human breast carcinoma. *Journal of drug delivery science and technology* (2020), 57:101478.

Trombino S., Servidio C., Curcio F., Cassano R., Strategies for hyaluronic acid- based hydrogels design in drug delivery. *Pharmaceutics* (2019), 11(8): 407.

ACKNOWLEDGEMENTS

Time flies so fast. I still cannot believe this journey has come to an end…
Now I would like to take a moment and thank all the people who have supported me during these three years.

Starting from the very beginning of this journey I would like to acknowledge my supervisors Prof. Roberta Cassano and Prof. Francesca Iemma for their guidance, and all my colleagues of the Pharmaceutical Technology Laboratory (University of Calabria), in particular Elisabetta.

I would like to express my sincerest gratitude to my supervisor at EPFL Prof. Francesco Stellacci for giving me the precious opportunity to join his research group. I would like to thank him for his hospitality, advises, support and guidance. This visiting period added an important value to my thesis.

A special thanks goes to Dr. Paulo H. Jacob Silva for his constant help and encouragement.

Thanks to all my colleagues in SuNMIL, Anna, Adeline, Cecilia, Chihui, Francesca, Hanna, Harita, Heyun, Laura, Lukasz, Melis, Nicolò, Pamina, Simone, Suiyang and Vincenzo. In particular, I would like to acknowledge Carla, Matteo, Quy, Lixia, Xufeng and Colleen for the fruitful discussions and collaborations.

A sincere and heartfelt thanks goes to Ting and Yong, for being not only amazing colleagues but also great and true friends. Lausanne would not be home without you, we have countless memories together that I will never forget…感谢一切!

I would like to thank my long-time friends Lorenza, Veronica, Francesco, Ludovica, Mariafrancesca and Alexia who have always supported and “sopported” :D me.

Last but not least, I want to express my deepest gratitude to my family for the constant and precious presence, guidance and love. Non ce l’avrei mai fatta senza di voi. Grazie.

Cosenza, 02-02-2022

C.S.